The effect of anatomical structures on particle transport mechanisms in the human upper airway

Zhaoqi Ma

M.Eng. The University of Sydney.

Supervisor: Associate Professor Agisilaos Kourmatzis

Associate Supervisor: Professor Hak-Kim Chan

A thesis submitted in fulfilment of

the requirements for the degree of

Doctor of Philosophy

School of Aerospace, Mechanical and Mechatronic Engineering

Faculty of Engineering

The University of Sydney

Australia

01 February 2025

Abstract

The geometry of the human upper airway is highly complex and varies from individual to individual. As a result, the aerosol aerodynamic performance in the different realistic human upper airways and their deposition mechanisms remains unclear. There is a paucity of studies that have been designed to investigate the effect of individual upper airway anatomical features on drug deposition. In this thesis, different anatomical features of the human pharynx (the uvula, epiglottis, and soft palate) were systematically isolated to investigate their independent influence on airflow dynamics and particle deposition characteristics in a geometrically realistic human airway. Computational Fluid Dynamics (CFD) using established turbulence models was initially employed to simulate the transport of mono-dispersed particles (3 μm) in the airway as a function of flow-rate, and it was found that 1) widening the space between the oral cavity and oropharynx and where the soft palate is situated leads to the most dramatic reduction in drug deposition in the upper airway; 2) exclusion of the uvula and epiglottis: a) affects flow dynamics in the airway; b) alters regional deposition behaviour; and c) does not significantly affect the total number of particles deposited in the pharynx. The deposition results from CFD study were validated in an experimental study using Next-Generation Impaction (NGI) and High-performance liquid chromatography (HPLC). The experimental work was also utilized to obtain detailed information on the fine particle fraction emanating from these different airway geometries. The experimental study highlights that widening the region near the soft palate increases the fine particle fraction (FPF) and reduces deposition. Furthermore, it was found that the resistance of practical inhaler devices and their interaction with anatomical features of the human airway are likely to play a significant role in determining subsequent lung dose. Whilst the experimental NGI and HPLC methods are suitable for assessing total deposition in the human upper airway, they are not able to rapidly assess regional deposition and particle dynamics within the upper airway. Taking into account this limitation, a novel approach was developed for analyzing the flow of drug particles in a realistic model of the human upper airway using paired laser and photodiode sensors. Signal analysis was utilized to examine drug particle velocity, escape time, and regional deposition at various locations along the airway. Results from the study suggest that this simple laser attenuation technique is advantageous to investigate the regional deposition and the transient drug particle flow information in the human upper airway models.

Acknowledgements

This thesis represents a tiny thread in the vast tapestry of pulmonary drug delivery research, and without the support of the people mentioned in this acknowledgment, even this small contribution would not have been possible.

First and foremost, my deepest gratitude goes to my lead supervisor, Associate Professor Agisilaos Kourmatzis, whose guidance, patience, and unwavering support have been instrumental throughout my PhD journey. His expertise in the field of Two-Phase Flows, Aerosol Drug Delivery Spray, and Optical Diagnostics, as well as his insightful feedback, have significantly influenced this work. I am equally indebted to my associate supervisor, Professor Hak-Kim Chan, whose extensive knowledge in pulmonary drug delivery and inhalation aerosols, along with his continuous encouragement, have significantly enhanced my understanding of the complex interactions between engineering and pharmacy. I am also deeply grateful to Associate Professor Shaokoon Cheng, whose ongoing support has significantly enhanced my understanding of the technical aspects of pulmonary drug delivery. His guidance has been invaluable in bridging the gap between theoretical concepts and practical application.

Their combined mentorship has not only been pivotal to the progression of this research but has also instilled in me a profound appreciation for scientific inquiry and rigorous research. I am incredibly grateful for their commitment to my development as a researcher and their dedication to advancing knowledge in the field of pulmonary drug delivery.

I would also like to extend my sincere thanks to Dr. Liam Milton-McGurk, Dr. Patricia Tang, and other colleagues, as well as other PhD students, for their valuable discussions, technical assistance, and collaborative efforts. Your contributions have greatly enriched this thesis, and I am deeply appreciative of your support.

On a more personal note, I would like to extend my heartfelt gratitude to my family for their unwavering support and understanding throughout this journey. Their encouragement made completing this thesis possible. I am also deeply thankful to the funding bodies that supported this research, especially Dino Farina from Proveris Scientific Corporation, Hudson, MA, United States, whose financial support was invaluable. Additionally, this work was funded, in part, by the Australian Research Council under grant LP190100511. This thesis is a testament to the collective effort of many, and I am sincerely grateful to each one of you.

Contents

List of Figures

List of Tables

List of Glossary

Abbreviations and Symbols (in alphabetical order)

ACI: Andersen Cascade Impactor

AD: Aerodynamic Diameter

AIT: Alberta Idealized Throat

APSD: Aerodynamic Particle Size Distribution

CFD: Computational Fluid Dynamics

CIs: Cascade Impactors

COPD: Chronic Obstructive Pulmonary Disease

CT: Computed Tomography

D10 (µm): Volume diameter under which 10% of the particles reside (obtained from laser diffraction)

D15.9 (µm): The mass-based size distribution where 15.9% of the volume is contained by particles smaller

D50 (µm): Volume diameter under which 50% of the particles reside (obtained by laser diffraction)

D84.1 (µm): The mass-based size distribution where 84.1% of the volume is contained by particles smaller

D90 (µm): Volume diameter under which 90% of the particles reside (obtained by laser diffraction)

DPM: Discrete Phase Model

DPIs: Dry Powder Inhalers

E: Removed Epiglottis

ET: Extrathoracic

FPD (mg): Fine Particle Dose

FPFem (%): Fine Particle Fraction

FPF: Fine Particle Fraction

GSD: Geometric Standard Deviation

HPLC: High-Performance Liquid Chromatography

IVIVCs: In-Vivo and In-Vitro Correlations

LES: Large-Eddy Simulation

LPM: Liter Per Minute

LRN: Low Reynolds Number

MMAD: Mass Median Aerodynamic Diameter

MMD: Mass Median Diameter

MOC: Micro-Orifice Collector

MRI: Magnetic Resonance Imaging

MT: Mouth Throat

NGI: Next-Generation Impactor

NW: Near-Wall

O: Original Model

OPC-MTs: Oropharyngeal Consortium Mouth-Throats

OPC: Oropharyngeal Consortium

OSA: Obstructive Sleep Apnea

OSAS: Obstructive Sleep Apnea Syndrome

PET: Positron Emission Tomography

p: Statistical p-value

pMDI: Pressurized Metered-Dose Inhaler

PIV: Particle Image Velocimetry

POD: Proper Orthogonal Decomposition

RANS: Reynolds-Averaged Navier–Stokes

RI: Refractive Index

SPECT: Single Photon Emission Computed Tomography

SP: Removed Soft Palate

SP+E: Removed Soft Palate and Epiglottis

SST: Shear-Stress Transport

Stk: Stokes Number

U: Removed Uvula

U+E: Removed Uvula and Epiglottis

USP: United States Pharmacopeia

UV: Ultraviolet

VCU-MTs: Virginia Commonwealth University Mouth-Throats

VCU: Virginia Commonwealth University

VMD: Volume Median Diameter

3D: Three-Dimensional

Chapter 1 Introduction

1.1 Motivation and Objectives

Inhalation therapies may have been used as early as 4000 years ago in ancient times, when Indian people utilized datura preparations to treat asthma and other respiratory disorders (P. J. Anderson, 2005). However, it was not until 1956 that the modern era of pulmonary drug delivery began since the first pressurized metered-dose inhaler (pMDI) for epinephrine and isoproterenol was marketed by Riker Laboratories (now 3M Drug Delivery Systems) (Sanders, 2007; S. W. Stein & Thiel, 2017). The complexity of the pulmonary drug delivery system requires a comprehensive understanding of integrating aspects from a wide range of traditional scientific and engineering disciplines, including aerosol mechanics, single-phase and multiphase fluid mechanics, interfacial science, pharmaceutics, respiratory physiology and anatomy, and pulmonology (W. H. Finlay, 2001). Over the past six decades, significant advancements have been made in this area, leading to the emergence of safer and more effective drugs for combating respiratory diseases. Despite this, rigorous investigation is still required to truly understand the physics of this entire system, allowing for better inhaler and aerosol optimization and improving inhalation therapeutic efficiency.

Pulmonary drug delivery is a critical area of research due to its unique advantages, including non-invasive administration, rapid therapeutic onset, and the potential for localized treatment of respiratory diseases while minimizing systemic side effects. However, achieving optimal drug deposition and delivery efficiency remains a significant challenge. This difficulty arises from several factors, including anatomical variability among patients (W. H. Finlay, 2001), such as differences in airway geometry (Ides et al., 2022) and body mass index (BMI) (Shaokoon Cheng et al., 2019), the influence of airflow dynamics on particle behavior, including turbulence, velocity gradients, and recirculating flow regions, and a limited understanding of how anatomical structures, such as the soft palate, uvula, and epiglottis, affect deposition patterns (A Kourmatzis et al., 2018).

Enhancing knowledge in this field is essential for several reasons:

1. Improved Therapeutic Outcomes: A deeper understanding of particle transport and deposition can inform inhaler design, ensuring that devices are tailored to individual patient anatomies and breathing patterns, ultimately leading to more effective treatments.

2.Reduced Drug Waste: Inefficient pulmonary drug delivery often results in significant medication waste, increasing costs and reducing treatment reliability. Identifying key factors influencing deposition can guide strategies to optimize drug delivery and reduce losses (Hoppentocht et al., 2014).

3. Enhanced Patient Compliance: Inhalation therapies are often preferred over invasive methods like injections. By improving inhaler design and drug delivery efficiency, treatments can be made more accessible, tolerable, and user-friendly, enhancing patient adherence.

4. Addressing Knowledge Gaps: Despite advancements in pulmonary drug delivery, critical questions remain about the role of upper airway structures in particle deposition and transport, particularly under varying flow conditions and inhaler designs. This study directly addresses these unresolved challenges.

To achieve these goals, the following research objectives were carefully defined, aligning directly with the motivation:

1. Develop and validate computational and experimental methods to study particle behavior in anatomically realistic upper airway models.

2. Quantify the impact of anatomical structures (e.g., soft palate, uvula, and epiglottis) on drug deposition and transport.

3. Investigate how flow rates and particle sizes influence deposition patterns, providing insights for optimizing inhaler performance.

4. Introduce a novel laser-based experimental technique to capture temporal and spatial aerosol dynamics, enhancing the validation of computational models.

5. Compare deposition patterns between different inhaler designs (e.g., Handihaler and Osmohaler) to identify critical design factors influencing efficiency.

6. Synthesize findings to provide actionable insights for improving pulmonary drug delivery in clinical applications.

This thesis contributes to the advancement of pulmonary drug delivery by integrating computational modeling, experimental validation, and innovative measurement techniques, offering new insights into particle behavior in the human airway and strategies for improving inhaler performance. imization and improving inhalation therapeutic efficiency.

1.2 Plan of thesis

Chapter 2 shall provide a general literature review of the project including:

- The human respiratory tract and existing mouth-throat models used in the field.
- A review of inhaled pharmaceutical particles.
- Simulation study of airway models.
- Experimental methods in the pulmonary drug delivery (Pharmaceutical-related).
- Imaging and laser techniques in the area (Engineering-related).

Chapter 3 shall be the first chapter outlining the simulation results and will focus on:

- Simulation studies the effect of individual upper airway anatomical features on drug deposition

Chapter 4 shall present experimental results and will cover:

- Validating the simulation results with experimental data
- The experimental study of the effect of individual upper airway anatomical features on the deposition of dry powder inhaler formulations using impaction and high performance liquid chromatography

Chapter 5 introduces a new experimental method for measuring the flow behavior of drug aerosols in the human upper airway models and shall involve:

- Using laser attenuation to measure drug particle deposition and velocity in a human upper airway model.
- The comparison of the new experimental method with computational fluid dynamics (CFD) data

Chapter 6 concludes the thesis by summarizing the findings and suggesting areas for further research.

Chapter 2 Literature Review

2.1 Introduction

The aim of this chapter is to provide an overview of the research conducted in the field of pulmonary drug delivery that is directly relevant to the project in this thesis. The review will encompass several key areas. Firstly, it will cover the fundamental anatomy of the human respiratory system and the airway models used for *in-vivo* and *in-vitro* correlations (IVIVCs) studies. This scientific information is essential for gaining a comprehensive understanding of the complex geometry of human airways and comprehending the function of different parts of the airway system. The second component will delve into reviewing the basic physics of drug particles in the human airway. Following this, a comprehensive review of drug delivery methods and research techniques in the field will be conducted, encompassing CFD, NGI, HPLC, laser technology, and dissolution.

2.2 Airway fundamentals

The human airway can be divided into three main regions: (1) the extrathoracic region (mouth-throat region), which comprises the nasal cavity, oral cavity, pharynx, and larynx to the entrance of the trachea, (2) the tracheobronchial region, which consists of the proximal conducting airways (start from the trachea to the terminal bronchioles), and (3) the alveolar region, which ranges from respiratory bronchioles to the alveoli (Ahookhosh et al., 2020; Hofmann, 2011). The anatomical structure of the human airway is highly intricate, and the understanding of the precise of the human respiratory tract remains limited (W. H. Finlay, 2001; Ides et al., 2022; Yaqub et al., 2022). This lack of understanding can be attributed to several factors. Firstly, there is a significant variation in respiratory tract geometry from individual to individual (W. H. Finlay, 2001; Z. Ma et al., 2022) and the human airway can be affected by many factors such as gender, age, BMI (Shaokoon Cheng et al., 2019; Bingjie Ma et al., 2020; S. Martin et al., 1997) and many health-related problems (A Kourmatzis et al., 2018; Walsh et al., 2008). Secondly, the complex intricacies of the lung, such as the presence of millions of

alveoli (the mean alveolar number was 480 million, ranging from 274 to 790 million) with diameters ranging in the order of a few hundred microns, each possessing unique shapes, render it impractical to fully specify this level of detailed information (Ochs et al., 2004; Xi et al., 2020). The geometry of the respiratory tract is dynamic and subject to change over time due to the nature of breathing. While alveoli Due to the limitation expand and contract during inhalation and exhalation, these changes are not limited to the alveoli. Significant geometric variations also occur in the oral cavity, pharynx, and upper respiratory tract regions, influenced by factors such as soft tissue movement, airway muscle activity, and airflow patterns (Balásházy et al., 2008; W. H. Finlay, 2001). Related to this dynamic behaviour, the shape of the oral cavity can be altered by the positioning of the tongue and jaws and their muscular movements, resulting in a much more complex upper airway geometry (Finlay, 2001; A Kourmatzis et al., 2018). While capturing detailed motion of airway changes remains challenging due to the limitations of current medical imaging techniques, recent advancements have made significant progress in this area. For example, studies (Bates et al., 2019; Bates et al., 2018) have introduced innovative methods using CFD and static MRI with non-rigid registration to map upper airway movement. These techniques provide valuable insights into the relationship between airway motion and airflow dynamics, addressing some of the challenges in characterizing airway geometry changes during breathing. However, despite this knowledge gap, there is sufficient understanding of the fundamental aspects of the respiratory tract to develop simplified models of its geometry (Ahookhosh et al., 2020; Karra et al., 2019; Z. Ma et al., 2022; West & Luks, 2020). The detailed review of human airway models will be further discussed in section 2.3. For reader's benefit, the schematic of the human respiratory tract is shown in Figure 2.1.

The upper airway plays a crucial role in the entire respiratory system, serving as the front line for the lower airway by preventing the entry of foreign particles (Newman, 2017). This function results in significant drug deposition in this region (Rogers et al., 2022), which reduces therapeutic efficiency of inhalation aerosols and increases intersubjective variability and side effects (P Worth Longest & Hindle, 2012; Newman et al., 2007; Sadeghi et al., 2024). The upper airway is comprised of the nasal cavities, oral cavity, pharynx, and larynx (Devine & Zur, 2021). The pharynx can be further categorized into the nasopharynx, oropharynx, and hypopharynx (Siddiqui & Connor, 2013). Figure 2.2 depicts the anatomy of the human upper airway, commencing with the nasal cavity and extending through the nasopharynx and oropharynx to the larynx (W. Faizal et al., 2020). This project primarily focuses on the mouth-

throat regions; therefore, the nasal cavity will not be addressed in this review section. Instead, anatomical features of the mouth-throat regions will be reviewed.

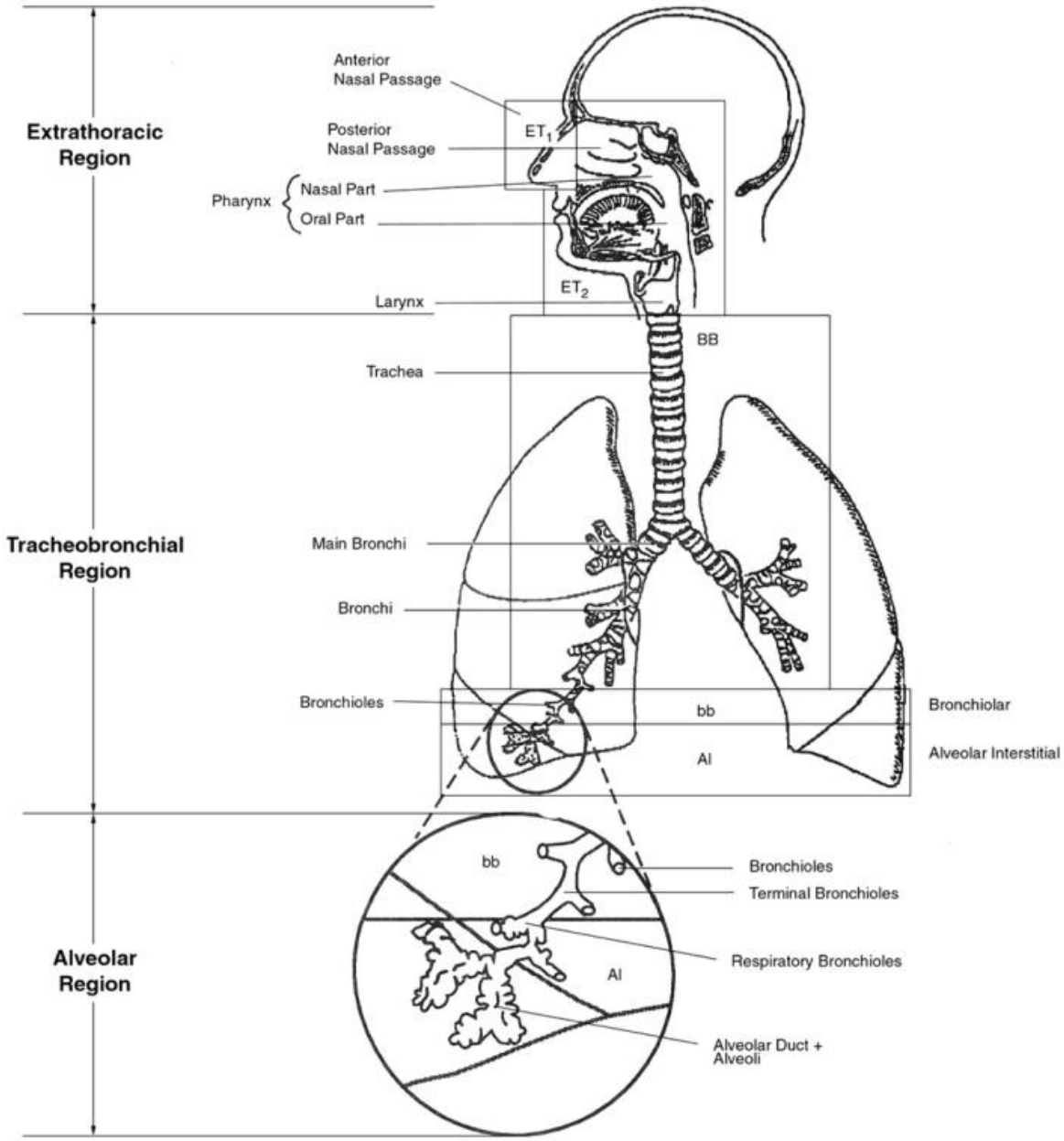

Figure 2. 1: Schematic of the human respiratory tract. Adapted from (Hofmann, 2011).

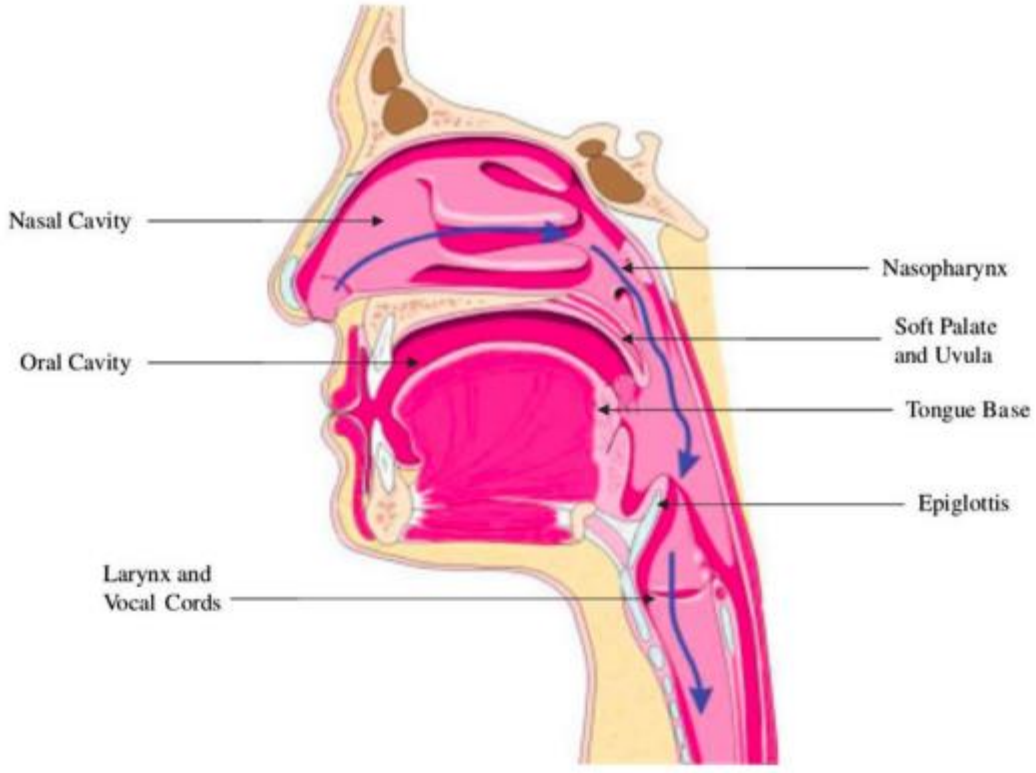

Figure 2. 2: The human upper airway including the nasal cavity, oral cavity, and the main carina at the lower end of the trachea. Adapted from (W. Faizal et al., 2020).

2.2.1 Oral cavity

Understanding the intricate dynamics of the oral cavity is essential for optimizing pulmonary drug delivery. The oral cavity, enclosed by the alveolar arch of the maxilla and the mandible, features teeth at the front, the hard and soft palates above, the anterior two-thirds of the tongue and its mucosa extending forward onto the mandible below, and the oropharyngeal isthmus behind (Joseph, 1982; Marani et al., 2018). These structures play a crucial role in determining airflow patterns and drug deposition during inhalation, thereby impacting the overall efficiency of pulmonary drug delivery systems (Rana et al., 2020; Vara Almirall et al., 2022). The oral teeth, situated at the front of the oral cavity, significantly influence the initial dispersion and direction of inhaled aerosols (Ehtezazi et al., 2004; He et al., 2024; X. Zhou et al., 2024). Teeth have the potential to create turbulent airflow, leading to premature deposition of drug particles on the oral surfaces rather than allowing them to reach the lower respiratory tract (Vara

Almirall et al., 2022). Misalignments or irregularities in the teeth further exacerbate this issue, emphasizing the need for optimization inhalation techniques and device designs to minimize such deposition and enhance drug delivery efficiency (Cataldo et al., 2022; Rogliani et al., 2017).

Geometrical factors of the mouth and throat significantly influence the deposition of orally inhaled aerosols. A comprehensive parametric study examined the effect of various mouth-throat geometrical features, such as oral cavity size, pharyngeal curvature, and airway diameter, on aerosol deposition patterns (Xi et al., 2016). Their findings highlighted that even small variations in geometry can lead to substantial changes in deposition efficiency, emphasizing the need to account for anatomical differences when designing inhalers. This work provides critical insights into the role of the oral cavity in particle dynamics and underscores the importance of including realistic geometrical models in pulmonary drug delivery studies.

Similarly, the hard and soft palates also play crucial roles in pulmonary drug delivery. The hard palate, which forms the roof of the mouth, provides structural support and stability, while the more flexible soft palate can alter its position during breathing and swallowing (Brand et al., 2023; Matsuo et al., 2010). At the distal of the soft palate is a small fleshy extension called the uvula (Gibb, 1872; Joseph, 1982), which can contribute to airway obstruction when improperly positioned (Hagberg et al., 2005). Additionally, the uvula plays a role in speech and swallowing, with its movement coordinated with that of the soft palate (Back et al., 2004; Donner et al., 1985). A lowered or improperly positioned soft palate can obstruct airflow, leading to increased drug deposition in the upper airway (BASKAR et al., 2021; Z. Ma et al., 2022). This obstruction significantly impacts the efficiency of drug delivery to the lungs as it disrupts airflow dynamics (Z. Ma et al., 2022).

The tongue, particularly its volume and muscle composition, has a profound impact on airway geometry and drug delivery (Mekonnen et al., 2022). A large tongue can obstruct the airway, creating a narrower passage for airflow, which complicates the effective delivery of inhaled medications (Bingjie Ma et al., 2020). Additionally, the muscle and fat composition of the tongue affects its size and positioning (Mekonnen et al., 2022). The intrinsic muscles of the tongue, including the superior longitudinal, inferior longitudinal, transverse, and vertical muscles, contribute to its shape and mobility (Sakamoto, 2018). The extrinsic muscles, such as the genioglossus, hyoglossus, styloglossus, and palatoglossus, control the tongue's position and movement (A Kourmatzis et al., 2018). Increased tongue fat, often seen in conditions like

obesity, further narrows the airway and exacerbates issues related to obstructive sleep apnea (OSA) (Kim et al., 2014), making pulmonary drug delivery less efficient (Bingjie Ma et al., 2020). A sagittal perspective of the human upper airway, presenting the anatomy and musculature is shown in Figure 2.3.

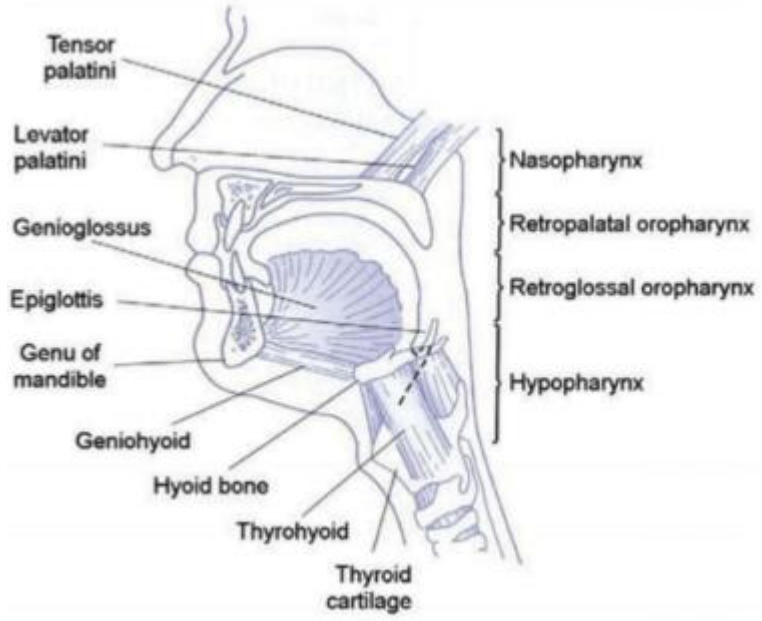

Figure 2. 3: The sagittal perspective of the human upper airway, presenting the anatomy and musculature. Adapted from (A Kourmatzis et al., 2018).

2.2.2 Epiglottis

Behind the tongue and in front of the laryngeal inlet is a leaf-shaped flap composed of elastic cartilage tissue covered with a mucous membrane known as the epiglottis (Suárez-Quintanilla & Sharma, 2019). The epiglottis is anchored to the thyroid cartilage and connected to the hyoid bone via the hyoepiglottic ligament (Ardran & Kemp, 1967; Suárez-Quintanilla & Sharma, 2019). It functions as a valve, preventing food and liquids from entering the trachea and lungs (Ardran & Kemp, 1967; Pitts, 2014).

The efficient administration of aerosolized medications to the lungs relies on unobstructed passage through the upper airway (Darquenne et al., 2024; W. H. Finlay, 2001). The epiglottis is likely to play a significant role in influencing the effectiveness of inhaled therapies in pulmonary drug delivery and deposition since the airway narrows dramatically at this level from an anatomical point of view (Mekonnen et al., 2022), and from a fluid mechanics

perspective, it creates a natural barrier for particles to be transported to the deep of human lungs due to the complex transition flow behavior in the local region (A Kourmatzis et al., 2018). Numerous studies have been conducted on obstructive sleep apnea (OSA), which is caused by the obstruction or narrowing of the airway at various levels (Catalfumo et al., 1998; Delakorda & Ovsenik, 2019; Torre et al., 2016). An earlier study (Catalfumo et al., 1998) investigated the relationship between the epiglottis and obstructive sleep apnea syndrome (OSAS) and revealed that partial or total hypopharyngeal obstruction by the epiglottis may contribute to OSAS, and the position of the epiglottis with respect to the base of the tongue during deep inspiration over 45 degrees may be the major contributing factor for the OSAS. Torre et al also argued that the collapse of the epiglottis is more likely to lead to OSA (Torre et al., 2016). However, limited research has been conducted in pulmonary drug delivery regarding the impact of the epiglottis on lung deposition, local drug particle flow, and deposition mechanisms (A Kourmatzis et al., 2018). Moreover, the position of the epiglottis will be changed due to the muscle motion during respiration (Ardran & Kemp, 1967), and the effect of these movements on drug particle deposition mechanisms remains unclear (A Kourmatzis et al., 2018). In addition, other systemic pathophysiological changes in the upper airway could impact inhaled drug delivery in Chronic obstructive pulmonary disease (COPD) (Mekonnen et al., 2022). For instance, research has shown that chronic inflammation of the nasal mucosa and enlargement of the tonsils and adenoids in COPD patients might lead to increased airway resistance (Lambert et al., 1993; Owens et al., 2017).

2.2.3 Pharynx

The pharynx is a muscular tube that extends from the base of the skull to the level of the sixth cervical vertebra, transitioning into the esophagus, and it is anatomically divided into three regions: the nasopharynx, oropharynx, and laryngopharynx (Donner et al., 1985; Karaosmanoglu & Ozgen, 2022). The nasopharynx is located posterior to the nasal cavity and above the soft palate (Moss, 1989; Sobiesk & Munakomi, 2019), the oropharynx is behind the oral cavity and extends from the soft palate to the hyoid bone (DelGaudio & Chen, 2010), and the laryngopharynx is situated posterior to the larynx (Suárez-Quintanilla & Sharma, 2019). During respiration, the pharynx serves as a passageway for directing air from both the nasal cavity and mouth to the larynx and trachea (Robinson & Furlow, 2007).

The pharynx is a crucial anatomical region in pulmonary drug delivery, as it is the initial pathway that inhaled medications must navigate to reach the lungs (Gonda, 2000). In the oropharynx, inertial impaction is responsible for delivering most pharmaceutical aerosols from inhaler devices, and oropharyngeal filtration significantly impacts the aerosols that can reach the deep lungs (A. Clark et al., 1998; Voss et al., 2022). Oropharyngeal filtering affects both overall lung drug deposition and its variability, with inhalers delivering the smallest lung doses showing the highest variability (Borgström et al., 2006). Furthermore, the complex anatomy and dynamic functions of the pharynx, including the coordinated muscular movements during breathing, significantly influence the flow dynamics and deposition patterns of inhaled drugs (Shaokoon Cheng et al., 2019; A Kourmatzis et al., 2018). A research (Shaokoon Cheng et al., 2019) found that deformation of the upper airway pharynx at the level of the soft palate in the lateral direction, rather than in the anteroposterior direction, has a significant impact on throat deposition, fine particle fraction (FPF), and in vitro lung dose as measured using a Next Generation Impactor (NGI). However, the detailed physical mechanisms behind this phenomenon remain unclear (Shaokoon Cheng et al., 2019). Additionally, combined with the Next Generation Impactor (NGI), mouth-throat models have been extensively used to study *in vitro-in vivo* correlations (IVIVCs), providing deep insights into particle transport and deposition mechanisms in the respiratory tract (Chow et al., 2021; Wei et al., 2018).

Several anatomical mouth-throat models have been developed over the last two decades based on the oropharyngeal geometries of healthy human subjects, and these mouth-throat models will be further discussed in section 2.3.

2.3 Realistic Mouth-Throat models

The anatomical geometry of the human upper airway is complex and forms a natural barrier against foreign particles, including inhaled pharmaceutical aerosols (Newman, 2017). A fundamental technique to test the efficacy of inhaled pharmaceutical aerosols involves analyzing the aerodynamic properties of drug particles using a cascade impactor, such as the Next Generation Impactor (NGI), alongside mouth-throat models to establish *in vitro-in vivo* correlations (IVIVCs) (Chow et al., 2021; Newman & Chan, 2020; Wei et al., 2018). The United States Pharmacopeia (USP) induction port, serving as a simplified mouth-throat model with a 90° bent tube, has been considered a standard tool for evaluating the performance of aerosols (USP, 2023). S. Stein and Gabrio (2000) observed that deposition in the USP induction port primarily occurred at the entrance. However, in a realistic upper airway model, deposition

was found to occur in both the mouth and the pharynx due to inertial impaction and turbulence (Ghahramani et al., 2014; S. Stein & Gabrio, 2000). Dolovich and Rhem (1998) compared seven different impactor inlets to the Andersen Cascade Impactor (ACI) showing that the fine particle dose (FPD) of particles less than 5.8μm varied almost three-fold, from 34.1% to 91.1% of the emitted dose, depending on the mouth-throat model used. Additionally, Borgström et al. (2006) argued that throat deposition emerged as the primary source of inter-subject variability observed in clinical lung deposition studies. These studies have indicated that the deposition of aerosols in the lungs is significantly influenced by the human upper airway geometries, underscoring the importance of developing appropriate mouth-throat models.

There are three main approaches employed to develop realistic mouth-throat models for inhaled drug aerosols: (a) geometries derived from cadaveric cast data found in existing literature, (b) geometries that replicate individual airways based on Computed Tomography (CT) or Magnetic Resonance Imaging (MRI) data, and (c) idealized geometries that incorporate critical airway dimensions (Byron et al., 2010; Golshahi et al., 2022; Newman & Chan, 2020). CT and MRI have emerged as the primary tools for developing mouth-throat models, as cadaver casts often suffer from distortions caused by post-mortem tissue shrinkage (Byron et al., 2010). Moreover, the advancement in manufacturing techniques, particularly 3D printing, has significantly improved the ability to create realistic upper airway models that accurately replicate anatomical structures for various research purposes (Bücking et al., 2017).

Over the past two decades, three primary designs of anatomical mouth-throat have been developed and are shown in Figure 2.4. The differences between AIT, VCU, and OPC will be discussed as follows. All of these designs are based on the oropharyngeal geometries of healthy human subjects (Newman & Chan, 2020; Wei, 2015).

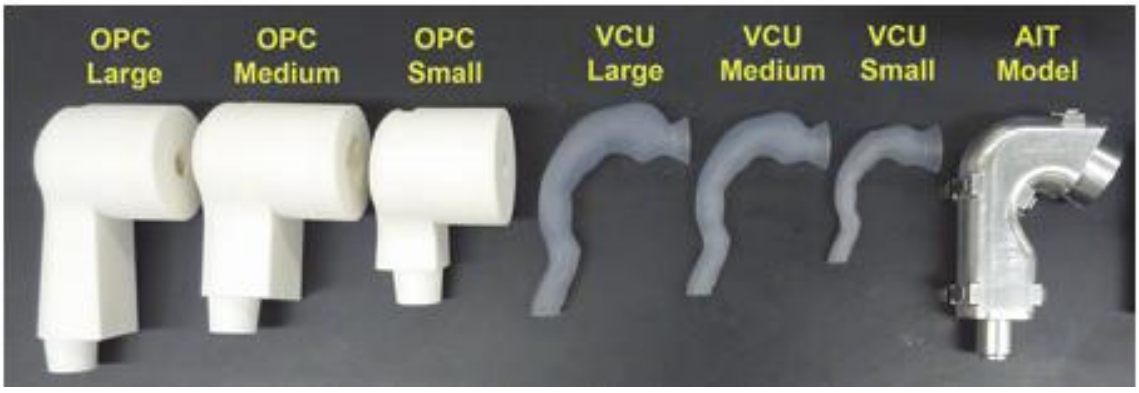

Figure 2. 4: Three main designs of mouth-throat models. Adapted from (Wei, 2015).

AIT

The Alberta Idealized mouth-throat (AIT) was constructed from metal (commercially available from Copley Scientific, Nottingham, UK) and designed by scientists at the University of Alberta in Edmonton, Canada, developed based on dimensions obtained from MRI images, CT images, and airway geometries available in the literature to mimic the anatomical features of a realistic human upper airway (W. Finlay et al., 2010; W. Finlay et al., 2004; Golshahi et al., 2022; Newman & Chan, 2020; Stapleton et al., 2000; Wei, 2015). This model aims to represent the anatomical geometric characteristics of an average adult oropharynx and its fluid dynamic properties concerning aerosol capture (Newman & Chan, 2020; Wei, 2015). To account for the variability in oropharyngeal dimensions among adult subjects, the idealized mouth-throat geometry can be proportionally scaled by 30% to approximate the upper and lower bounds (W. Finlay et al., 2010). Although the AIT can be separated into two halves to potentially ease the differentiation between deposition in the mouth and the pharynx (Newman & Chan, 2020), it has unrealistically smooth interior surfaces (Byron et al., 2013), lacks anatomical features such as the uvula (though it includes the epiglottis) (S. S. Y. Leung et al., 2015; Stapleton et al., 2000), and requires an airtight adapter to correctly position and angle an inhaler into the mouth region of the model (Byron et al., 2013). Additionally, pediatric models are also available; however, the primary focus of this thesis is on adult airways, so models for child and infant airways will not be addressed.

VCU

Pharmaceutical scientists at Virginia Commonwealth University (VCU) developed small, medium, and large Virginia Commonwealth University mouth-throat models (VCU-MTs) with internal volumes of 26.6 cm^3, 61.6 cm^3, and 96.1 cm^3, respectively (Delvadia et al., 2012; P Worth Longest & Hindle, 2012; Wei, 2015). The internal volumes of VCU-MTs align with the 95% confidence intervals (CI) derived from the mean ± 2SD values reported by Burnell et al (Burnell et al., 2007; Wei, 2015). VCU-MTs were developed using CT imaging data of healthy adults from Xi and Longest (2007) and Xi et al. (2008). Additionally, these models also incorporated the first three generations of the lung airways (trachea to upper bronchi) modeled on asymmetrically branching tracheobronchial airway data from Yeh and Schum (1980) and Tian et al. (2011). VCU-MTs are typically fabricated from transparent resin and polyurethane

(Newman & Chan, 2020), with polished gold-plated steel also employed for the medium-sized VCU model in the existing study (Kaviratna et al., 2019b). Additionally, anatomical features such as the uvula and epiglottis have been removed in the VCU-MTs (Delvadia et al., 2012).

OPC

The Oropharyngeal Consortium mouth-throats (OPC-MTs) were established as a collaborative effort by AstraZeneca, GlaxoSmithKline, and Sanofi-Aventis to encompass the full spectrum of dimensions present in diverse human subjects of mixed genders (Burnell et al., 2007). OPC-MTs, fabricated by stereolithography from MRI imaging data, have internal volumes of 27.6 cm^3, 91.7 cm^3, and 84.4 cm^3 for the small, medium, and large sizes, respectively (Wei, 2015). Small, medium, and large OPC-MTs (Emmace Consulting AB, Sodra Sandby, Sweden), made from sintered polyamide, have been acquired for utilization in laboratory research (Wei et al., 2018). The selection of the small, medium, and large OPC models was based on the Consortium's assessment of aerosol deposition, rather than on measurements of the internal geometries of the models themselves (Burnell et al., 2007). Moreover, in comparison to Virginia Commonwealth University mouth-throats (VCU-MTs) and AIT models, OPC-MTs incorporate more detailed anatomical features such as the hard palate, tongue, soft palate, and epiglottis (Burnell et al., 2007).

2.4 Particles

The effectiveness of inhalation therapy largely depends on the properties of the drug particles, including particle size, shape, density, and surface characteristics (Carvalho et al., 2011; Chew & Chan, 2002; W. H. Finlay, 2001; Stuart, 1984). These factors influence the deposition pattem within the respiratory tract. The optimal particle size for inhalation aerosols typically ranges from 1 to 5 μm (Bosquillon et al., 2001; W. H. Finlay, 2001; Parumasivam et al., 2016). Larger drug particles (particle size > 5 μm) are more likely to be deposited in the upper airways and do not reach the deep lung region, while small particles (particle size < 1 μm) tend to remain in suspension and are expelled during exhalation (Patton & Byron, 2007; Thakur et al., 2020; Yu & Taulbee, 1975). However, having the particle size fall within the appropriate range is not everything. An earlier study contended that agglomeration tended to occur due to the Van der

Waals and electrostatic forces (Edwards et al., 1998). Additionally, with respect to the particle shape and particle density, there are two simplifying assumptions that are commonly accepted in the existing literature: (1) The particle is assumed to be spherical; and (2) the particle density is assumed to be much larger than that of the surrounding fluid (W. H. Finlay, 2001; A Kourmatzis et al., 2018).

Aerosols used in pulmonary drug delivery are broadly categorized into solid particles, commonly delivered via dry powder inhalers (DPIs), and liquid droplets, typically administered through sprays and nebulizers. The behavior of these two types of aerosols differs significantly (W. H. Finlay, 2001). This thesis primarily focuses on solid particles. In the following section, a comprehensive review of inhalation particles will be provided, covering the fundamental physics of particle motion in fluid and its correlation to airway dynamics. Additionally, the distribution of particle sizes will also be discussed.

2.4.1 Mechanism of particle motion and deposition

When drug particles travel along the human airway, they are exposed to various external influences, such as turbulence, gravitational forces, and inertial effects, that may cause them to deviate from the streamlines of the inhaled air. These interactions can lead to particle deposition on the surrounding airway surfaces, although many tracer particles closely follow the streamlines under typical conditions (Carvalho et al., 2011). There are five primary mechanisms for the deposition of drug particles in the lungs, primarily based on particle size: inertial impaction, sedimentation, diffusion by Brownian motion, interception, and electrostatic precipitation (Carvalho et al., 2011; Hofmann, 2011; Mortensen et al., 2014; Patton & Byron, 2007). Interception and electrostatic precipitation are generally considered minor factors compared to impaction, sedimentation, and diffusion in particle deposition (Darquenne, 2020). Consequently, they are not addressed in this thesis. The effects of particle shape (e.g., elongated particles) and electrostatic charges, which are associated with these lesser mechanisms, have been thoroughly reviewed in other studies (Gonda, 2004; Zeng et al., 2001). The particle motion and deposition mechanisms of inhaled particles in the lung are illustrated in Figure 2.5:

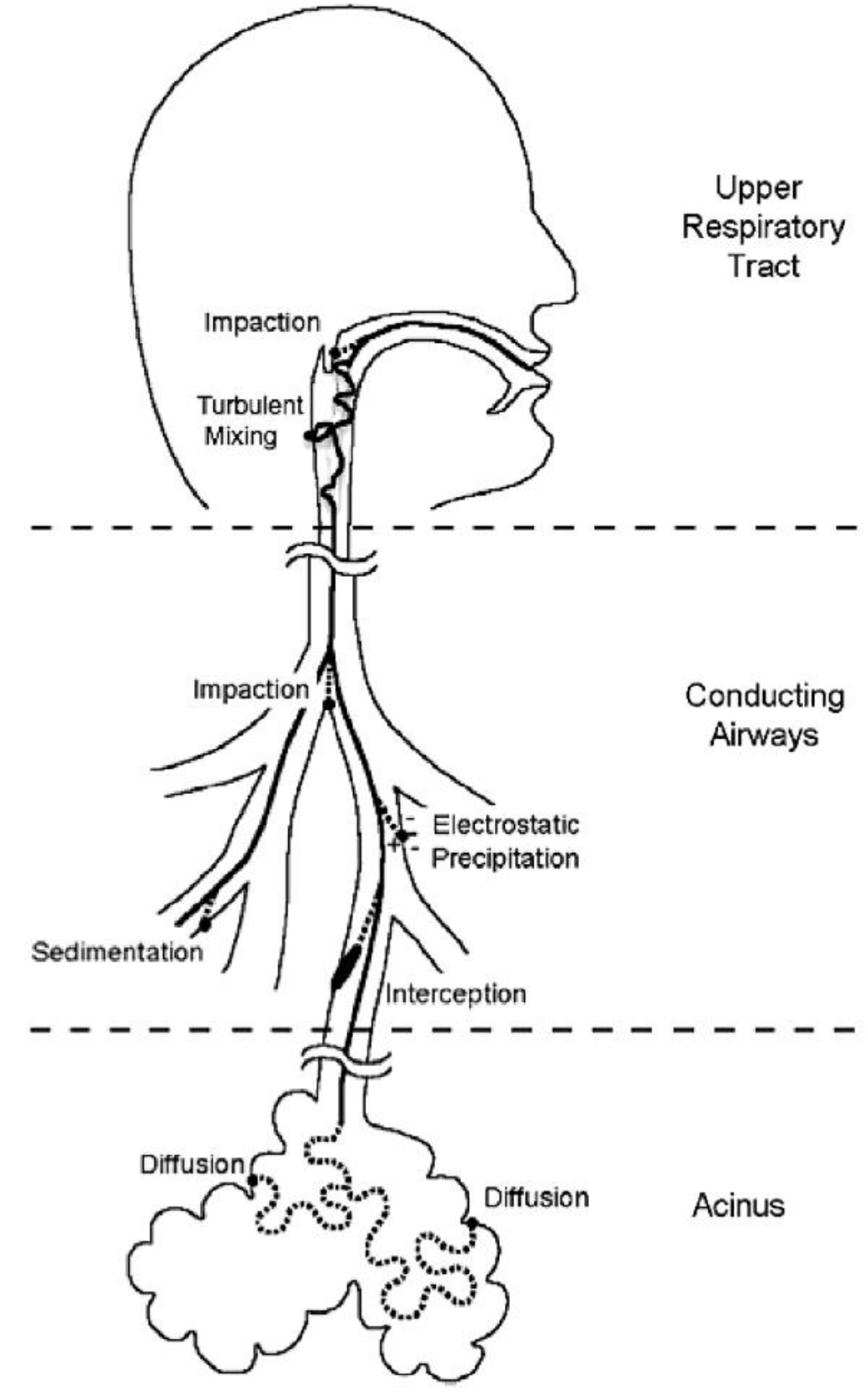

Figure 2.5: The deposition mechanisms of inhaled particles in the lung. Adapted from (Darquenne, 2020)

Inertial impaction

Inertial impaction primarily occurs in the upper and conducting airways, particularly in the mouth-throat region, trachea and bronchial regions where the airways bifurcate and narrow. In these areas of the human respiratory tract, airborne particles have sufficient momentum to maintain their trajectory despite changes in airflow direction, causing them to collide with the walls of the airway. The likelihood of deposition via impact increases when drug particles travel longer distances (S), which depends on their mobility (velocity per unit force) (B), mass (m), and velocity (v), as described by Eq.1 (Hickey, 2003) :

$$S = B \times m \times v \tag{1}$$

The Stokes number (Stk), as described by Eq.2, is a dimensionless parameter that characterizes the behavior of particles suspended in a fluid flow, particularly in relation to their ability to follow the flow streamlines, and it describes the probability of particle deposition in the airways via impaction (Carvalho et al., 2011). A higher Stokes number suggests an increased likelihood of particles being deposited due to inertial impaction.

$$Stk = \frac{\rho_p \times d^2 \times V}{18 \times \mu \times \mathrm{R}} \tag{2}$$

In this equation, ρ_p represents the particle density, d denotes the particle diameter, V signifies the air velocity, μ refers to the air viscosity, and R indicates the airway radius.

In vitro experiments performed by Grgic, Finlay, and Heenan (2004) in an idealized mouth-throat geometry showed that deposition efficiency increased with increasing flow rate, even if the Stokes number was held constant, indicating a dependence on the flow Reynolds number Re (Eq.3). An empirical Reynolds number correction was applied to the Stokes number ($Stk \cdot Re^{0.37}$), leading to better collapse of extrathoracic deposition onto a single curve.

$$R_e = \frac{\rho_a \times V \times d}{\mu} \tag{3}$$

Where ρ_a is the density of air, V is the flow velocity, d is the diameter of the passageway and μ is to the air viscosity. This equation is primarily applicable to regions of the respiratory airway where a representative diameter (d) can be reasonably approximated, such as the mouth-throat or trachea. It is important to note that the diameter of the airway varies significantly

along its length, ranging from a few centimeters in the mouth and trachea to millimeters in the bronchioles. Therefore, this equation is most relevant to larger airway regions where the geometry remains relatively uniform over the length considered. For smaller, highly variable regions, such as the bronchioles, the equation serves as a general framework but may require refinement or local adjustments to account for geometric variability. This distinction ensures the equation is appropriately interpreted within the context of specific airway regions.

Sedimentation

Sedimentation primarily occurs in the smaller airways and alveolar regions of the respiratory tract (Carvalho et al., 2011; Stuart, 1984). This process is time-dependent and is most significant in areas where airflow slows down, such as in the bronchioles and alveoli, allowing particles to settle due to gravity (Carvalho et al., 2011; Hofmann, 2011). Furthermore, slow breathing is most effective for promoting sedimentation because it allows for longer residence times of particles in the airways (Hofmann, 2011; Zeng et al., 2000). Additionally, Stokes' Law operates under the assumption that there is no relative velocity between the particle's surface and the surrounding airstream. For spherical particles with unit density ranging from 1 to 40 µm, this law can be applied to estimate the terminal settling velocity (also referred to as the "sedimentation velocity") V_{ts}, as shown below in Eq.4 (Gonda, 2000):

$$V_{ts} = \frac{(\rho_p - \rho_a) \times d^2 \times g}{18 \times \mu} \quad (4)$$

In which, ρ_p is the density of the particle, ρ_a represents the density of air, d is the particle diameter, g indicates the gravitational acceleration and µ refers to the air viscosity.

However, the assumption of Stokes' Law is not suitable for inhaled small particles. A slip correction factor (C_C), as derived by Cunningham (1910) and given in Eq.5, should be applied to Stokes' Law for particles smaller than 10 µm (Crowder et al., 2002).

$$C_C = 1 + Kn \times \left[A_1 + A_2 \times \exp\left(-\frac{A_3}{\text{kn}}\right)\right] \quad (5)$$

In which, Kn is the Knudsen Number, and A_1, A_2 and A_3 are constants. The values for A_1, A_2 and A_3 are derived from experimental measurements of drag on small particles, and most commonly used values, determined by Davies in 1945 (Davies, 1945), are reported by Reist (Reist, 1993) and Hinds & Zhu (Hinds & Zhu, 2022) as $A_1 = 1.257, A_2 = 0.4$ and $A_3 = 1.1$.

The Knudsen number represents the ratio of the mean free path of gas molecules to the particle size (as shown in Eq. 6). It is influenced by the transfer of heat, mass, and momentum between the particles and the surrounding carrier gas.

$$Kn = \frac{2\lambda}{d} \tag{6}$$

where λ represents the mean free path of the gas molecules, and d indicates the particle diameter. The mean free path of gas molecules can be calculated using Eq.7.

$$\lambda = v\left(\frac{\pi m}{2kT}\right)^{1/2} \tag{7}$$

where v represents the kinematic viscosity of the gas, m is the molecular mass, k refers to Boltzmann's constant, and T is the absolute temperature (Friedlander & Smoke, 2000).

Moreover, the slip correction factor should be incorporated into the calculation of particle settling velocity, as shown in Eq.8 (Crowder et al., 2002).

$$V_{ts} = \frac{\rho_p \times d^2 \times g \times C_C}{18 \times \mu} \tag{8}$$

Numerous studies have explored the impact of sedimentation on particle deposition within the human airways. A study noted that in a realistic human upper airway model, the deposition of particles due to inertial impaction and sedimentation exhibited non-linear behavior in relation to particle diameters (Martonen et al., 2002). Sedimentation became increasingly dominant over inertial impaction under slow breathing conditions (i.e. Q ≤ 7.5 L/min) (Kleinstreuer et al., 2007). A recent study (Ou et al., 2020) found that gravitational sedimentation is primarily influenced by the Stokes number (St) and the ratio of St to Re^2. Moreover, the alteration of gravity also has an impact on the sedimentation of particles in the human lungs (Darquenne, 2014; Darquenne et al., 2000).

Brownian diffusion

For particles of extremely small size (<1 μm), collisions with randomly moving air molecules cause a nondeterministic random walk known as Brownian motion, allowing these particles to diffuse easily due to molecular interactions within the gas (Carvalho et al., 2011; W. H. Finlay, 2001). The diffusion rate is proportional to the Brownian diffusion coefficient, which is related

to particle size and can be described by the Stokes–Einstein equation, as shown in Eq.9 (Gonda, 2000).

$$D_B = \frac{C_C \mathrm{kT}}{3\pi\mu\mathrm{d}} \tag{9}$$

Where D_B is the diffusion coefficient, C_C is the Cunningham correction factor, k is Boltzmann's constant, T represents the absolute temperature, μ is to the air viscosity and d indicates the particle diameter. Unlike impaction and sedimentation mechanisms, diffusional deposition is inversely related to particle size and particularly becoming the primary deposition mechanism for particles smaller than 0.5 μm in diameter (Carvalho et al., 2011; Darquenne, 2020).

2.4.2 Particle size distribution

Most inhaled pharmaceutical aerosols are 'polydisperse,' containing particles of varying sizes, whereas 'monodisperse' aerosols-composed of uniform-sized particles-are typically impractical for pharmaceutical use (W. H. Finlay, 2001) but are commonly employed in CFD studies (W. Longest & Farkas, 2019; Rygg & Longest, 2016; Tian et al., 2015). Understanding the particle size distribution within an aerosol is crucial, as it significantly influences the deposited drug dose and the spatial distribution of aerosols within the lungs (W. H. Finlay & Darquenne, 2020). Additionally, while aerosol particle size distributions are inherently discrete, continuous functions, such as count distributions, mass distributions, and commonly used models like the Rosin-Rammler distribution, serve as valuable conceptual tools for describing these distributions (W. H. Finlay, 2001; W. H. Finlay & Darquenne, 2020).

Count distribution

The size distribution of an aerosol can be described by its frequency distribution $f(d_p)$, such that the fraction of particles with diameters between d_p and $d_p + \Delta d_p$ is $f(d_p)\Delta d_p$, Δd_p is also represented as the area under the frequency distribution curve $f(d_p)$ within the infinitesimal range. The count distribution $n(d_p)$ is related to the frequency distribution $f(d_p)$ and shown below in Eq.10 (W. H. Finlay, 2001; W. H. Finlay & Darquenne, 2020).

$$n(d_p) = N_p f(d_p) \tag{10}$$

In which, N_p represents the total number of particles in the aerosol.

Mass distribution

Count and frequency distributions provide the number of particles within specific size ranges, but for aerosolized drugs, measuring particle count is often impractical (W. H. Finlay & Darquenne, 2020). Instead, mass is typically used to quantify inhalation drug aerosols. When considering mass, it is standard practice to refer to the cumulative mass distribution $M(d_p)$, which represents the total mass of particles with diameters less than a specified value, obtained by calculating the area under the mass distribution curve from zero to the given diameter d_p (W. H. Finlay & Darquenne, 2020). The relationship between the mass and cumulative mass distributions is provided in Eq.11.

$$M(d_p) = \int_0^{d_p} m(x)\, dx \tag{11}$$

In which, $m(x)\ dx$ represents the mass of particles with diameters between x and $x + dx$. In mass distributions, the mass median diameter (MMD) is a widely utilized metric, representing the diameter at which half of the total aerosol mass is contained. When considering aerodynamic diameters, the mass median aerodynamic diameter (MMAD) is calculated and serves as a widely used metric for inhaled aerosols (W. H. Finlay & Darquenne, 2020; Wiggins, 1991).

Beyond cumulative mass distributions, the log-normal distribution, as described by Eq.12, is another commonly encountered size distribution in aerosol science (W. H. Finlay, 2001).

$$m(d_p) = \frac{1}{d_p\sqrt{2\pi}} \exp\left[\frac{-(lnd_p - lnMMAD)^2}{2(lnGSD)^2}\right] \tag{12}$$

In which, d_p is the particle diameters, MMAD (or MMD) is the mass median diameter and GSD is the geometric standard deviation.

The MMAD is calculated by first identifying the aerodynamic diameter at 50% of the mass or by locating the 50% point on the cumulative distribution curve. To obtain the GSD and evaluate the variability of the distribution, the aerodynamic diameter at 15.9% of the mass and 84.1% of the mass volume was also determined. The GSD was calculated using Eq.13, with $D_{84.1}$ and $D_{15.9}$ representing the diameters at which 84.1% and 15.9% of the mass volume are composed of smaller particles (USP, 2023; Wiggins, 1991).

$$GSD = \sqrt{\frac{D_{84.1}}{D_{15.9}}} \quad (13)$$

Given the MMAD (or MMD) and GSD of an aerosol, along with the number N of aerosol particles per unit volume and the particle density ρ_p, the mass M of particulates per unit volume of air can be determined by Eq.14 (W. H. Finlay & Darquenne, 2020).

$$M = \frac{\rho_p N\pi}{6}(MMAD)^3 \exp\left[\frac{-9(lnGSD)^2}{2}\right] \quad (14)$$

Aerosol size distributions are not always well-represented by a lognormal model, leading to the development of alternative continuous functions to characterize these distributions (Hinds & Zhu, 2022). An alternative distribution is the Rosin-Rammler distribution (see Eq.15), originally described by Rosin and Rammler in 1933 (Rosin, 1933), which characterizes aerosol size distributions based on cumulative mass data.

$$M_{normalized}(d_p) = 1 - \exp\left[\left(\frac{-d_p}{\delta}\right)^n\right] \quad (15)$$

where δ and n are specified constants (Michaelides et al., 2016).

2.5 CFD

Pulmonary drug delivery is a multidisciplinary field that encompasses the study of fluid dynamics and airway geometries. Computational Fluid Dynamics (CFD) has been utilized in research related to airway studies. This section will focus on the application of CFD in human upper airway research, starting with the mathematical aspects of the CFD model.

2.5.1 CFD basics

The advancement in computational power has significantly accelerated the application of computational fluid dynamics (CFD) models in the design of pharmaceutical inhalers (Conor A Ruzycki et al., 2013) and in predicting the behavior of aerosols within the respiratory tract (Fen Huang et al., 2021; Jahed et al., 2024; Y. Kim et al., 2019). By leveraging the Navier-Stokes equations, CFD models provide a robust framework for quantifying gas flow and aerosol dynamics within the respiratory tract, including comprehensive assessments of both total and regional aerosol deposition patterns in the human upper airways (P Worth Longest &

Holbrook, 2012). The Navier-Stokes equations are typically expressed as follows (Constantin & Foiaş, 1988):

Continuity equation (Conservation of mass):

$$\nabla \cdot u = 0 \tag{16}$$

Momentum equation (Conservation of Momentum):

$$\rho\left(\frac{\partial u}{\partial t} + u \cdot \nabla u\right) = -\nabla p + \rho g + \mu \nabla^2 u \tag{17}$$

Where u denotes the fluid velocity vector with components u_x, u_y, u_z, ρ is the fluid density, p is the pressure field, μ is the dynamic viscosity of the fluid, and ρg represents the gravitational force acting on the fluid.

In addition, CFD offers a variety of turbulence models suited to different flow conditions, including commonly used models such as k-epsilon (k-ε), k-omega (k-ω), Reynolds Stress models, and Large Eddy Simulation (LES) (W. Faizal et al., 2020). The choice of model depends on the specific application and the flow characteristics being studied. The RANS equations, as detailed in Eq.18 and Eq.19, are derived from the Navier-Stokes equations by decomposing the instantaneous velocity and pressure fields into mean and fluctuating components (Alfonsi, 2009).

Continuity equation (for incompressible flow):

$$\nabla \cdot \bar{u} = 0 \tag{18}$$

Momentum equation:

$$\rho\left(\frac{\partial \bar{u}}{\partial t} + \bar{u} \cdot \nabla \bar{u}\right) = -\nabla \bar{p} + \rho g + \mu \nabla^2 \bar{u} - \nabla \cdot \overline{u'u'} \tag{19}$$

Where $\bar{u}$ is the time-averaged velocity vector, $\bar{p}$ is the time-averaged pressure field, u' is the fluctuating component of the velocity and $\overline{u'u'}$ is the Reynolds stress tensor, capturing the effects of turbulence.

2.5.2 Different turbulence models in human upper airway

RANS models, the most widely used turbulence models in pulmonary drug delivery, are favored for their robustness and significantly lower computational costs compared to DNS or LES, as they simplify the analysis by decomposing the instantaneous turbulent velocity into

mean flow velocity and time-dependent fluctuations, solving only the Reynolds-averaged Navier-Stokes equations (both mass and momentum) to predict the mean flow properties (Fen Huang et al., 2021; Mihaescu et al., 2008).

Standard k-ε and k-ω models

The standard k-ε and k-ω models, both commonly used RANS approaches, link Reynolds stress to turbulent kinetic energy (k) and its dissipation rate (ε) or specific dissipation rate (ω), and are classified as two-transport-equation models (Fen Huang et al., 2021).

The standard k-ε model, which serves as the default in k-ε turbulence modelling, is efficient and performs well in simulating flows with small pressure gradients, such as in free-stream regions, it has been found to perform poorly in predicting flows in the extrathoracic (ET) region, where recirculating zones, free-shear layers, and mean streamline curvature are present (P. Koullapis et al., 2018; Stapleton et al., 2000). The k-ε model is optimally suited for flow regions distant from walls, such as free surface flows, but it is not well-suited for low Reynolds number turbulent flows in the near-wall (NW) region. To enhance the simulation accuracy in the NW region, Matida et al. (2006) introduced a anisotropic turbulence correction, while P Worth Longest and Xi (2007) stressed precise velocity interpolation. However, the standard k-ω model, outperforming the standard k-ε in NW and ET regions, closely aligns with in vivo data but is sensitive to inlet condition variations (Ball et al., 2008; P. Koullapis et al., 2018). Mylavarapu et al. (2009) investigated the CFD models used for human airway simulation and found that the standard k-ω turbulence model more accurately predicts experimental wall static pressures in patient-specific airway geometries, with an average error of approximately 20% across all measurement ports.

LRN k-ε and k-ω models

Low-Reynolds Number (LRN) models were developed to simulate turbulent flows in the NW region, providing superior predictions of near-wall flow dynamics, including pressure drop, velocity distributions, shear stress, and the transition from laminar to turbulent flow (Huang et al., 2022). CFD simulations utilizing LRN models were able to predict particle deposition in transitional and turbulent flows within the extrathoracic (ET) region and across airway bifurcations (Y. Chen et al., 2023; Launder & Sharma, 1974).

Numerous studies have employed LRN models to investigate drug particle behavior within the human airway. Luo and Liu (2008) employed a Low Reynolds Number (LRN) k-ω turbulence model to simulate inspiratory flow in a CT-scan-based respiratory model, revealing that airflow preferentially diverts toward the left main bronchus and extends further downstream with the increase of Reynolds numbers. Forman et al. (2007) investigated aerosol deposition in a CT-scan-based respiratory tract model using the LRN k-ε turbulence model, concluding that higher Reynolds numbers enhance aerosol deposition due to the generation of turbulence. Additionally, a few study have observed that LRN k-ε model demonstrated better agreement with experimental data compared to the LRN k-ω model (Y. Chen et al., 2023; Ghahramani et al., 2014). However, this finding has been contested by several other studies (P. Koullapis et al., 2018; Zhe Zhang & Kleinstreuer, 2003). P. Koullapis et al. (2018) contended that the LRN k-ω model was effective in predicting both flow fields and deposition in the human airway, particularly for particles larger than 5 μm in size, although it tended to overpredict the deposition of smaller particles.

Shear-stress transport turbulence models

Shear-stress transport (SST) turbulence models integrate the strengths of both k-ε and k-ω models, applying the k-ω approach near the wall regions and the k-ε model in the mainstream flow (Huang et al., 2022). This hybrid approach allows the k-ω SST model to function effectively as a Low-Reynolds Number turbulence model without the need for additional damping functions. Kolanjiyil and Kleinstreuer (2016) utilized the k-ω SST model to simulate airflow throughout the entire lung, while Jayaraju et al. (2007) investigated flow dynamics and particle deposition in a realistic mouth-throat (MT) model using the LRN SST model, with their findings showing strong correlation with both simulation results and experimental data (Martonen et al., 2002). Ciciliani et al. (2017) also employed the k-ω SST model to analyze flow behavior in the tracheobronchial (TB) region.

2.5.3 DPM

To investigate aerosol behavior in the human airway using CFD, the Discrete Phase Model (DPM), within the Eulerian-Lagrangian framework, is commonly employed, where all particles are treated as Lagrangian point particles, and the forces acting on them are analyzed in Cartesian coordinates, as described by the following equations (X. Chen et al., 2012; F. Huang et al., 2021):

$$\frac{d(u_p)}{dt} = F_D(u - u_p) + \frac{g(\rho_p - \rho)}{\rho_p} \tag{20}$$

$$F_D = \frac{18\mu}{\rho_p d_a^2}\frac{C_D Re}{24} \tag{21}$$

$$Re = \frac{\rho_p d_p |u_p - u|}{\mu} \tag{22}$$

$$C_D = a_1 + \frac{a_2}{Re} + \frac{a_3}{Re^2} \tag{23}$$

Where u is the velocity, μ is the dynamic viscosity, and ρ is the density, u_p, ρ_p, d_a are the velocity, density and diameter of particles, Re is the Reynolds number, C_D is the drag coefficient, and g is the acceleration of gravity.

The majority of studies employing CFD-DPM models for aerosol transport in the respiratory tract operate under the assumption that the aerosol phase is sufficiently sparse, thereby exerting minimal impact on the airflow, and that interactions between particles are negligible (Dehbi, 2008; Dong et al., 2021; Dong et al., 2019). This approach is referred to as one-way coupling (Dehbi, 2008). Since impaction and sedimentation are the main mechanisms of micron-sized particle deposition in the extrathoracic (ET) region, pressure gradient, added mass, and Basset forces are often omitted from the CFD-DPM models (Fen Huang et al., 2021; Jõgi et al., 2021; Li, 2012). Most research focuses on fluid drag force and/or gravitational force (X. Chen et al., 2012; Guha, 2008; Fen Huang et al., 2021). Baoshun Ma and Lutchen (2009) found that omitting gravity led to a reduction of up to 10% in total aerosol deposition. CFD-DPM models have been extensively utilized to investigate the deposition of drug particles in the human airway. A study (X. Chen et al., 2012) employing a CFD-DPM approach revealed that, under transient flow conditions, obstructions in the pulmonary airways not only decrease airflow rates at the blockage and in downstream generations but also result in a more widespread and

dispersed deposition area compared to steady inlet conditions. Rahman et al. (2021) utilized a CFD-DPM approach to investigate how aging influences airflow patterns and micron-particle behavior in the human lung, finding that as age increases, more particles tend to accumulate in the upper airway, while fewer particles reach the deeper regions of the lungs. Additionally, CFD-DPM is also utilized in simulating nasal cavity dynamics. A study (Shang & Inthavong, 2019) used a CFD-DPM model to study how micron-sized particles deposit in the human nasal cavity, finding that larger particles, due to their higher inertia, mainly accumulate in the main nasal passage.

2.6 Experimental methods

Obtaining quantitative data on extrathoracic deposition is essential because it directly affects the amount of inhaled particles that reach the thoracic region of the respiratory tract. Real-time analysis of particle transport in the human airway is often challenging due to significant deposition of unwanted drug particles in the upper airway (W. H. Finlay, 2001; Grgic, Finlay, Burnell, et al., 2004; Pham et al., 2021) and inherent limitations of current imaging technologies (A Kourmatzis et al., 2018). Standard nuclear imaging techniques, such as two-dimensional (2D) gamma scintigraphy, X-ray computed tomography (CT), Positron Emission Tomography (PET), Single Photon Emission Computed Tomography (SPECT), and Magnetic Resonance Imaging (MRI), play a crucial role in assessing pulmonary drug delivery by providing measurements of anatomical features. However, these methods have limitations; they can only assess drug deposition using radiolabeled drug particles, offering relatively low resolution and typically only capturing data after deposition has occurred (Conway, 2012; Milne & King, 2014; Venegas et al., 2013). It is challenging to accurately capture details like extrathoracic airflow mechanics or particle trajectories during inhalation because of the limitations in both temporal and spatial resolution. (A Kourmatzis et al., 2018). Numerous in-vivo and in-vitro correlation (IVIVC) studies have been conducted in the area of pulmonary drug delivery to investigate the flow dynamics of drug particles within the human upper airway (Keith T. Ung et al., 2016; Xi & Longest, 2007). In this section, experimental methods for IVIVC studies are discussed.

2.6.1 Cascade impactors

Cascade impactors, such as the Andersen Cascade Impactor (ACI) and the Next Generation Impactor (NGI), are frequently utilized for in-vitro testing of inhaled drugs, particularly for determining the aerodynamic particle size distribution (APSD) under specific flow rates and inhalation conditions (Mohan et al., 2017). Measuring aerodynamic particle size distribution (APSD) is crucial for the development, evaluation, and quality control of dry powder inhalers (DPIs) (Yoshida et al., 2017). Particles with aerodynamic diameters smaller than 5 microns are classified as fine particles, capable of reaching the lower airways, and are linked to the treatment of respiratory conditions (Newman, 2022). Fine particle fraction (FPF) data derived from cascade impactors are frequently utilized to determine if a specific inhaler can effectively deliver its formulation to the lungs (Colthorpe et al., 2013). To obtain essential data, cascade impactors need to be used alongside mouth-throat (MT) models, such as the commonly used United States Pharmacopeia (USP) induction port model (USP, 2023), the Virginia Commonwealth University (VCU) (Delvadia et al., 2012) model, Alberta Idealized Throat (AIT) (Stapleton et al., 2000), and the Oropharyngeal Consortium (OPC) model (Burnell et al., 2007).

A standard experimental setup of the NGI with USP induction port is shown in Figure 2.6.

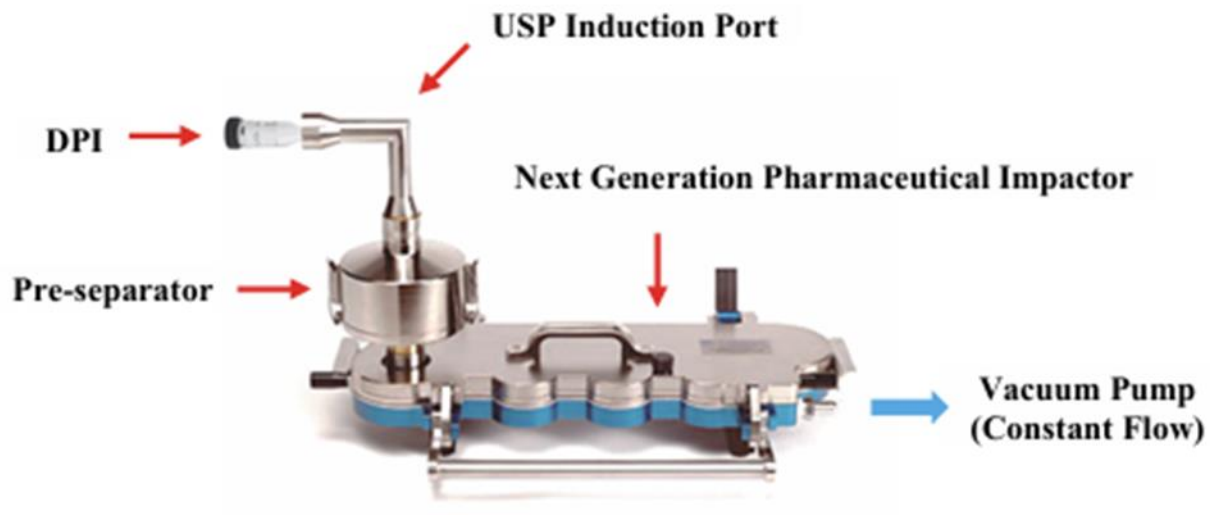

Figure 2. 6: A standard experimental setup of the NGI with USP induction port. Adapted from (Wei, 2015)

As depicted in Figure 2.6, pharmacopeial methods are used to measure aerodynamic particle size distributions (APSDs) for dry powder inhalers (DPIs) under steady airflow and volume

conditions. In these setups, aerosol from the inhaler passes through a 90° bent induction port into a calibrated Next Generation Pharmaceutical Impactor (NGI), with a pre-separator removing larger particles, and a vacuum pump on the NGI's left side ensuring a consistent flow (Wei, 2015).

The NGI, a sophisticated tool commonly used in pulmonary drug delivery (Abdelrahim & Chrystyn, 2009; Okuda et al., 2017), employs inertial impaction to separate aerosol particles by aerodynamic diameter, accurately assessing how effectively drugs are delivered to the lungs (Kamiya et al., 2004; Marple et al., 2003; Roberts & Mitchell, 2016a). The distribution of particles across the multiple stages of the NGI provides a profile that reflects the aerodynamic particle size distribution (APSD) of the product, which is a key quality indicator for inhaled medications (Mohan et al., 2017). Each stage of the NGI targets a specific size range, simulating deposition in different parts of the respiratory tract, by capturing particles based on their aerodynamic cut-off diameter, allowing for detailed analysis of particle distribution and lung deposition (J. Mitchell, 2019; Yoshida et al., 2017). The early stages of the impactor trap larger particles intended to settle in the upper respiratory tract, while the subsequent stages capture smaller particles capable of reaching deeper lung regions (Marple et al., 2003; Mohan et al., 2017). The last stage, known as the micro-orifice collector (MOC), gathers the smallest particles that make it to the alveolar area (J. P. Mitchell & Nagel, 2003). A top view of the NGI seal body for each stage is depicted in Figure 2.7.

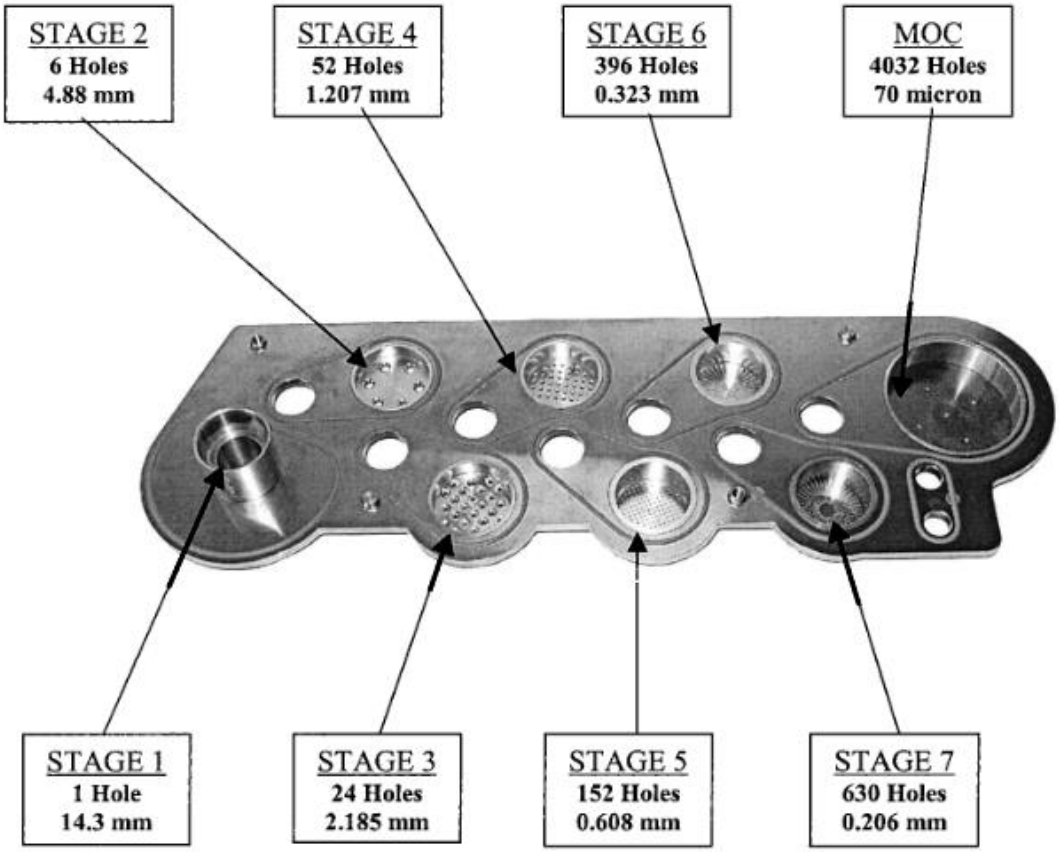

Figure 2. 7: A top view of the NGI seal body.Adapted from (Marple, Roberts, et al., 2003).

Furthermore, in order to determine the diameter of each stage, it is essential to take into account the cut-off diameter. The initial calculation of the cut-off diameter was first mentioned by Marple, Roberts, et al. (2003). The calculated values of the cut-off diameter for the pre-separator and stages 1 to 7 (and D80 for the MOC) at flow rates of 30, 60, and 100 LPM are presented in Table 2.1.

Table 2. 1: The calculated values of the cut-off diameter, D50 (µm), for the pre-separator and stages 1 to 7 (and D80 (µm), for MOC) at flow rates of 30, 60, and 100 LPM (Marple et al., 2003).

Pre-separator and NGI stages	Flow rates		
	30 LPM	60 LPM	100 LPM
Pre-separator	14.9	12.8	10.0
Stage 1	11.7	8.06	6.12
Stage 2	6.40	4.46	3.42
Stage 3	3.99	2.82	2.18
Stage 4	2.30	1.66	1.31
Stage 5	1.36	0.94	0.72
Stage 6	083	0.55	0.40
Stage 6	0.54	0.34	0.24
MOC (D_{80})	0.36	0.14	0.07

The relevant equations for the calculation of the cut-off diameter are presented below:

Pre-separator:

$$D_{50} = 12.8 - 0.07(Q - 60) \quad (24)$$

Stages 1-7:

$$D_{50} = A(\frac{60}{Q})^{B} \quad (25)$$

MOC:

$$D_{80} = 0.14(\frac{60}{Q})^{1.36} \quad (26)$$

The stage cut-off diamater coefficients (A and B) are provided in table 2.2.

Table 2. 2: Coefficients (A and B) for stage cut-off diameter (Marple et al., 2003).

Stages	A	B
Stage 1	8.06	0.54
Stage 2	4.46	0.52

Stage 3	2.82	0.50
Stage 4	1.66	0.47
Stage 5	0.94	0.53
Stage 6	0.55	0.60
Stage 7	0.34	0.67

Later, J. Mitchell and Nagel (2004) and Taki et al. (2010) introduced a new equation to adjust for the cut-off diameter of a multi-stage impactor across different flow rates.

NGI is commonly used as a device for testing inhalation aerosols. K. Leung et al. (2005) utilized the NGI to measure the particle size distribution of live measles vaccine from the IPI nebulizer by analyzing its ability to size wet aerosols. Wong et al (Wong et al., 2022) conducted a study using the Next Generation Impactor (NGI) alongside two respiratory epithelial cell lines to examine the aerodynamic performance of dry powder inhalers and to track the fate of aerosolized drugs after they were deposited in the lungs. Furthermore, when combined with airway models and HPLC, the NGI can be utilized to assess drug deposition in the upper airway (Shaokoon Cheng et al., 2019). In addition, NGI is not without its flaws. Many studies found that NGI plates can cause particle bounce during inhalation dry powder testing, resulting in imprecise APSD measurements and stage overloading (Grasmeijer et al., 2012; Khalili et al., 2018; Roberts & Mitchell, 2016a, 2016b).

2.6.2 High-performance liquid chromatography (HPLC)

To determine the mass of aerosol drug in each stage of NGI, HPLC is typically utilized (Omer et al., 2019; Yoshida et al., 2017). In HPLC, the detector converts a chemical or physical characteristic into a measurable signal that indicates the concentration or identity of a compound (Scott, 1996; Snyder et al., 2011). HPLC can detect physical or chemical properties through four main methods: bulk property measurement, analyte-specific detection, modifying the mobile phase, and using hyphenated techniques (Snyder et al., 2011).

The refractive index (RI) detector, commonly used for bulk property detection, responds to all analytes and depends on the column's selectivity for separation, but it has limited sensitivity (Swartz, 2010). RI detectors work by measuring the change in optical refractive index between the mobile phase and the sample, making them suitable for analyzing compounds like sugars, triglycerides, and organic acids, which do not need chromophores (Mozdzanowski & Burman, 2004; Swartz, 2010). The most widely used RI detector, the deflection refractometer, directs light through two wedge-shaped cells, with one containing static mobile phase and the other receiving column effluent; differences in light refraction between these cells are detected by photodiodes and converted to an output voltage (Swartz, 2010).

Another commonly used detector is the Ultraviolet (UV) detector, which targets specific analytes by responding to those that absorb UV light at certain wavelengths. While UV detectors are generally selective for compounds with chromophores, they become more universal at wavelengths under 210 nm, where almost all organic compounds show absorption (Snyder et al., 2011; Swartz, 2010). UV detectors measure absorbance within the UV and visible spectrum (190–600 nm), determining sample concentration based on the amount of light passing through the detector cell, as described by Beer's Law in Eq.27:

$$A = \log\left(\frac{I_0}{I}\right) = \in bc \qquad (27)$$

Where A represents absorbance, I_0 is the initial light intensity, I represents the intensity of the transmitted light, ϵ denotes the molar extinction coefficient, b is the path length of the cell in cm, and c indicates the molar concentration of the sample.

HPLC works by pumping a liquid solvent through a column filled with a stationary phase to separate, detect, and quantify components in a sample based on their interactions with the stationary and mobile phases (Snyder et al., 2011). To interpret an HPLC signal from the detector, analyze the chromatogram peaks for retention time and peak area, which indicate the identity and concentration of compounds, respectively (Gong et al., 2004; Swartz, 2010). An example of a sugar signal detected by an RI detector is illustrated in Figure 2.8.

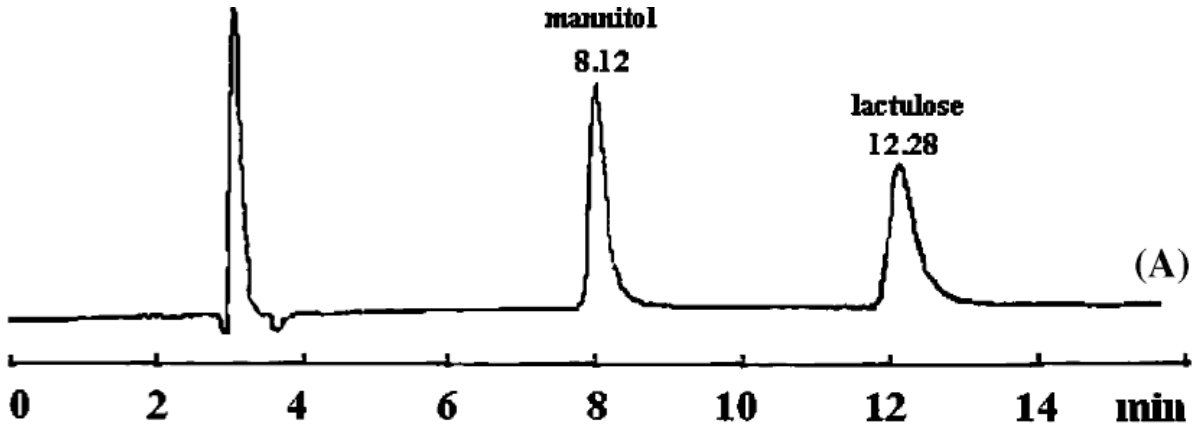

Figure 2. 8: HPLC signal with RID of dual sugars. Adapted from (Liu et al., 2004)

To analyze the drug deposition in each plate of the NGI, HPLC is used to identify and quantify the collected particles by dissolving the drug particles from each stage in a suitable solvent, injecting the solution into the HPLC system, and then separating and detecting the components based on their retention times and peak areas (Shaokoon Cheng et al., 2019; Gondhale et al., 2022). A combination of NGI and HPLC can be utilized for the assessment of inhalation aerosol performance (Keith T Ung et al., 2014). Chan et al. (2011) used NGI and HPLC to investigate mannitol delivery via vibrating mesh nebulization, finding that adding sodium chloride significantly enhanced nebulizer efficiency and reduced droplet size, overcoming the limitations of nebulizing mannitol alone.

2.6.3 Laser techniques

Laser diffraction

Laser diffraction is extensively used in various industries as a non-invasive technique for real-time analysis of sprays and aerosols (A Kourmatzis et al., 2018). A laser diffraction analyzer detects how a collimated light beam is scattered by particles in a sample, with larger particles scattering light at narrower angles and smaller particles at broader angles, enabling the determination of particle size distribution through Mie theory (for small particles) or Fraunhofer diffraction theory (for large particles) (Loizeau et al., 1994; Wriedt, 2012). The connection between particle size and scattering pattern can be explained using Fraunhofer diffraction theory.

A simplified expression of this relationship is:

$$d = \frac{sin(\theta)}{\lambda} \tag{28}$$

Where d is the particle diameter, λ is the wavelength of light, and $sin(\theta)$ is the scattering angle.

A notable device using laser diffraction technology is the Spraytec by Malvern. A previous study (A. R. Clark, 1995) examined this technique for assessing droplet size distributions in medical nebulizers, demonstrating its reliability and robustness. The findings showed a strong correlation with radiolabel deposition profiles and predictions from empirical deposition models, highlighting its significance in clinical applications. Additionally, research by Thomas et al. (2021), identified a relationship between the volume median diameter (VMD) and the percentage of peripheral airway deposition relative to total lung deposition in 12 patients with acquired immunodeficiency syndrome, who inhaled aerosolized pentamidine through eight different nebulizers.

Particle Image Velocimetry (PIV)

The section on Particle Image Velocimetry (PIV) is a laser-based technique widely used in aerosol and flow studies. Although not directly applied in this study, its relevance provides important context for understanding alternative experimental approaches.

Particle Image Velocimetry (PIV) is a sophisticated optical method that tracks tracer particle movement over time to measure particle velocities, allowing for visualization and analysis of fluid flow dynamics (Hain & Kähler, 2007). The basic formula for finding the velocity v in PIV is (Hain & Kähler, 2007; Scarano, 2012):

$$v = \frac{\Delta x}{\Delta t} \tag{29}$$

PIV has been widely utilized for the validation of CFD results (Bingjie Ma et al., 2020; Xu et al., 2020). Xu et al. (2020) validated CFD predictions by measuring flow characteristics in the trachea of a realistic human upper airway model using PIV under three steady inhalation and exhalation conditions, finding good agreement between the CFD and PIV results. Additionally, Shinneeb and Pollard (2012a) and Shinneeb and Pollard (2012b) used PIV and proper orthogonal decomposition (POD) to study simplified airway geometries, discovering that significant turbulence in the epiglottal region and streamwise flow bursts are key sources of Reynolds shear stress.

2.7 Summary

This chapter provided a review of key topics relevant to pulmonary drug delivery, focusing on the interplay between airway anatomy, particle dynamics, computational modeling, and experimental techniques. It began with an overview of airway fundamentals, detailing the anatomy of the human respiratory system and the complexity of airway geometries that influence airflow and drug deposition. The discussion then explored the oral cavity and pharynx, emphasizing the role of structures such as the teeth, soft palate, and epiglottis in modifying airflow patterns and affecting particle transport within the upper airway.

To better understand pulmonary drug delivery mechanisms, realistic mouth-throat models were introduced, highlighting their role in experimental studies designed to replicate physiological airway conditions. The dynamics of particle motion and deposition were also examined, with particular focus on key mechanisms such as inertial impaction, gravitational sedimentation, and diffusion, which determine how inhaled aerosols interact with airway surfaces.

The chapter further reviewed the application of Computational Fluid Dynamics (CFD) in pulmonary research, discussing various turbulence models used to simulate airflow and particle transport in the respiratory tract. The strengths and limitations of CFD in capturing complex

flow phenomena were evaluated, along with its role in predicting drug deposition patterns. Additionally, experimental methods such as the Next Generation Impactor (NGI), High-Performance Liquid Chromatography (HPLC), and laser-based techniques were described, emphasizing their importance in validating CFD models and characterizing aerosol properties in drug delivery studies.

By synthesizing these key topics, this chapter established a foundation for understanding the mechanisms governing pulmonary drug delivery. It underscored the critical role of airway geometry, particle behavior, and advanced modeling techniques in optimizing inhaler performance and improving therapeutic outcomes.

The next chapter will be the first study and will focus on the interaction between anatomical features and the flow and deposition of drug particles in order to gain a comprehensive understanding of the effects of anatomical feature changes on the human upper airway.

2.8 References for Chapter 2

1. Abdelrahim, M. E., & Chrystyn, H. (2009). Aerodynamic characteristics of nebulized terbutaline sulphate using the next generation impactor (NGI) and CEN method. *Journal of aerosol medicine and pulmonary drug delivery*, *22*(1), 19-28.
2. Ahookhosh, K., Pourmehran, O., Aminfar, H., Mohammadpourfard, M., Sarafraz, M. M., & Hamishehkar, H. (2020). Development of human respiratory airway models: A review. *European Journal of Pharmaceutical Sciences*, *145*, 105233.
3. Alfonsi, G. (2009). Reynolds-averaged Navier–Stokes equations for turbulence modeling.
4. Anderson, P. J. (2005). History of aerosol therapy: liquid nebulization to MDIs to DPIs. *Respiratory care*, *50*(9), 1139-1150.
5. Ardran, G., & Kemp, F. (1967). The Mechanism of the Larynx—II The epiglottis and closure of the larynx. *The British Journal of Radiology*, *40*(473), 372-389.
6. Back, G., Nadig, S., Uppal, S., & Coatesworth, A. (2004). Why do we have a uvula?: literature review and a new theory. *Clinical Otolaryngology & Allied Sciences*, *29*(6), 689-693.
7. Balásházy, I., Hofmann, W., Farkas, Á., & Madas, B. G. (2008). Three-dimensional model for aerosol transport and deposition in expanding and contracting alveoli. *Inhalation toxicology*, *20*(6), 611-621.
8. Ball, C., Uddin, M., & Pollard, A. (2008). High resolution turbulence modelling of airflow in an idealised human extra-thoracic airway. *Computers & Fluids*, *37*(8), 943-964.
9. BASKAR, S., VISHNUPRIYA, V., & GAYATHRI, R. (2021). Upper airway sleep disorders and dental treatment. *The journal of contemporary issues in business and government*, *27*(2), 2300-2308.
10. Bates, A. J., Higano, N. S., Hysinger, E. B., Fleck, R. J., Hahn, A. D., Fain, S. B., . . . Woods, J. C. (2019). Quantitative assessment of regional dynamic airway collapse in

neonates via retrospectively respiratory-gated 1H ultrashort echo time MRI. *Journal of Magnetic Resonance Imaging, 49*(3), 659-667.
11. Bates, A. J., Schuh, A., McConnell, K., Williams, B. M., Lanier, J. M., Willmering, M. M., . . . Amin, R. S. (2018). A novel method to generate dynamic boundary conditions for airway CFD by mapping upper airway movement with non-rigid registration of dynamic and static MRI. *International Journal for Numerical Methods in Biomedical Engineering, 34*(12), e3144.
12. Borgström, L., Olsson, B., & Thorsson, L. (2006). Degree of throat deposition can explain the variability in lung deposition of inhaled drugs. *Journal of aerosol medicine, 19*(4), 473-483.
13. Bosquillon, C., Lombry, C., Preat, V., & Vanbever, R. (2001). Influence of formulation excipients and physical characteristics of inhalation dry powders on their aerosolization performance. *Journal of controlled release, 70*(3), 329-339.
14. Brand, R. W., Isselhard, D. E., & Smith, A. (2023). *Anatomy of Orofacial Structures-E-Book: A Comprehensive Approach*: Elsevier Health Sciences.
15. Bücking, T. M., Hill, E. R., Robertson, J. L., Maneas, E., Plumb, A. A., & Nikitichev, D. I. (2017). From medical imaging data to 3D printed anatomical models. *PloS one, 12*(5), e0178540.
16. Burnell, P. K., Asking, L., Borgström, L., Nichols, S. C., Olsson, B., Prime, D., & Shrubb, I. (2007). Studies of the human oropharyngeal airspaces using magnetic resonance imaging IV—the oropharyngeal retention effect for four inhalation delivery systems. *Journal of aerosol medicine, 20*(3), 269-281.
17. Byron, P. R., Hindle, M., Lange, C. F., Longest, P. W., McRobbie, D., Oldham, M. J., . . . Finlay, W. H. (2010). In vivo–in vitro correlations: predicting pulmonary drug deposition from pharmaceutical aerosols. *Journal of aerosol medicine and pulmonary drug delivery, 23*(S2), S-59-S-69.
18. Byron, P. R., Wei, X., Delvadia, R. R., & Longest, P. W. (2013). Standardizing in vitro test methods to support aerosol drug evaluation in the clinic. *RDD Europe, 1*, 85-92.
19. Carvalho, T. C., Peters, J. I., & Williams III, R. O. (2011). Influence of particle size on regional lung deposition–what evidence is there? *International Journal of Pharmaceutics, 406*(1-2), 1-10.
20. Cataldo, D., Hanon, S., Peche, R. V., Schuermans, D. J., Degryse, J. M., De Wulf, I. A., . . . Derom, E. (2022). How to choose the right inhaler using a patient-centric approach? *Advances in therapy, 39*(3), 1149-1163.
21. Catalfumo, F. J., Golz, A., Westerman, S. T., Gilbert, L. M., Joachims, H. Z., & Goldenberg, D. (1998). The epiglottis and obstructive sleep apnoea syndrome. *The Journal of Laryngology & Otology, 112*(10), 940-943.
22. Chan, J. G. Y., Kwok, P. C. L., Young, P. M., Chan, H.-K., & Traini, D. (2011). Mannitol delivery by vibrating mesh nebulisation for enhancing mucociliary clearance. *Journal of pharmaceutical sciences, 100*(7), 2693-2702.
23. Chen, X., Zhong, W., Sun, B., Jin, B., & Zhou, X. (2012). Study on gas/solid flow in an obstructed pulmonary airway with transient flow based on CFD–DPM approach. *Powder technology, 217*, 252-260.
24. Chen, Y., Feng, X., Shi, X., Cai, W., Li, B., & Zhao, Y. (2023). Evaluation of computational fluid dynamics models for predicting pediatric upper airway airflow characteristics. *Medical & Biological Engineering & Computing, 61*(1), 259-270.
25. Cheng, S., Kourmatzis, A., Mekonnen, T., Gholizadeh, H., Raco, J., Chen, L., . . . Chan, H.-K. (2019). Does upper airway deformation affect drug deposition? *International Journal of Pharmaceutics, 572*, 118773.

26. Chew, N. Y., & Chan, H.-K. (2002). The role of particle properties in pharmaceutical powder inhalation formulations. *Journal of aerosol medicine, 15*(3), 325-330.
27. Chow, M. Y. T., Tai, W., Chang, R. Y. K., Chan, H.-K., & Kwok, P. C. L. (2021). In vitro-in vivo correlation of cascade impactor data for orally inhaled pharmaceutical aerosols. *Advanced drug delivery reviews, 177*, 113952.
28. Ciciliani, A.-M., Langguth, P., & Wachtel, H. (2017). In vitro dose comparison of Respimat® inhaler with dry powder inhalers for COPD maintenance therapy. *International journal of chronic obstructive pulmonary disease*, 1565-1577.
29. Clark, A., Newman, S., & Dasovich, N. (1998). Mouth and oropharyngeal deposition of pharmaceutical aerosols. *Journal of aerosol medicine, 11*(s1), S-116-S-121.
30. Clark, A. R. (1995). The use of laser diffraction for the evaluation of the aerosol clouds generated by medical nebulizers. *International Journal of Pharmaceutics, 115*(1), 69-78.
31. Colthorpe, P., Voshaar, T., Kieckbusch, T., Cuoghi, E., & Jauernig, J. (2013). Delivery characteristics of a low-resistance dry-powder inhaler used to deliver the long-acting muscarinic antagonist glycopyrronium. *Journal of drug assessment, 2*(1), 11-16.
32. Constantin, P., & Foiaş, C. (1988). *Navier-stokes equations*: University of Chicago press.
33. Conway, J. (2012). Lung imaging—two dimensional gamma scintigraphy, SPECT, CT and PET. *Advanced drug delivery reviews, 64*(4), 357-368.
34. Crowder, T. M., Rosati, J. A., Schroeter, J. D., Hickey, A. J., & Martonen, T. B. (2002). Fundamental effects of particle morphology on lung delivery: predictions of Stokes' law and the particular relevance to dry powder inhaler formulation and development. *Pharmaceutical Research, 19*, 239-245.
35. Cunningham, E. (1910). On the velocity of steady fall of spherical particles through fluid medium. *Proceedings of the Royal Society of London. Series A, Containing Papers of a Mathematical and Physical Character, 83*(563), 357-365.
36. Darquenne, C. (2014). Aerosol deposition in the human lung in reduced gravity. *Journal of aerosol medicine and pulmonary drug delivery, 27*(3), 170-177.
37. Darquenne, C. (2020). Deposition mechanisms. *Journal of aerosol medicine and pulmonary drug delivery, 33*(4), 181-185.
38. Darquenne, C., Corcoran, T. E., Lavorini, F., Sorano, A., & Usmani, O. S. (2024). The effects of airway disease on the deposition of inhaled drugs. *Expert opinion on drug delivery, 21*(8), 1175-1190.
39. Darquenne, C., Paiva, M., & Prisk, G. K. (2000). Effect of gravity on aerosol dispersion and deposition in the human lung after periods of breath holding. *Journal of Applied Physiology, 89*(5), 1787-1792.
40. Davies, C. (1945). Definitive equations for the fluid resistance of spheres. *Proceedings of the Physical Society, 57*(4), 259.
41. Dehbi, A. (2008). A CFD model for particle dispersion in turbulent boundary layer flows. *Nuclear engineering and design, 238*(3), 707-715.
42. Delakorda, M., & Ovsenik, N. (2019). Epiglottis shape as a predictor of obstruction level in patients with sleep apnea. *Sleep and Breathing, 23*, 311-317.
43. DelGaudio, J. M., & Chen, A. Y. (2010). Oral cavity and oropharynx. *Anatomic basis of tumor surgery*, 1-54.
44. Delvadia, R. R., Longest, P. W., & Byron, P. R. (2012). In vitro tests for aerosol deposition. I: Scaling a physical model of the upper airways to predict drug deposition variation in normal humans. *Journal of aerosol medicine and pulmonary drug delivery, 25*(1), 32-40.

45. Devine, C., & Zur, K. (2021). Upper Airway Anatomy and Physiology. *Diagnostic and Interventional Bronchoscopy in Children*, 17-37.
46. Dolovich, M., & Rhem, R. (1998). Impact of oropharyngeal deposition on inhaled dose. *Journal of aerosol medicine, 11*(s1), S-112-S-115.
47. Dong, J., Li, J., Tian, L., & Tu, J. (2021). Transport and deposition of ultrafine particles in the upper tracheobronchial tree: a comparative study between approximate and realistic respiratory tract models. *Computer Methods in Biomechanics and Biomedical Engineering, 24*(10), 1125-1135.
48. Dong, J., Ma, J., Tian, L., Inthavong, K., & Tu, J. (2019). Inhalation exposure analysis of lung-inhalable particles in an approximate rat central airway. *International Journal of Environmental Research and Public Health, 16*(14), 2571.
49. Donner, M. W., Bosnia, J. F., & Robertson, D. L. (1985). Anatomy and physiology of the pharynx. *Gastrointestinal radiology, 10*, 197-212.
50. Edwards, D. A., Ben-Jebria, A., & Langer, R. (1998). Recent advances in pulmonary drug delivery using large, porous inhaled particles. *Journal of Applied Physiology, 85*(2), 379-385.
51. Ehtezazi, T., Horsfield, M. A., Barry, P. W., & O'callaghan, C. (2004). Dynamic change of the upper airway during inhalation via aerosol delivery devices. *Journal of aerosol medicine, 17*(4), 325-334.
52. Faizal, W., Ghazali, N. N. N., Khor, C., Badruddin, I. A., Zainon, M., Yazid, A. A., . . . Razi, R. M. (2020). Computational fluid dynamics modelling of human upper airway: A review. *Computer methods and programs in biomedicine, 196*, 105627.
53. Finlay, W., Golshahi, L., Noga, M., & Flores-Mir, C. (2010). *Choosing 3-D mouth-throat dimensions: A rational merging of medical imaging and aerodynamics.* Paper presented at the Respiratory drug delivery.
54. Finlay, W., Zhang, Y., Grgic, B., Heenan, A., Burnell, P., Matida, E., . . . Lange, C. (2004). Solving a major in vitro-in vivo correlation problem: impactor induction ports. *Respiratory Drug Delivery IX, 1*, 203-210.
55. Finlay, W. H. (2001). *The mechanics of inhaled pharmaceutical aerosols: an introduction*: Elsevier.
56. Finlay, W. H., & Darquenne, C. (2020). Particle size distributions. *Journal of aerosol medicine and pulmonary drug delivery, 33*(4), 178-180.
57. Forman, M., Jícha, M., & Katolický, J. (2007). Aerosol deposition in human airways during breathing cycle.
58. Friedlander, S. K., & Smoke, D. (2000). Haze: Fundamentals of aerosol dynamics. In: Oxford University Press, New York.
59. Ghahramani, E., Abouali, O., Emdad, H., & Ahmadi, G. (2014). Numerical analysis of stochastic dispersion of micro-particles in turbulent flows in a realistic model of human nasal/upper airway. *Journal of Aerosol Science, 67*, 188-206.
60. Gibb, G. D. (1872). THE USES OF THE UVULA. *The Lancet, 99*(2528), 180-182.
61. Golshahi, L., Finlay, W. H., & Wachtel, H. (2022). Use of airway replicas in lung delivery applications. *Journal of aerosol medicine and pulmonary drug delivery, 35*(2), 61-72.
62. Gonda, I. (2000). The ascent of pulmonary drug delivery. *Journal of pharmaceutical sciences, 89*(7), 940-945.
63. Gondhale, P., Deshmukh, M., Omase, R., Arbune, A., Kolsure, P., Bhope, S., & Padmanabhan, S. (2022). Comparative Evaluation of Fine Particle Fraction and T2 Fraction by Using Next Generation Impactor (NGI) and Glass Twin Impinger (GTI) on Formoterol Fumarate and Tiotropium Dry Powder Inhaler (DPI) Marketed Products. *Pharmaceutical Chemistry Journal, 56*(5), 720-726.

64. Gong, F., Liang, Y.-Z., Fung, Y.-S., & Chau, F.-T. (2004). Correction of retention time shifts for chromatographic fingerprints of herbal medicines. *Journal of Chromatography A, 1029*(1-2), 173-183.
65. Grasmeijer, F., Hagedoorn, P., Frijlink, H. W., & de Boer, A. H. (2012). Characterisation of high dose aerosols from dry powder inhalers. *International Journal of Pharmaceutics, 437*(1-2), 242-249.
66. Grgic, B., Finlay, W. H., Burnell, P. K., & Heenan, A. F. (2004). In vitro intersubject and intrasubject deposition measurements in realistic mouth–throat geometries. *Journal of Aerosol Science, 35*(8), 1025-1040.
67. Guha, A. (2008). Transport and deposition of particles in turbulent and laminar flow. *Annu. Rev. Fluid Mech., 40*(1), 311-341.
68. Hagberg, C., Georgi, R., & Krier, C. (2005). Complications of managing the airway. *Best Practice & Research Clinical Anaesthesiology, 19*(4), 641-659.
69. Hain, R., & Kähler, C. (2007). Fundamentals of multiframe particle image velocimetry (PIV). *Experiments in fluids, 42*, 575-587.
70. He, J., Li, J., Chen, B., Yang, W., Yu, X., Zhang, F., . . . Zhu, X. (2024). Study of aerosol dispersion and control in dental practice. *Clinical Oral Investigations, 28*(1), 120.
71. Hickey, A. J. (2003). *Pharmaceutical inhalation aerosol technology*: CRC Press.
72. Hinds, W. C., & Zhu, Y. (2022). *Aerosol technology: properties, behavior, and measurement of airborne particles*: John Wiley & Sons.
73. Hofmann, W. (2011). Modelling inhaled particle deposition in the human lung—A review. *Journal of Aerosol Science, 42*(10), 693-724.
74. Hoppentocht, M., Hagedoorn, P., Frijlink, H., & De Boer, A. (2014). Technological and practical challenges of dry powder inhalers and formulations. *Advanced drug delivery reviews, 75*, 18-31.
75. Huang, F., Zhang, Y., Tong, Z. B., Chen, X. L., Yang, R. Y., & Yu, A. B. (2021). Numerical investigation of deposition mechanism in three mouth–throat models. *Powder Technology, 378*, 724-735.
76. Huang, F., Zhou, X., Dai, W., Yu, J., Zhou, Z., Tong, Z., & Yu, A. (2022). In Vitro and In Silico Investigations on Drug Delivery in the Mouth-Throat Models with Handihaler®. *Pharmaceutical Research, 39*(11), 3005-3019.
77. Huang, F., Zhu, Q., Zhou, X., Gou, D., Yu, J., Li, R., . . . Yang, R. (2021). Role of CFD based in silico modelling in establishing an in vitro-in vivo correlation of aerosol deposition in the respiratory tract. *Advanced Drug Delivery Reviews, 170*, 369-385. doi:https://doi.org/10.1016/j.addr.2020.09.007
78. Ides, K. M., De Backer, W. A., Lanclus, M., Leemans, G., Dierckx, W., Lauwers, E., . . . De Backer, J. W. (2022). The effect of posture on airflow distribution, airway geometry and air velocity in healthy subjects. *BMC Pulmonary Medicine, 22*(1), 477.
79. Jahed, M., Kozinski, J., & Pakzad, L. (2024). Mucus, airway and plume temperature effects on pMDI-drug delivery in a mouth-throat airway: Experimental and numerical studies. *Journal of Aerosol Science, 181*, 106436.
80. Jayaraju, S., Brouns, M., Verbanck, S., & Lacor, C. (2007). Fluid flow and particle deposition analysis in a realistic extrathoracic airway model using unstructured grids. *Journal of Aerosol Science, 38*(5), 494-508.
81. Jõgi, R., Mattila, L., Vahteristo, M., Takala, A., Lähelmä, S., Vartiainen, V. A., & Lindqvist, A. (2021). Inspiratory flow parameters through dry powder inhalers in healthy volunteers and patients with chronic obstructive pulmonary disease (COPD): device resistance does not limit use in COPD. *International Journal of Chronic Obstructive Pulmonary Disease*, 1193-1201.

82. Joseph, J. (1982). The Oral Cavity and Palate. In *A Textbook of Regional Anatomy* (pp. 286-295): Springer.
83. Kamiya, A., Sakagami, M., Hindle, M., & Byron, P. R. (2004). Aerodynamic sizing of metered dose inhalers: an evaluation of the Andersen and next generation pharmaceutical impactors and their USP methods. *Journal of pharmaceutical sciences, 93*(7), 1828-1837.
84. Karaosmanoglu, A. A., & Ozgen, B. (2022). Anatomy of the pharynx and cervical esophagus. *Neuroimaging Clinics, 32*(4), 791-807.
85. Karra, N., Swindle, E., & Morgan, H. (2019). Drug delivery for traditional and emerging airway models. *Organs-on-a-Chip, 1*, 100002.
86. Kaviratna, A., Tian, G., Liu, X., Delvadia, R., Lee, S., & Guo, C. (2019). Evaluation of bio-relevant mouth-throat models for characterization of metered dose inhalers. *AAPS PharmSciTech, 20*, 1-9.
87. Khalili, S. F., Ghanbarzadeh, S., Nokhodchi, A., & Hamishehkar, H. (2018). The effect of different coating materials on the prevention of powder bounce in the next generation impactor. *Research in pharmaceutical sciences, 13*(3), 283-287.
88. Kim, A. M., Keenan, B. T., Jackson, N., Chan, E. L., Staley, B., Poptani, H., . . . Schwab, R. J. (2014). Tongue fat and its relationship to obstructive sleep apnea. *Sleep, 37*(10), 1639-1648.
89. Kim, Y., Tong, Z., Chan, H., & Yang, R. (2019). CFD modelling of air and particle flows in different airway models. *Journal of Aerosol Science, 134*, 14-28.
90. Kleinstreuer, C., Zhang, Z., & Kim, C. S. (2007). Combined inertial and gravitational deposition of microparticles in small model airways of a human respiratory system. *Journal of Aerosol Science, 38*(10), 1047-1061.
91. Kolanjiyil, A. V., & Kleinstreuer, C. (2016). Computationally efficient analysis of particle transport and deposition in a human whole-lung-airway model. Part I: Theory and model validation. *Computers in biology and medicine, 79*, 193-204.
92. Koullapis, P., Kassinos, S. C., Muela, J., Perez-Segarra, C., Rigola, J., Lehmkuhl, O., . . . Jicha, M. (2018). Regional aerosol deposition in the human airways: The SimInhale benchmark case and a critical assessment of in silico methods. *European Journal of Pharmaceutical Sciences, 113*, 77-94.
93. Kourmatzis, A., Cheng, S., & Chan, H.-K. (2018). Airway geometry, airway flow, and particle measurement methods: implications on pulmonary drug delivery. *Expert opinion on drug delivery, 15*(3), 271-282.
94. Lambert, R., Wiggs, B., Kuwano, K., Hogg, J., & Pare, P. (1993). Functional significance of increased airway smooth muscle in asthma and COPD. *Journal of Applied Physiology, 74*(6), 2771-2781.
95. Launder, B. E., & Sharma, B. I. (1974). Application of the energy-dissipation model of turbulence to the calculation of flow near a spinning disc. *Letters in heat and mass transfer, 1*(2), 131-137.
96. Leung, K., Louca, E., Gray, M., Tipples, G., & Coates, A. L. (2005). Use of the next generation pharmaceutical impactor for particle size distribution measurements of live viral aerosol vaccines. *Journal of aerosol medicine, 18*(4), 414-426.
97. Leung, S. S. Y., Tang, P., Zhou, Q., Tong, Z., Leung, C., Decharaksa, J., . . . Chan, H.-K. (2015). De-agglomeration effect of the US pharmacopeia and Alberta throats on carrier-based powders in commercial inhalation products. *The AAPS journal, 17*, 1407-1416.
98. Li, Z. (2012). Particle deposition in oral-tracheal airway models with very low inhalation profiles. *Journal of Bionic Engineering, 9*(2), 252-261.

99. Liu, H., Zhang, S., Yu, A., Qu, L., Zhao, Y., Huang, H., & Li, J. (2004). Studies on intestinal permeability of cirrhotic patients by analysis lactulose and mannitol in urine with HPLC/RID/MS. *Bioorganic & medicinal chemistry letters, 14*(9), 2339-2344.
100. Loizeau, J. L., Arbouille, D., Santiago, S., & Vernet, J. P. (1994). Evaluation of a wide range laser diffraction grain size analyser for use with sediments. *Sedimentology, 41*(2), 353-361.
101. Longest, P. W., & Hindle, M. (2012). Condensational growth of combination drug-excipient submicrometer particles for targeted high efficiency pulmonary delivery: comparison of CFD predictions with experimental results. *Pharmaceutical Research, 29*, 707-721.
102. Longest, P. W., & Holbrook, L. T. (2012). In silico models of aerosol delivery to the respiratory tract—development and applications. *Advanced drug delivery reviews, 64*(4), 296-311.
103. Longest, P. W., & Xi, J. (2007). Effectiveness of direct Lagrangian tracking models for simulating nanoparticle deposition in the upper airways. *Aerosol Science and Technology, 41*(4), 380-397.
104. Longest, W., & Farkas, D. (2019). Development of a new inhaler for high-efficiency dispersion of spray-dried powders using computational fluid dynamics (CFD) modeling. *The AAPS journal, 21*, 1-15.
105. Luo, H., & Liu, Y. (2008). Modeling the bifurcating flow in a CT-scanned human lung airway. *Journal of biomechanics, 41*(12), 2681-2688.
106. Ma, B., Kourmatzis, A., Zhao, Y., Yang, R., Chan, H.-K., Salehi, F., & Cheng, S. (2020). Potential effects of lingual fats on airway flow dynamics and particle deposition. *Aerosol Science and Technology, 54*(3), 321-331.
107. Ma, B., & Lutchen, K. R. (2009). CFD simulation of aerosol deposition in an anatomically based human large–medium airway model. *Annals of Biomedical Engineering, 37*, 271-285.
108. Ma, Z., Kourmatzis, A., Milton-McGurk, L., Chan, H.-K., Farina, D., & Cheng, S. (2022). Simulating the effect of individual upper airway anatomical features on drug deposition. *International Journal of Pharmaceutics, 628*, 122219.
109. Marani, E., Heida, C., Marani, E., & Heida, C. (2018). Oral Cavity: Tongue, Palate and Teeth. *Head and Neck: Morphology, Models and Function*, 133-160.
110. Marple, V. A., Olson, B. A., Santhanakrishnan, K., Mitchell, J. P., Murray, S. C., & Hudson-Curtis, B. L. (2003). Next generation pharmaceutical impactor (a new impactor for pharmaceutical inhaler testing). Part II: Archival calibration. *Journal of aerosol medicine, 16*(3), 301-324.
111. Martin, S., Mathur, R., Marshall, I., & Douglas, N. (1997). The effect of age, sex, obesity and posture on upper airway size. *European Respiratory Journal, 10*(9), 2087-2090.
112. Martonen, T., Zhang, Z., Yue, G., & Musante, C. (2002). 3-D particle transport within the human upper respiratory tract. *Journal of Aerosol Science, 33*(8), 1095-1110.
113. Matida, E. A., Finlay, W. H., Breuer, M., & Lange, C. F. (2006). Improving prediction of aerosol deposition in an idealized mouth using large-eddy simulation. *Journal of aerosol medicine, 19*(3), 290-300.
114. Matsuo, K., Metani, H., Mays, K., & Palmer, J. (2010). Effects of respiration on soft palate movement in feeding. *Journal of dental research, 89*(12), 1401-1406.
115. Mekonnen, T., Cai, X., Burchell, C., Gholizadeh, H., & Cheng, S. (2022). A review of upper airway physiology relevant to the delivery and deposition of inhalation aerosols. *Advanced Drug Delivery Reviews*, 114530.

116. Michaelides, E., Crowe, C. T., & Schwarzkopf, J. D. (2016). *Multiphase flow handbook*: CRC Press.
117. Mihaescu, M., Murugappan, S., Kalra, M., Khosla, S., & Gutmark, E. (2008). Large Eddy Simulation and Reynolds-Averaged Navier–Stokes modeling of flow in a realistic pharyngeal airway model: An investigation of obstructive sleep apnea. *Journal of biomechanics, 41*(10), 2279-2288.
118. Milne, S., & King, G. G. (2014). Advanced imaging in COPD: insights into pulmonary pathophysiology. *Journal of thoracic disease, 6*(11), 1570.
119. Mitchell, J. (2019). Aerodynamic Particle Size Testing. In *Pharmaceutical Inhalation Aerosol Technology, Third Edition* (pp. 541-587): CRC Press.
120. Mitchell, J., & Nagel, M. (2004). Particle size analysis of aerosols from medicinal inhalers. *KONA Powder and Particle Journal, 22*, 32-65.
121. Mitchell, J. P., & Nagel, M. W. (2003). Cascade impactors for the size characterization of aerosols from medical inhalers: their uses and limitations. *Journal of aerosol medicine, 16*(4), 341-377.
122. Mohan, M., Lee, S., Guo, C., Peri, S. P., & Doub, W. H. (2017). Evaluation of abbreviated impactor measurements (AIM) and efficient data analysis (EDA) for dry powder inhalers (DPIs) against the full-resolution next generation impactor (NGI). *AAPS PharmSciTech, 18*, 1585-1594.
123. Moss, W. T. (1989). The nasopharynx. *Radiation oncology, 6th edn. St Louis, MO: The CV Mosby Company*, 198-214.
124. Mozdzanowski, J., & Burman, S. (2004). Detection methods. *Protein Purification Protocols*, 389-410.
125. Mylavarapu, G., Murugappan, S., Mihaescu, M., Kalra, M., Khosla, S., & Gutmark, E. (2009). Validation of computational fluid dynamics methodology used for human upper airway flow simulations. *Journal of biomechanics, 42*(10), 1553-1559.
126. Newman, S. P. (2017). Drug delivery to the lungs: challenges and opportunities. *Therapeutic delivery, 8*(8), 647-661.
127. Newman, S. P. (2022). Fine particle fraction: The good and the bad. *Journal of aerosol medicine and pulmonary drug delivery, 35*(1), 2-10.
128. Newman, S. P., & Chan, H.-K. (2020). In vitro-in vivo correlations (IVIVCs) of deposition for drugs given by oral inhalation. *Advanced drug delivery reviews, 167*, 135-147.
129. Newman, S. P., Steed, K. P., Reader, S. J., Pavia, D., & Sohal, A. K. (2007). An in vitro study to assess facial and ocular deposition from Respimat® Soft Mist™ inhaler. *Journal of aerosol medicine, 20*(1), 7-12.
130. Ochs, M., Nyengaard, J. R., Jung, A., Knudsen, L., Voigt, M., Wahlers, T., . . . Gundersen, H. J. G. (2004). The number of alveoli in the human lung. *American journal of respiratory and critical care medicine, 169*(1), 120-124.
131. Okuda, T., Tang, P., Yu, J., Finlay, W. H., & Chan, H.-K. (2017). Powder aerosol delivery through nasal high-flow system: In vitro feasibility and influence of process conditions. *International Journal of Pharmaceutics, 533*(1), 187-197.
132. Omer, H. K., Husein, N. R., & Hamadameen, H. A. (2019). Comparison between the next generation impactor and the twin glass impinge as model pulmonary drug delivery devices. *Zanco Journal of Medical Sciences (Zanco J Med Sci), 23*(1), 74-80.
133. Ou, C., Hang, J., & Deng, Q. (2020). Particle deposition in human lung airways: effects of airflow, particle size, and mechanisms. *Aerosol and Air Quality Research, 20*(12), 2846-2858.

134. Owens, R. L., Macrea, M. M., & Teodorescu, M. (2017). The overlaps of asthma or COPD with OSA: a focused review. *Respirology, 22*(6), 1073-1083.
135. Parumasivam, T., Chang, R. Y. K., Abdelghany, S., Ye, T. T., Britton, W. J., & Chan, H.-K. (2016). Dry powder inhalable formulations for anti-tubercular therapy. *Advanced drug delivery reviews, 102*, 83-101.
136. Patton, J. S., & Byron, P. R. (2007). Inhaling medicines: delivering drugs to the body through the lungs. *Nature reviews Drug discovery, 6*(1), 67-74.
137. Pham, D. T., Chokamonsirikun, A., Phattaravorakarn, V., & Tiyaboonchai, W. (2021). Polymeric micelles for pulmonary drug delivery: a comprehensive review. *Journal of Materials Science, 56*, 2016-2036.
138. Pitts, T. (2014). Airway protective mechanisms. *Lung, 192*(1), 27-31.
139. Rahman, M. M., Zhao, M., Islam, M. S., Dong, K., & Saha, S. C. (2021). Aging effects on airflow distribution and micron-particle transport and deposition in a human lung using CFD-DPM approach. *Advanced Powder Technology, 32*(10), 3506-3516.
140. Rana, S., Kharbanda, O., & Agarwal, B. (2020). Influence of tongue volume, oral cavity volume and their ratio on upper airway: A cone beam computed tomography study. *Journal of Oral Biology and Craniofacial Research, 10*(2), 110-117.
141. Reist, P. C. (1993). *Aerosol science and technology*.
142. Roberts, D. L., & Mitchell, J. (2016a). The Next Generation Impactor (NGI™)–Manufacturing Control: Part I. Nozzles. *Inhalation, 10*(2), 12-19.
143. Roberts, D. L., & Mitchell, J. (2016b). The Next Generation Impactor (NGI™)–Manufacturing Control: Part II. Collection Cups and the Critical Jet-to-Plate Distance. In: Inhalation.
144. Robinson, N. E., & Furlow, P. W. (2007). Anatomy of the respiratory system. *Equine respiratory medicine and surgery*, 3-17.
145. Rogers, T. D., Button, B., Kelada, S. N., Ostrowski, L. E., Livraghi-Butrico, A., Gutay, M. I., . . . Grubb, B. R. (2022). Regional differences in mucociliary clearance in the upper and lower airways. *Frontiers in Physiology, 13*, 842592.
146. Rogliani, P., Calzetta, L., Coppola, A., Cavalli, F., Ora, J., Puxeddu, E., . . . Cazzola, M. (2017). Optimizing drug delivery in COPD: the role of inhaler devices. *Respiratory medicine, 124*, 6-14.
147. Rosin, P. (1933). The laws governing the fineness of powdered coal. *J. Inst. Fuel, 7*(31), 29-36.
148. Ruzycki, C. A., Javaheri, E., & Finlay, W. H. (2013). The use of computational fluid dynamics in inhaler design. *Expert opinion on drug delivery, 10*(3), 307-323.
149. Rygg, A., & Longest, P. W. (2016). Absorption and clearance of pharmaceutical aerosols in the human nose: development of a CFD model. *Journal of aerosol medicine and pulmonary drug delivery, 29*(5), 416-431.
150. Sadeghi, T., Fatehi, P., & Pakzad, L. (2024). Effect of Nasal Inhalation on Drug Particle Deposition and Size Distribution in the Upper Airway: With Soft Mist Inhalers. *Annals of Biomedical Engineering, 52*(5), 1195-1212.
151. Sakamoto, Y. (2018). Structural arrangement of the intrinsic muscles of the tongue and their relationships with the extrinsic muscles. *Surgical and radiologic anatomy, 40*(6), 681-688.
152. Sanders, M. (2007). Inhalation therapy: an historical review. *Primary care respiratory journal, 16*(2), 71-81.
153. Scarano, F. (2012). Tomographic PIV: principles and practice. *Measurement Science and Technology, 24*(1), 012001.
154. Scott, R. P. (1996). *Chromatographic detectors: Design: Function, and operation*: CRC Press.

155. Shang, Y., & Inthavong, K. (2019). Numerical assessment of ambient inhaled micron particle deposition in a human nasal cavity. *Experimental and computational multiphase flow, 1*, 109-115.
156. Shinneeb, A.-M., & Pollard, A. (2012a). Identification of vortical structures inside the human pharynx/larynx region from POD-reconstructed velocity fields. *Experiments in fluids, 53*, 353-367.
157. Shinneeb, A.-M., & Pollard, A. (2012b). Investigation of the flow physics in the human pharynx/larynx region. *Experiments in fluids, 53*, 989-1003.
158. Siddiqui, A., & Connor, S. (2013). Imaging of the pharynx and larynx. *Imaging, 22*(1), 91047403.
159. Snyder, L. R., Kirkland, J. J., & Dolan, J. W. (2011). *Introduction to modern liquid chromatography*: John Wiley & Sons.
160. Sobiesk, J. L., & Munakomi, S. (2019). Anatomy, head and neck, nasal cavity.
161. Stapleton, K. W., Guentsch, E., Hoskinson, M., & Finlay, W. H. (2000). On the suitability of k–ε turbulence modeling for aerosol deposition in the mouth and throat: a comparison with experiment. *Journal of Aerosol Science, 31*(6), 739-749.
162. Stein, S., & Gabrio, B. (2000). Understanding throat deposition during cascade impactor testing. *Respir Drug Deliv, 2*, 287-290.
163. Stein, S. W., & Thiel, C. G. (2017). The history of therapeutic aerosols: a chronological review. *Journal of aerosol medicine and pulmonary drug delivery, 30*(1), 20-41.
164. Stuart, B. O. (1984). Deposition and clearance of inhaled particles. *Environmental health perspectives, 55*, 369-390.
165. Suárez-Quintanilla, J., & Sharma, S. (2019). Anatomy, head and neck, larynx.
166. Swartz, M. (2010). HPLC detectors: a brief review. *Journal of Liquid Chromatography & Related Technologies, 33*(9-12), 1130-1150.
167. Taki, M., Marriott, C., Zeng, X.-M., & Martin, G. P. (2010). Aerodynamic deposition of combination dry powder inhaler formulations in vitro: a comparison of three impactors. *International Journal of Pharmaceutics, 388*(1-2), 40-51.
168. Thakur, A. K., Kaundle, B., & Singh, I. (2020). Mucoadhesive drug delivery systems in respiratory diseases. In *Targeting chronic inflammatory lung diseases using advanced drug delivery systems* (pp. 475-491): Elsevier.
169. Thomas, C. L., Hernandez-Allica, J., Dunham, S. J., McGrath, S. P., & Haefele, S. M. (2021). A comparison of soil texture measurements using mid-infrared spectroscopy (MIRS) and laser diffraction analysis (LDA) in diverse soils. *Scientific Reports, 11*(1), 16.
170. Tian, G., Hindle, M., Lee, S., & Longest, P. W. (2015). Validating CFD predictions of pharmaceutical aerosol deposition with in vivo data. *Pharmaceutical Research, 32*, 3170-3187.
171. Tian, G., Longest, P. W., Su, G., Walenga, R. L., & Hindle, M. (2011). Development of a stochastic individual path (SIP) model for predicting the tracheobronchial deposition of pharmaceutical aerosols: Effects of transient inhalation and sampling the airways. *Journal of Aerosol Science, 42*(11), 781-799.
172. Torre, C., Camacho, M., Liu, S. Y. C., Huon, L. K., & Capasso, R. (2016). Epiglottis collapse in adult obstructive sleep apnea: a systematic review. *The Laryngoscope, 126*(2), 515-523.
173. Ung, K. T., Rao, N., Weers, J. G., Clark, A. R., & Chan, H.-K. (2014). In vitro assessment of dose delivery performance of dry powders for inhalation. *Aerosol Science and Technology, 48*(10), 1099-1110.

174. Ung, K. T., Rao, N., Weers, J. G., Huang, D., & Chan, H.-K. (2016). Design of spray dried insulin microparticles to bypass deposition in the extrathoracic region and maximize total lung dose. *International Journal of Pharmaceutics, 511*(2), 1070-1079. doi:https://doi.org/10.1016/j.ijpharm.2016.07.073
175. USP. (2023). General Chapter, ⟨601⟩ Inhalation and Nasal Drug Products: Aerosols, Sprays, and Powders—Performance Quality Tests. In. Rockville, MD: United States Pharmacopeia.
176. Vara Almirall, B., Inthavong, K., Bradshaw, K., Singh, N., Johnson, A., Storey, P., & Salati, H. (2022). Flow patterns and particle residence times in the oral cavity during inhaled drug delivery. *Pharmaceuticals, 15*(10), 1259.
177. Venegas, J., Winkler, T., & Harris, R. S. (2013). Lung physiology and aerosol deposition imaged with positron emission tomography. *Journal of aerosol medicine and pulmonary drug delivery, 26*(1), 1-8.
178. Voss, S., Vutlapalli, S. C., Saalfeld, P., Arens, C., & Janiga, G. (2022). CFD simulations of inhalation through a subject-specific human larynx–Impact of the unilateral vocal fold immobility. *Computers in biology and medicine, 143*, 105243.
179. Walsh, J. H., Leigh, M. S., Paduch, A., Maddison, K. J., Philippe, D. L., Armstrong, J. J., . . . Eastwood, P. R. (2008). Evaluation of pharyngeal shape and size using anatomical optical coherence tomography in individuals with and without obstructive sleep apnoea. *Journal of sleep research, 17*(2), 230-238.
180. Wei, X. (2015). *Development of clinically relevant in vitro performance tests for powder inhalers*: Virginia Commonwealth University.
181. Wei, X., Hindle, M., Kaviratna, A., Huynh, B. K., Delvadia, R. R., Sandell, D., & Byron, P. R. (2018). In vitro tests for aerosol deposition. VI: realistic testing with different mouth–throat models and in vitro—in vivo correlations for a dry powder inhaler, metered dose inhaler, and soft mist inhaler. *Journal of aerosol medicine and pulmonary drug delivery, 31*(6), 358-371.
182. West, J. B., & Luks, A. M. (2020). *West's Respiratory Physiology*: Lippincott Williams & Wilkins.
183. Wiggins, N. A. (1991). The development of a mathematical approximation technique to determine the mass median aerodynamic diameter (MMAD) and geometric standard deviation (GSD) of drug particles in an inhalation aerosol sprat. *Drug development and industrial pharmacy, 17*(14), 1971-1986.
184. Wong, C. Y. J., Cuendet, M., Spaleniak, W., Gholizadeh, H., Marasini, N., Ong, H. X., & Traini, D. (2022). Validation of a cell integrated next-generation impactor to assess in vitro drug transport of physiologically relevant aerosolised particles. *International Journal of Pharmaceutics, 624*, 122024.
185. Wriedt, T. (2012). Mie theory: a review. *The Mie theory: Basics and applications*, 53-71.
186. Xi, J., & Longest, P. (2007). Transport and deposition of micro-aerosols in realistic and simplified models of the oral airway. *Annals of biomedical engineering, 35*(4), 560-581.
187. Xi, J., Longest, P. W., & Martonen, T. B. (2008). Effects of the laryngeal jet on nano-and microparticle transport and deposition in an approximate model of the upper tracheobronchial airways. *Journal of Applied Physiology, 104*(6), 1761-1777.
188. Xi, J., Talaat, M., Si, X. A., Han, P., Dong, H., & Zheng, S. (2020). Alveolar size effects on nanoparticle deposition in rhythmically expanding-contracting terminal alveolar models. *Computers in biology and medicine, 121*, 103791.

189. Xi, J., Yuan, J. E., Yang, M., Si, X., Zhou, Y., & Cheng, Y.-S. (2016). Parametric study on mouth–throat geometrical factors on deposition of orally inhaled aerosols. *Journal of Aerosol Science, 99*, 94-106.
190. Xu, X., Wu, J., Weng, W., & Fu, M. (2020). Investigation of inhalation and exhalation flow pattern in a realistic human upper airway model by PIV experiments and CFD simulations. *Biomechanics and modeling in mechanobiology, 19*(5), 1679-1695.
191. Yaqub, N., Wayne, G., Birchall, M., & Song, W. (2022). Recent advances in human respiratory epithelium models for drug discovery. *Biotechnology Advances, 54*, 107832.
192. Yeh, H.-C., & Schum, G. (1980). Models of human lung airways and their application to inhaled particle deposition. *Bulletin of mathematical biology, 42*(3), 461-480.
193. Yoshida, H., Kuwana, A., Shibata, H., Izutsu, K.-i., & Goda, Y. (2017). Comparison of aerodynamic particle size distribution between a next generation impactor and a cascade impactor at a range of flow rates. *AAPS PharmSciTech, 18*, 646-653.
194. Yu, C., & Taulbee, D. (1975). A theory of predicting respiratory tract deposition of inhaled particles in man. *Inhaled particles, 4*, 35-47.
195. Zeng, X. M., Martin, G. P., & Marriott, C. (2000). *Particulate interactions in dry powder formulation for inhalation*: CRC Press.
196. Zhang, Z., & Kleinstreuer, C. (2003). Low-Reynolds-number turbulent flows in locally constricted conduits: a comparison study. *AIAA journal, 41*(5), 831-840.
197. Zhou, X., Li, Y., Miao, H., Zhang, Y., Yu, A., Huang, F., . . . Tong, Z. (2024). Numerical study on the effect of the realistic mouth-inhaler positions on orally inhaled drug delivery in pediatric intersubject upper airways. *Powder technology, 432*, 119163.

Chapter 3 Simulating the effect of individual upper airway anatomical features on drug deposition

(Published in the International Journal of Pharmaceutics, Volume 628, 122219)

As evidenced through the literature, anatomical features of the extrathoracic airway play a crucial role in defining the deposition mechanics of dry powders from inhaler devices. Understanding the effect of the airway is critical towards informing the design of replicas used as induction ports for cascade impactors. This study aims to systematically isolate different anatomical features of the human pharynx with the goal to investigate their independent influence on airflow dynamics and particle deposition characteristics in a geometrically realistic human airway. Specifically, the effects of the uvula, epiglottis and soft palate on drug particle deposition are studied systematically, by carefully removing each of these anatomical features from reconstructed models based on MRI data and comparing them to a benchmark realistic airway model. Computational Fluid Dynamics using established turbulence models is employed to simulate the transport of monodispersed particles (3 µm) in the airway at two flow-rates. The simulations suggest three findings: 1) widening the space between the oral cavity and oropharynx and where the soft palate is situated leads to the most dramatic reduction in drug deposition in the upper airway; 2) exclusion of the uvula and epiglottis: a) affects flow dynamics in the airway; b) alters regional deposition behaviour; c) does not significantly affect the total number of particles deposited in the pharynx; and 3) the space adjacent to the soft palate is a key determinant for aerosol deposition in the extrathoracic region and is related to mechanisms of flow acceleration, diversion and recirculation.

3.1 Introduction

Respiratory diseases, such as asthma (Nurmagambetov et al., 2018; Usmani, 2019), chronic obstructive pulmonary disease (COPD) (Gayle et al., 2022; Zhu et al., 2018) and chronic bronchitis (Dotan et al., 2019) are devastating. Prevailing medical conditions and aggregated morbidity, mortality and mental health associated with these diseases are known to incur immense economic costs of over €380 billion annually in Europe alone (Manfrin et al., 2021). The direct cost implication of COPD ranges between $6,000 to $10,000 per patient in both Asia and the USA (Gutiérrez Villegas et al., 2021). Improved understanding of the diseases

and the advent of medical technologies have introduced treatments that span from oral medication, inhaled drug delivery, intramuscular injection, and intravenous injection to reduce the mortality associated with these respiratory diseases (Newman, 2018). Among these treatments, there is an increase in the development of inhaled pulmonary drug delivery related technologies, given that this treatment modality presents higher therapeutic efficacy and is associated with benefits that include rapid drug uptake, higher drug bioavailability, and less drug waste (Cazzola et al., 2020; N. Renee Labiris & Myrna B. Dolovich, 2003).

The geometry of the human upper airway is highly complex and has physiological properties that present a natural barrier for foreign particles, including inhaled drug particles (Newman, 2017). The upper airway, which is the only conduit to the lung, consists of several distinct sections, namely the nasopharynx, oropharynx, laryngopharynx, and trachea (A. Kourmatzis et al., 2018). The geometries of these different sections of the human upper airway can vary between individuals (Burchell et al., 2022; W. H. Finlay, 2001), and some of these sections can also change during respiration (S. Cheng et al., 2008; Wagshul et al., 2013). The above complexity is further compounded by the change in upper airway physiology with disease state and risk factors, such as regional inflammation and obesity, which are known to change the anatomical structure of the human pharynx (A. Kourmatzis et al., 2018; Walsh et al., 2008). These factors present challenges to understanding the details of drug deposition mechanisms in the extrathoracic airway.

A fundamental technique to test the efficacy of inhaled drug delivery technology is by analyzing the aerodynamic properties of drug particles in a cascade impactor, where the desired measurement outcome is a sufficient mass of fine particles between 1 – 5 μm. The cascade impactor is connected to an induction port, with the United States Pharmacopeia (USP) mouth throat model being the standard airway replica used in these experiments, albeit having little resemblance to the human throat, as it only comprises a 90° bent tube (Tang et al., 2012; Xi et al., 2016; Yu Zhang et al., 2006). Several geometrically realistic airway replicas have been commercialized over the years with the aim to realize stronger in vitro-in vivo correlations in the testing of inhaled drug delivery related technologies. Some of these induction ports include the Virginia Commonwealth University (VCU) (Kaviratna et al., 2019a; Newman & Chan, 2020) throat, the Alberta Idealized Throat (AIT) (Keith T. Ung et al., 2016; Wei et al.), and the Oropharyngeal Consortium (OPC) model (Newman & Chan, 2020; Wei & Byron, 2016; Wei et al., 2018). The geometry of some of the aforementioned mouth throat models, despite being significantly different from the USP throat model, have idealized geometries that consist of the

absence of some distinctive upper airway anatomical features. The VCU mouth throat replica (Newman & Chan, 2020), for example, excludes anatomical features such as the uvula and epiglottis and has a wide oral cavity space that may represent the absence of the soft palate, at least for some humans. The AIT (Keith T. Ung et al., 2016), on the other hand, does not consist of the uvula, but includes the epiglottis and has a narrow space at the region of the soft palate that indicates the presence of the latter airway structure (Newman & Chan, 2020; Wei et al., 2018). On the other hand, the OPC-realistic airway model consists of the uvula, soft palate and epiglottis (Wei et al., 2018). While existing studies have demonstrated clear differences in drug deposition using different mouth throat models (Kaviratna et al., 2019a; Wei et al., 2018), there remains a limited understanding of what causes the disparity and, specifically, how they may be related to the absence of specific anatomical features in the human upper airway.

Understanding the potential effects caused by different anatomical features in the human upper airway is vital. This understanding is necessary to help provide critical insights on drug particle deposition mechanisms in the human pharynx, but also needed to interpret data obtained from experiments using cascade impactors connected to idealized extrathoracic airway geometries. Computational modelling has been commonly used to study drug deposition in the upper airway (W. M. Faizal et al., 2020; Y. H. Kim et al., 2019; P. Worth Longest et al., 2019; Bingjie Ma et al., 2020; Shang et al., 2019; Y. Zhang et al., 2004; Zhe Zhang & Kleinstreuer, 2011), as it can provide detailed information on the regional deposition of particles in the pharynx, which can be otherwise challenging to obtain using other methods. The transport behaviour of particles and droplets has been proven to be accurately simulated by using Eulerian-Eulerian and Eulerian-Lagrangian numerical models (Ariyaratne et al.). The discrete phase model (DPM), for example, is a commonly used model developed from an Eulerian-Lagrangian approach. Xu et al. (2020) investigated the flow behaviour in a realistic human upper airway by using four different turbulence models, including LRN k-ε, RNG k-ε, SST $k-\omega$ and SST-Transition. They found that all cases show good agreement with experimental measurements obtained using particle image velocimetry.

This study examines the effects of individual upper airway anatomical features (i.e. the uvula, epiglottis and soft palate), on drug deposition in the human airway by systematically removing these features from a geometrically realistic pharynx derived from human MRI images. Only one specific feature of each model is removed at a time, thereby keeping the inflow and outflow conditions fixed and all other features of the geometry fixed. This results in six different models, and together with a USP computational model for validation purposes, 7 models are

investigated in this current study. With the soft palate removed, the study geometry resembles some existing idealized throat models. We hypothesized that removing the soft palate would result in the least number of particles deposited in the airway and that each of the anatomical features investigated would have varying degrees of impact on the fluid mechanics in the airway, which in turn can cause variation in deposition behaviour between the different model's geometries.

3.2 Methods:

3.2.1 Computational models

A three-dimensional (3D) upper airway model was reconstructed from MRI images of a healthy human (Female, aged 56, BMI 21.5 ± 2.7) with no history of respiratory diseases using 3D Slicer (https://www.slicer.org/). Prior to the reconstruction, the images were visually scanned to ensure that anatomical details of the uvula, epiglottis and soft-palate region were sufficiently represented and were distinctive on the MRI images. A cube with a voxel size of 0.25 mm was utilized to generate an image stack (276 voxels*448 voxels*468 voxels) in 3D slicer. To generate the basic model that includes all the detailed anatomical features of the upper airway, specific airway boundaries surrounding the uvula, epiglottis and soft palate were carefully traced on 3D slicer for every MRI image slice.

As oral-only inhalation conditions are investigated in this work, the nasal cavity was removed. Six models were developed, including the basic model. The other five models were developed by ensuring that the upper airway boundaries were the same as the basic model except at the regions where some of the key anatomical features are situated, which were explicitly removed to produce variations of the pharynx model. The models generated are, 1.) A model without the uvula only, 2.) A model without the epiglottis only, 3.) A model without the uvula and epiglottis, 4.) A model without the soft palate, and 5.) A model without the soft palate and epiglottis. All the models were then exported to Rhinoceros (Rhino 7, Robert McNeel&Associates, Seattle, Washington), where the poly-surfaces, inlet and outlet were generated before they were exported as STL files to Ansys (2021R1, Canonsburg, Pennsylvania, United States) for meshing and simulations. The six different airway geometries are shown in Figure 3.1.

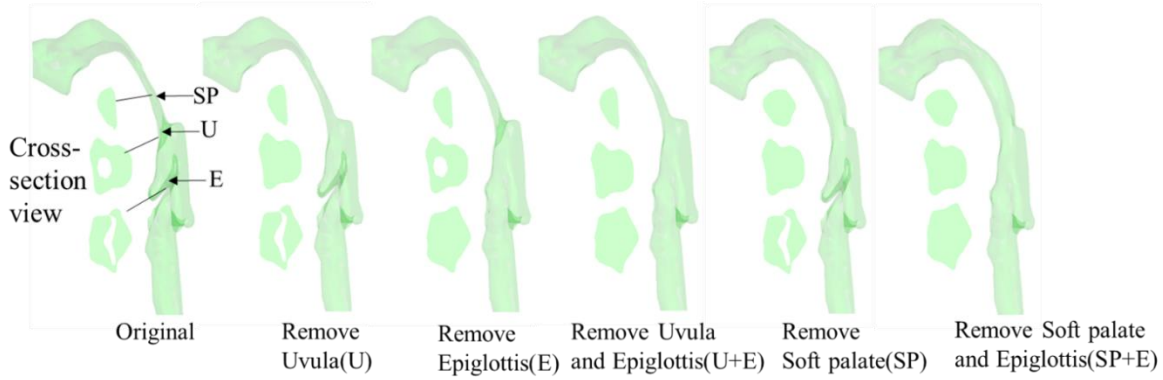

Figure 3. 1: The original pharynx model (far left) and five other models with specific airway anatomical features removed from the original model (Soft palate: SP, Uvula: U, Epiglottis: E).

3.2.2 Numerical method

The mesh of all six models was generated using ICEM-CFD in the commercial software ANSYS workbench (2021 R1, Canonsburg, Pennsylvania, United States). Steady-state conditions were considered in this study, with flowrates of 40LPM and 70LPM prescribed at the inlet. The average flow behaviour is generally governed by the Reynolds averaged Navier-Stokes (NS) equations. The momentum equation is presented in its general form for completeness, but the time-dependent term was omitted in the steady-state simulations conducted in this study.

$$\nabla \cdot (\bar{u}) = 0$$

$$\rho \frac{\partial(\bar{u})}{\partial t} + \rho \nabla \cdot (\bar{u}\bar{u}) = -\nabla \mathrm{P} + \nabla \cdot (\tau) + \rho g + \rho \nabla \cdot (-\overline{u' u'})$$

where ρ is the fluid density, τ is the fluid viscous stress tensor and $\bar{u}$ is the fluid mean velocity, respectively. P is the pressure, and g is the gravitational acceleration. The $k-\omega$ SST numerical scheme was used to model the turbulent scales. Previous studies(Shang et al., 2019; Xu et al., 2020) have demonstrated the accuracy of simulating the flow and particle transport in the human airway using the $k-\omega$ SST model.

In the DPM model, all particles are treated as Lagrangian point particles, and the force was analysed in Cartesian coordinates(F. Huang et al., 2021). The equations are described as follows:

$$\frac{d(u_p)}{dt} = F_D(u - u_p) + \frac{g(\rho_p - \rho)}{\rho_p}$$

$$F_D = \frac{3\mu C_D Re}{4\rho_p d_p^2}$$

$$Re = \frac{\rho d_p |u_p - u|}{\mu}$$

$$C_D = a_1 + \frac{a_2}{Re} + \frac{a_3}{Re^2}$$

Where u is the velocity, μ is the dynamic viscosity, and ρ is the density, u_p, ρ_p, d_p are the velocity, density and diameter of particles, Re is the Reynolds number, C_D is the drag coefficient, g is the acceleration of gravity and a_1, a_2, a_3 are constants determined by the Re.

Tetrahedral and Hexahedral meshes were generated in ICEM-CFD, and three inflation layers were generated using near-wall prism layers. The mesh was subsequently converted into advanced cells (Polyhedral) in ANSYS Fluent (2021R1, Canonsburg, Pennsylvania, United States). Mesh independence testing was conducted for models with 1, 2, 4, and 8 million mesh elements, and velocity profiles averaged across planes at the pharynx, epiglottis, and trachea regions were monitored to assess flow characteristics. The difference in velocity between the models with 4 and 8 million mesh elements was less than 5%, indicating that the results are independent of the mesh size. Therefore, the model with 4 million mesh elements was selected for all the simulations. Mono-dispersed particles (3 μm) were implemented and prescribed at the inlet surface. The discrete random walk model was enabled in the studies, which also enabled easier control of the injected number of particles prescribed at the inlet.

A particle number independence test was also conducted to ensure that the regional deposition results are also consistent regardless of the simulated particle numbers. Particle numbers of 1000, 2000, 5000, 10000 and 20000 were investigated. The particle deposition fraction (particles deposited in the airway/total number of injected particles) was similar for the 10000 and 20000 particles, and hence, 10000 particles were used for all the other simulations. In this current work, velocity has been prescribed at the inlet of the airway to generate flow, with a zero gauge pressure outlet. Boundary conditions to generate flow by setting pressure difference across the flow domain have been presented by Shang et al.(Shang et al., 2019). Previous work(Bingjie Ma et al., 2020; Zhao et al., 2020) demonstrated that comparisons between experimental flow-field data (from PIV) and CFD predictions based on boundary conditions like those deployed here provide a reasonable estimate of the average flow-field. The inlet

surface area (196.9 mm^2) was measured in ANSYS SpaceClaim, and the velocities associated with the inlet flow rate of 40LPM and 70LPM were prescribed at the inlet of all the six airway models. Preliminary simulations were performed to compare monodisperse and polydisperse simulation outcomes. Given the very narrow size distribution of Mannitol, including polydispersity did not significantly change the outcomes of this study and therefore for simplicity, and to focus only the effects of anatomical changes, the manuscript presents data from monodisperse simulations only. The direction of gravity is specified such that it is perpendicular to the outlet surface and towards the ground. Trap condition was prescribed at the boundaries of the airway wall, and all particles were allowed to escape from the outlet. The data was exported from Fluent and then post-processed in CFD-post.

3.3 Results

3.3.1 Validation of computational models

The numerical scheme and settings prescribed in the model were validated by comparing simulations of a USP throat computational model with published experimental data (Shaokoon Cheng et al., 2019) on Mannitol. A Rosin Rammler function (M. S. Islam et al., 2018; Shrestha et al., 2022) was used to model the particle size distribution of Mannitol in Fluent, and the particles were prescribed randomly at the inlet of the USP computational model. The results of Figure 3.2 show that the deposition fraction in the USP computational model matches well with the experimental data, and differences are less than 5% for all flow rates conducted, demonstrating the fidelity of the computational model and numerical schemes in estimating particle deposition in the airway.

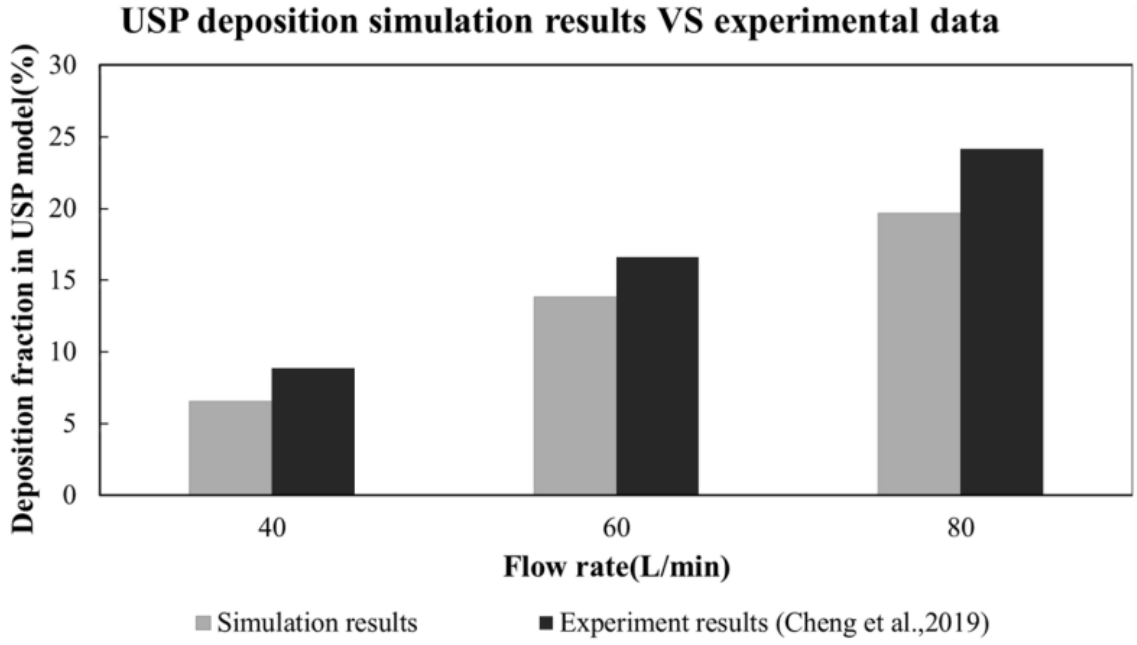

Figure 3. 2: Computational model validation with experiment results.

3.3.2 Effects of upper airway anatomical structures on average velocity

This section discusses how specific anatomical structures affect flow characteristics in the pharynx models. A steady-state flow rate of 40LPM was prescribed at the inlet of the airway. Figure 3.3(a) shows the change in average velocity (spatial average at each cutting plane shown) at different specific locations of the airway (P1 – P7). Specifically, two of the locations are at the oral cavity, and five of the locations are spread at equal distances along the oropharynx and laryngopharynx region, with one of them placed at the tip of the epiglottis (P5) to study the effects of this anatomical structure on airflow dynamics. The average velocities analyzed at planes perpendicular to the airway path length in all the models, range between 2m/s to 29m/s except for the models without the soft palate. In the models without the soft palate, the maximum average velocity analyzed across the 7 locations is 5m/s which is 5 fold less than the models with the soft palate, demonstrating the effects of this anatomical structure and the implication of widening the airway at this region of the pharynx (P3 – P4). In addition to the difference in average velocity, the location of the first peak of the highest average velocity can be found between P3 and P4 in the models without the soft palate, which is further upstream of the airway compared to those models with the soft palate, where the location of the highest

average velocity is consistently at P4. The presence of the soft palate appears to significantly impact flow adjacent to this structure from P2 to P5, and has a lesser impact on the flow dynamics downstream, where the average velocity in all models appear to converge to a range between 5m/s to 10m/s at P5 which decreases further to between 2m/s and 5m/s at P6. The distal section of the airway is the tracheal, which has geometry that has not been altered in any of the models. The average velocity is ~ 10m/s at the distal end of the airway, and this is consistent in all models, demonstrating that regardless of the upstream change in anatomical features, the flow re-develops in the tracheal region.

Figure 3.3(b) shows the normalized change in average velocity (normalising against the original airway geometry, i.e. altered model velocity/original model velocity) at the 7 different locations, with the effects of both the uvula and epiglottis being clearer. Removing the uvula appears to have varying effects on the average velocity downstream of the structure. In the model where only the uvula is removed, the average velocity is ~ 2 to 3 fold higher than the original geometry. The further exclusion of the epiglottis appears to have the effect of reducing the impact associated with the sole absence of the uvula, such that the average velocity profiles are similar to the original geometry, with the maximum variation being only as high as ~ 10% at P5. The impact related to the sole exclusion of the epiglottis is apparently lesser than when only the uvula is removed in terms of the change in average velocity normalized against the results of the original model. Removing the epiglottis reduces the average velocity by ~30% at P5, where the tip of the epiglottis lies, and increases the average velocity by ~20% further downstream of the anatomical structure (P6), when compared to the original airway geometry. In the model without the soft palate, further exclusion of the epiglottis leads to a ~30% drop in average velocity at P6. Hence, depending on the original configuration of the pharynx, the inclusion of the epiglottis will produce variable effects on the average velocity downstream of this anatomical structure. The results also suggest that the uvula can have a significant impact on the local behaviour of the flow.

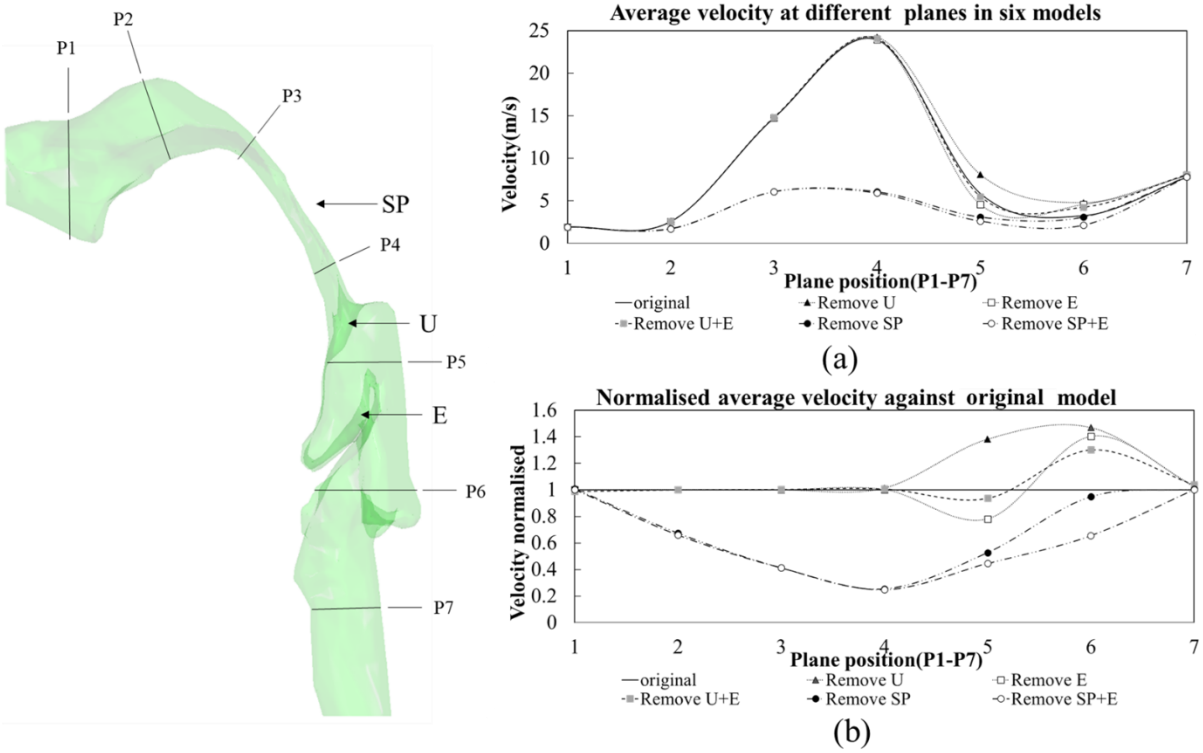

Figure 3. 3: Average velocity in the six pharynx models with different anatomical features removed. Panel (a): Average velocity at different planes (P1 – P7; see figure on the left) in the six pharynx models. Panel (b): Average velocity normalised against the velocity in the original model at the same plane. (Soft palate: SP, Uvula: U, Epiglottis: E).

3.3.3 Effects of upper airway anatomical structures on the velocity field, flow bifurcation, streamlines, and turbulent kinetic energy

Figure 3.4 shows the mean velocity magnitude in the midsagittal planes of the six different mouth throat models under 40LPM inhalation flow conditions. The results show that the maximum velocity in all the models occurs at the soft palate region, which has the narrowest cross-sectional area at this section of the airway for all the models. These results are also consistent with the data presented in figure 3(a), which demonstrate that the highest maximum average velocity occurs near P4, a location that is slightly upstream of the uvula. The commonly reported jet flow phenomenon adjacent to the epiglottis (Zhao et al., 2020) is apparent in the original model, though clearer in the model without the soft palate (but with the

epiglottis). This may be related to a more significant flow convergence as it arrives at the epiglottis, though this must be subject to further investigation.

Results from the vector fields presented in the coronal plane (Figure 4(b)) show that the epiglottis and uvula are anatomical features in the original pharynx model that can cause flow bifurcation. The vectors were three-dimensional and were plotted on a 2D plane (orthogonal to the airway path length) for clarity. There are three distinctive flow bifurcation zones in the original airway model - one situated at the uvula (See circle inset), and the other two at the aryepiglottic folds (See top of the square inset in Fig 4(b)) along the supraglottic section of the airway. The exclusion of the uvula from the original pharynx geometry is associated with non-symmetrical flow separation at the uvula structure, which becomes more apparent in the model that excludes the epiglottis only. Flow bifurcation is less obvious in the models without both the uvula and epiglottis and the two other models where the soft palate is removed.

Figure 3.4(c) shows the flow streamlines in the mid-sagittal plane. There is a small recirculation zone at the tip of the tongue, with the intensity of the recirculating flow being slightly different between the models. This observation is minor and suggests how airway structures downstream of the airway might affect airflow dynamics upstream in the oral cavity. Traces of recirculating flows are prominent in all the models and in the models without the soft palate; recirculating flow anterior to the epiglottis is notable, which appears to be more intense when the epiglottis is removed.

The results of Figure 3.4(d) show how subtle changes in the original geometry, such as removing the epiglottis or uvula, can significantly impact the turbulent kinetic energy. When the oral space downstream of the oral cavity is widened, such as in those models where the soft palate is removed, high turbulent kinetic energy is less localized in the oropharynx and appears to linger along the entire section of the airway caudal to the uvula.

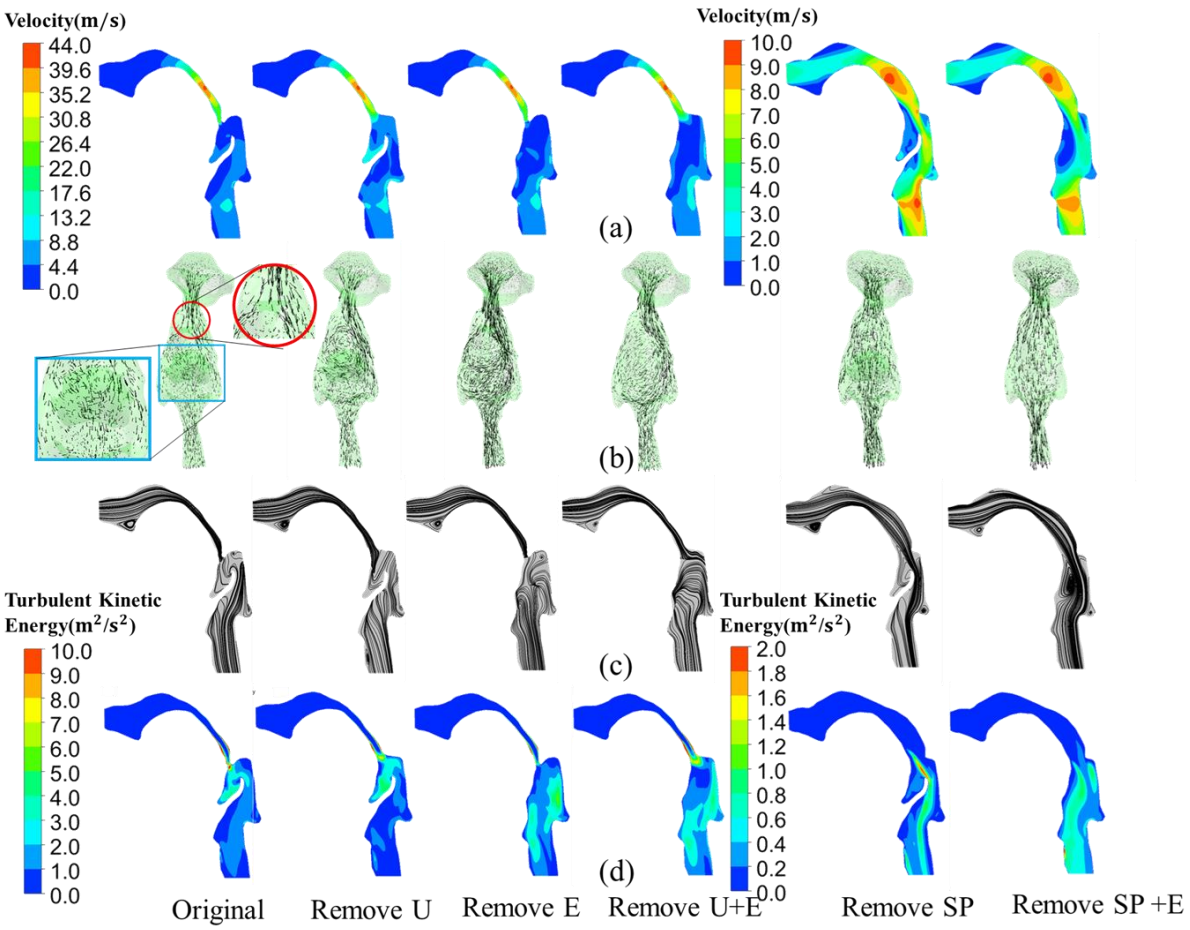

Figure 3. 4: Velocity field (a), flow bifurcation (b), streamlines(c), and turbulent kinetic energy (d) in the six upper airway models.

3.3.4 Effects of upper airway anatomical structures on particle deposition at two different flow rates.

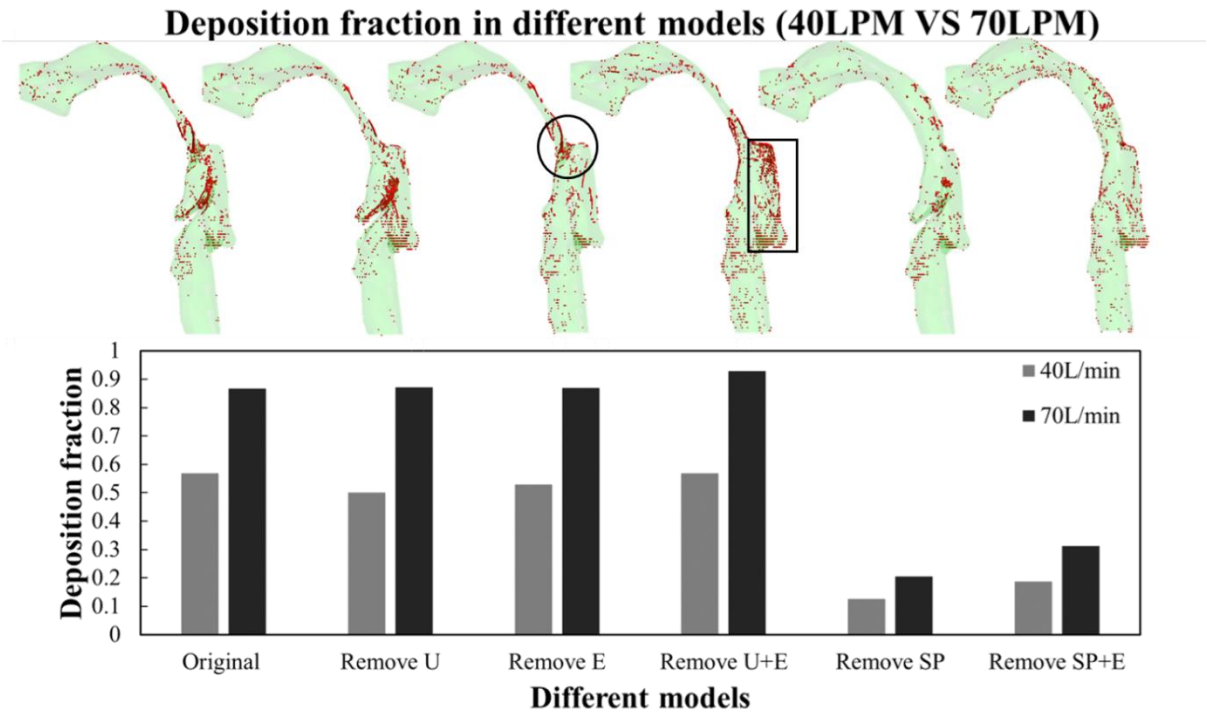

Figure 3. 5: Overall deposition in different models at 40LPM and 70LPM flow rates

Figure 3.5 shows the results of the simulated deposition fraction in the upper airway based on 3um sized monodisperse particles and at flow rates of 40LPM and 70LPM. The locations of the deposited particles and their regions of concentration can also be observed in figure 3.5 (e.g. see circled and squared airway insets). Particle deposition is higher in the high flow rate cases for all the six models, and deposition efficiency is ~90%, which is the highest in the model without both the uvula and epiglottis. Results from the model without both the uvula and epiglottis demonstrate that the absence of protruding anatomical structures increases the number of particles trapped in the pharynx, at least based on the particle size and geometry of the pharynx investigated this study. Fig. 4 demonstrated a high-velocity region of flow diverted towards the back pharyngeal wall of the airway with no uvula or epiglottis (with minimal flow bifurcation), which results in an increase in deposition in that region (as also evident through the airway inset shown in Fig. 5). In contrast with the model with the sole exclusion of the epiglottis, despite the presence of traces of large recirculating regions, the flow appears to have

been disrupted at the lower half of the oropharynx. However, widening the airway space substantially above the oropharynx, which is represented by models without the soft palate, affects particle deposition and reduces the deposition fraction by 36% compared with the original model. The concurrent removal of the epiglottis with the soft palate did not result in an increase, but a further decrease in particles deposited in the airway for both flow rates. A volume threshold of the space where the soft palate is situated, above which significant reduction in the overall particles deposition in the pharynx can be observed, merits further investigation.

As can be noted from Figure 3.5, the locations of concentrated particle deposition are different between the models that include the soft palate despite them having similar total particle deposition in the pharynx. When only the epiglottis is removed from the original model, particles are concentrated at the uvula (see circle inset) region. Removal of the uvula tip and the epiglottis results in a dramatically higher deposition at the back of the oropharynx (see rectangle inset) and a slightly higher deposition at the oral cavity. Finally, the concurrent absence of both the soft palate and epiglottis is associated with particle deposition characteristics that appear to be the most homogeneously distributed throughout the airway inner walls and, unlike the other models, concentrated regions of particles deposition is the least apparent in this airway model.

The exact amount of particles deposited in the upper airway for all models analyzed at five different sections along the pharynx (See top right figure inset in Figure 3.6) is shown in figure 3.6 for the two different flow rates investigated in this current work. As noted from the figure, the number of particles deposited along the trachea is consistently low and is not affected by any changes in upper airway geometries upstream. Based on the average percentage of particles deposited in the upper airway, analyzed for all the 6 models, particle deposition at the oral cavity (mouth) is the second-lowest after the trachea. According to the standard deviation (error bars) presented in the figure, particles deposited along the airway section where the soft palate is located vary the least despite being removed in two models. Significant variation in the deposition fraction amongst the models is noted in the epiglottis region.

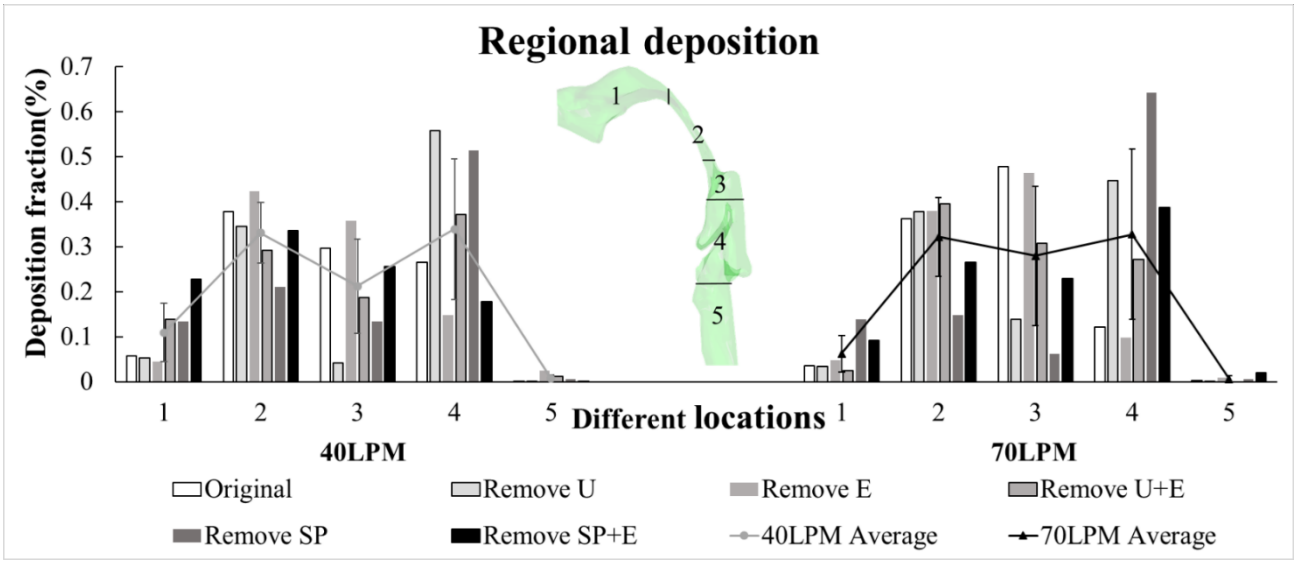

Figure 3. 6: Regional depositions in different models under 40LPM and 70LPM.

3.3.4 Effect of the BMI

The examination of the impact of anatomical features is conducted using a high BMI airway model. Although the removal of different anatomical features, particularly the soft palate, may result in different BMI models, it could be argued that this study is confined to a single subject. As such, the conclusions run the risk of either exaggerating or downplaying the effects of specific features by focusing solely on one individual. Therefore, this section examines a different airway model with a relatively low BMI (20.4 kg/m^2) compared to the high BMI (39.5 kg/m^2) model, in order to investigate the effect of anatomical fractures on intersubject differences and to ensure that the conclusion is consistent across various airway models with different BMI values.

Based on the study of the high BMI model, it is evident that the soft palate plays a significant role in drug deposition in the upper airway region. Removal of the soft palate will result in considerable changes to flow behavior in the upper airway, leading to a dramatic reduction in deposition in the extrathoracic region. Additionally, it is worth noting that the epiglottis also plays a major role in inducing symmetry in airflow within the human upper airway. Three variations of low BMI airway models, including the original (no features removed), Remove E (epiglottis removed), and Remove SP (soft palate removed), have been investigated. The velocity field, flow bifurcation, streamlines, and turbulent kinetic energy in these three upper airway models are shown in Figure 3.7.

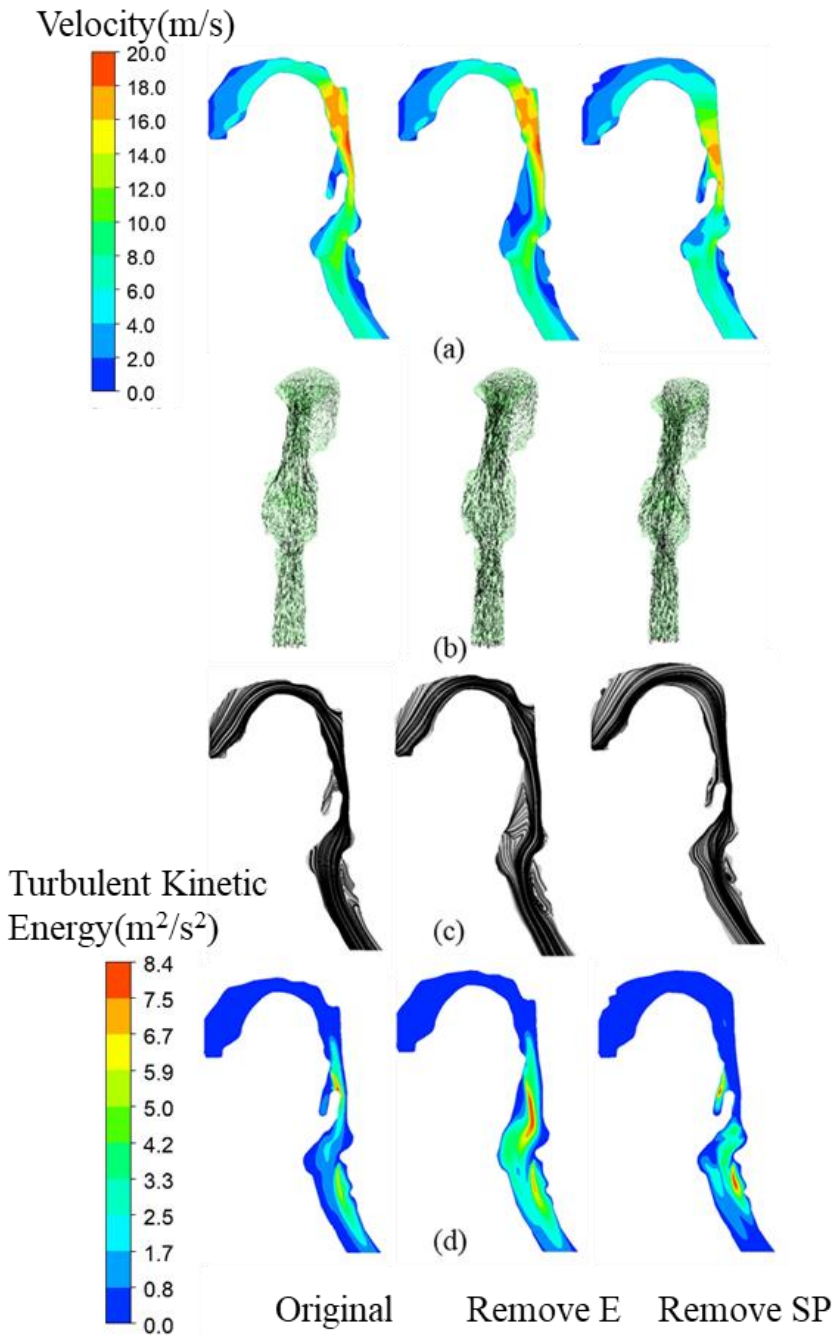

Figure 3. 7: Velocity field (a), flow bifurcation (b), streamlines(c), and turbulent kinetic energy (d) in the three upper airway models with low BMI values.

Figure 3. 7 (a) indicates the mean velocity magnitude in the midsagittal planes of the three different upper airway models with a low BMI value at flow rates of 40LPM. The results indicate that the maximum velocity occurs above the epiglottis and at the tongue base region. This differs slightly from the high BMI model, where the maximum velocity occurs in the soft palate region, as shown in Figure 3.3. This difference may be attributed to the movement and positioning of the tongue in these two cases (Bingjie Ma et al., 2020). Furthermore, the removal

of the soft palate appears to decrease localized velocity variations compared to the original model. This suggests the soft palate play critical roles in modulating airflow speed. The three-dimensional vectors, which were plotted on a 2D plane along the supraglottic section of the airway, are depicted in Fig. 7 (b). A minor flow bifurcation is observed in the original model, which becomes less apparent with the removal of the soft palate. Additionally, non-symmetrical flow is seen near below the tongue base when the epiglottis is removed.

Figure 3. 7 (c) illustrates the flow streamlines in the mid-sagittal plane. The recirculating flow posterior to the epiglottis is notable, and it appears to be more intense when the soft palate is removed. Furthermore, the intensity of the recirculating flow increases in the epiglottis region when the epiglottis itself is removed. Fig. 7 (d) shows the turbulent kinetic energy in the mid-sagittal plane. The results indicate that removing the epiglottis and the soft palate can significantly influence the distribution of higher turbulent kinetic energy. Lower turbulence can have an impact on the deposition patterns of particles (Guha, 2008), and changes in turbulent kinetic energy may consequently affect regional deposition.

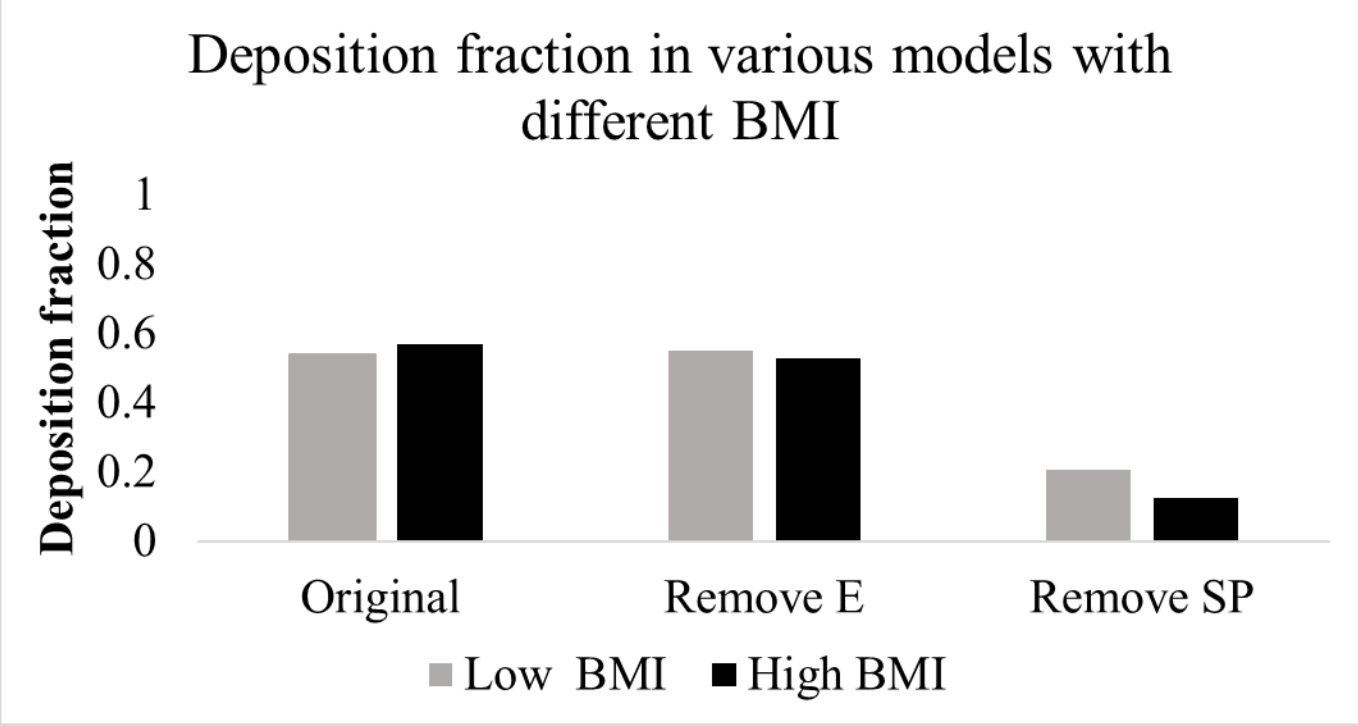

Figure 3. 8: Deposition fraction in the three upper airway models with different BMI values.

Figure 3.8 illustrates the simulated deposition fraction in the upper airway, based on 3um sized monodisperse particles under inhalation flow conditions of 40 LPM, in three upper airway models with different BMI values. After removing the soft palate (widening the airway space

substantially above the oropharynx), there is a 33.38% reduction in deposition fraction compared to the original model with low BMI (53.98%). This trend remains consistent across different BMI models, indicating a significant decrease in deposition fraction when the soft palate is removed. However, the removal of the epiglottis has little effect on overall drug deposition in the airway for different BMI cases.

When the soft palate is removed, there is a significant reduction in deposition fraction across different BMI models. This provides us with confidence in the findings of our present study. In the initial segment of the airway, inertial impaction plays a pivotal role. Drug particles have enough momentum to sustain their path despite alterations in airflow direction, causing them to collide with airway walls (Carvalho et al., 2011). The soft palate region is where the airflow significantly changes direction, typically from horizontal to perpendicular (Matsuo et al., 2010). Constriction in this area can significantly increase local velocity, while expansion could potentially decrease local velocity and, therefore, reduce deposition caused by inertial impaction.

Additionally, an interesting phenomenon is that the deposition fraction of particles in different original models at both high BMI and low BMI cases appears to be similar. In the individual with a high BMI, the narrowest region is located near the soft palate above the middle of the tongue. Conversely, in cases of low BMI, the narrowest region is situated near the base of the tongue. A prior study examined the impact of lingual fat on airway flow dynamics and particle deposition, revealing that pharyngeal narrowing with increased BMI, may alter airflow patterns and particle deposition in the upper airway (Bingjie Ma et al., 2020). Additionally, Xi and Yang (2019) also argued that different tongue positions will significant affect the airflow pattern and particle motions. This similarity in deposition fraction may be attributed to variations in airway structure among individuals, particularly in relation to the movement of the tongue. Further research is necessary to investigate the impact of tongue movement during the administration of pharmaceutical aerosols. That said, despite some changes in regional flow behaviour, generally speaking the overall conclusions with respect to the role of the soft palate are unaffected by the change in BMI.

3.4 Discussion

Despite the wide consensus that pharynx geometry can significantly impact deposition efficiency (Grgic, Finlay, et al., 2004b; Conor A. Ruzycki et al., 2017), there is a general lack of understanding of how key anatomical structures in the upper airway may affect particle deposition. To the best of the authors' knowledge, this is one of few studies demonstrating how the exclusion of specific anatomical features in a realistic upper airway could affect flow and regional deposition and the potential mechanisms underpinning those observations. The two primary findings generated through this study is that the space above the oropharynx, where the soft palate is located, is the most critical airway feature out of the three investigated (uvula, epiglottis and soft palate), that could have a significant impact on particle deposition efficiencies in an airway replica. Secondly, the underpinning mechanism appears to be related to the overall dynamics of the flow and specifically to the possibility for recirculating flows to develop and persist over time in the replica.

Whilst the soft palate results in large changes to the overall deposition fraction, other anatomical features can influence flow and regional deposition fraction significantly. The uvula and epiglottis appear to have the effect of enabling a symmetrical flow to be developed in the airway, despite the airway geometry being inherently non-symmetrical along the midsagittal plane. The removal of the uvula or epiglottis can lead to a less homogenized flow pattern with a flow that is more concentrated on one side of the airway. Removal of such anatomical features can also result in changes in flow diversion towards the back pharyngeal wall, which can significantly impact deposition, as was observed upon removal of the epiglottis and uvula. A few key observations can be drawn when observing how regional deposition is affected by differences in the pharynx geometry, which are also consistent for both flow rates. These observations are, i) the largest increase in regional deposition fraction from the region of the uvula to the epiglottis region is noted for the models without the uvula and without the soft palate and ii) the deposition fraction at the region of the uvula is always highest for the original model and the model without the epiglottis. The former observation is simply indicative of the controlling role that the uvula and epiglottis have in the flow (and hence deposition) in the oropharynx (back of tongue). Other changes to the airway models have less of an effect in that region as the removed features are either located upstream or downstream of that airway section between the uvula and epiglottis. The latter observation merits further study, but results from this current study provide evidence that the change in flowrate has more of an effect on some

airway regions than others. Whilst changes in regional deposition fraction are noteable, overall deposition fraction was most affected in models without the soft palate.

The current study demonstrates that the numerical scheme used to predict the number of particles deposited in the USP throat as a validation exercise is accurate, and while the walls of the USP computational models are set at a "trap" condition some particles may bounce off from a physical USP replica which is not accounted for here. However, there is clear evidence from the literature showing that such discrepancies may be minor for 3um size particles, and hence the "trap" settings prescribed to the model should not affect the outcome of this study. For example, in a well-known study, Y. Zhou et al. (2011) conducted physical experimentation on solid particle deposition in grease coated and uncoated USP throat using a range of flow rates. The deposition fraction in the upper airway for the 3um size particles is similar in the case with grease and without grease experimental configurations. This current study also shows that particle deposition is higher with a higher flow rate, consistent with existing in-vitro and in-vivo work (Shaokoon Cheng et al., 2019; F. Huang et al., 2021). It would be useful to provide further evidence on the accuracy of these results by using in-vivo comparisons, given that the original airway model used in this study is geometrically realistic and reconstructed from MRI data. Michael Y. Yang et al. (2017) performed an in-vivo lung deposition study using SPECT-CT and with mannitol particles with a mass medium aerodynamic diameter of 3um, which is close to the size of the particles simulated in this current work. Michael Y. Yang et al. (2017) show that lung deposition in eight human subjects is consistently higher when breathing through an osmohaler at low flow rate, and there is higher throat deposition in the subjects when breathing through the inhaler at a high flow rate. The amount of lung deposition in the study ranges between 10 – 50% in the subject cohort for a flow rate of between 50 – 70 LPM, and hence suggest that deposition in the inhaler and throat combined ranged between 50% to 90% based on the range of flow rate investigated. These results correspond very well with the deposition result of the "original" geometry in this current study, where particle deposition is ~ 50% and 84% for the 40LPM and 70LPM flow rate cases, respectively.

In this current study, the in-plane average velocity at different sections of the airway is analyzed. The results presented in the current work match with several existing works (Bingjie Ma et al., 2020; Xi & Longest, 2007). A recent work on the effects of airway wall motion on airway flow dynamics (Zhao et al., 2020) shows that pharynx tissue motion during inspiration could potentially reduce high-speed flow at the oropharynx, and results from the current work suggest that the effect of jet flow could also be reduced by expanding the space where the soft palate

is situated. Xi and Longest (2007) performed CFD on a pseudo-realistic pharyngeal model with a fairly large volumetric airway space between the oral cavity and the oropharynx, analogous to the model that is without the soft palate and the protruding epiglottis structure presented in this current work. Xi et al. (Xi & Longest, 2007) showed that the in-plane velocity in the airway has a magnitude that ranges between ~ 0.5m/s to 4.5m/s, and these results, along with the locations of concentrated particle deposition associated with the flow, are both consistent with the observations presented in this current study. Increasing the space where the soft palate is situated is likely to decrease the overall particle deposition in the airway, and this could be realistically achieved by deliberately advancing the mandible while concurrently positioning the tongue carefully such that it does not occlude the airway when biting on inhalers. Results from existing work (P. G. Koullapis et al., 2016; Z. Zhang & Kleinstreuer, 2004) have demonstrated that the above method is associated with fewer particles deposited in the airway, which is consistent with the results presented in this current work.

While this is one of very few studies that systematically isolate the effects of how key anatomical structures in a geometrically realistic human pharynx may contribute to particle deposition in the airway, several parametric studies have been undertaken in the literature to investigate how dimensions of the upper airway could affect deposition. For example, Xi et al. (2014) studied the effects of total airway volume, oral cavity volume, airway curvature, glottic cross-sectional area and total surface area on particle deposition using a pseudo-realistic mouth throat model. Results from that study show that the cross-sectional area of the airway is the most predominant factor that affects deposition with high deposition associated with smaller areas, and the effect is the most apparent for medium-sized particles ranging between 6 – 12 um. It is worth noting that changes in the cross-sectional area in the models are made consistent at different sections along the oropharynx and up to the level of the epiglottis, which is different from the present study, where the cross-section is altered by removing features of the airway, with removing the soft palate and epiglottis being the two cases that result in the largest change in cross-sectional area for the models investigated in this study. Results from this current work corroborated well with the work of Xi et al. (2014) by demonstrating a three-fold increase in deposition when the cross-sectional area where the soft palate is situated is halved through the explicit removal of this airway feature. However, particle deposition presented in this current work is ~ 8 times higher compared to Xi et al. (2014), and this is likely related to the inherent difference in pharynx geometry between the two studies.

Results from this current study suggest that all three airway replicas (USP, VCU and the AIT throat) are appropriate induction ports for cascade impaction studies as they replicate certain realistic features that are present in human airways. Our results show that the airway anatomical features integrated in the AIT model are particularly appropriate despite it being an idealized model that has excluded some anatomical features such as the uvula. This is because our work demonstrates that one of the key airway anatomical features, the soft palate, which the AIT model has, is likely to enable it to replicate in-vivo particle deposition accurately. This is also a plausible explanation as to why low particle deposition is commonly associated with the VCU and USP throat. It is important to note, though, that the space where the soft palate is located is likely variable between humans when they bite on inhalers which can be further complicated by tongue positioning, and when using inhalers with different mouthpiece sizes. Hence, while the AIT throat model may best produce physiologically realistic and relevant particles deposition in the airway for some conditions, further studies to investigate how a range of airway geometries obtained with subjects biting on different inhaler mouthpiece sizes may be best presented by a single airway replica is merited.

3.5 Limitations

There are several inherent limitations with the design of this current study that should be carefully considered when interpreting the results. First, the results from this study have been produced with monodisperse particles of only a given size and at a constant flow rate, both of which are non-realistic but were prescribed intentionally nonetheless, to remove any complexities associated with transient flow conditions and polydisperse distributions. Second, upper airway tissue motion has been a recent subject of interest, which has been demonstrated to have an impact on airflow dynamics. The modelling of dynamic wall behaviour, which includes the passive collapse of the airway, may influence the results variably for each model, and this warrants further investigation. Finally, it is important to remember that the extent to which how the uvula and epiglottis affect the flow dynamics and particle deposition characteristics are specific to the model representing the original airway geometry in the human subject. These structures are known to occlude the pharynx variably between humans and may be affected by body mass index (Shaokoon Cheng et al., 2014). Hence, the exclusion of these anatomical structures could result in more dramatic differences compared to the base model, further highlighting their importance in defining particle deposition in the human airway, which is not within the scope of this current study, and could be investigated in future work.

3.6 Conclusions

The effects that certain anatomical features in the upper airway have on drug particle deposition in the human upper airway have been investigated by using a coupled Eulerian-Lagrangian (RANS/DPM) CFD model. The flow field variation and drug deposition behaviour have been analysed. The soft palate is a major determining factor that dictates the overall throat deposition fraction in the human upper airway, and therefore models that do not include it are likely over-idealized. The findings generally demonstrate that the narrow region between the tongue and the soft palate is a key feature in dictating drug deposition. Additional specific conclusions follow below:

- The uvula and epiglottis both play a major role in inducing symmetry in airflow in the human upper airway
- The uvula and epiglottis alter local airflow behaviour and therefore affect regional deposition but do not significantly affect the overall deposition fraction in the airway for the conditions simulated
- Removing the soft-palate will considerably change the flow behaviour in the upper airway and dramatically reduce the deposition in the extrathoracic region. The recommendation is therefore that models which include a soft palate region are preferred when it comes to the analysis of physiologically realistic drug deposition behaviour.
- The removal of a particular physiological feature alters the local flow behaviour, which changes deposition in the upper airway. This effect seems to have a greater influence than a change in flowrate on regional deposition, though further work is required to substantiate this over a broader range of conditions.

Acknowledgement.

Funding for the research was made possible, in part, by the Australian Research Council through grant LP190100511. All authors have participated and contributed to the research, data analysis and preparation of the final version of this paper.

3.7 Appendix

This appendix provides further detail on the quality of the mesh chosen for simulations (see Figure 3.A1) as well as data demonstrating the mesh independence testing. Results from mesh independence testing are shown in Figure 3.A2 and demonstrate independence of the velocity profile with the mesh density at various locations along the airway model.

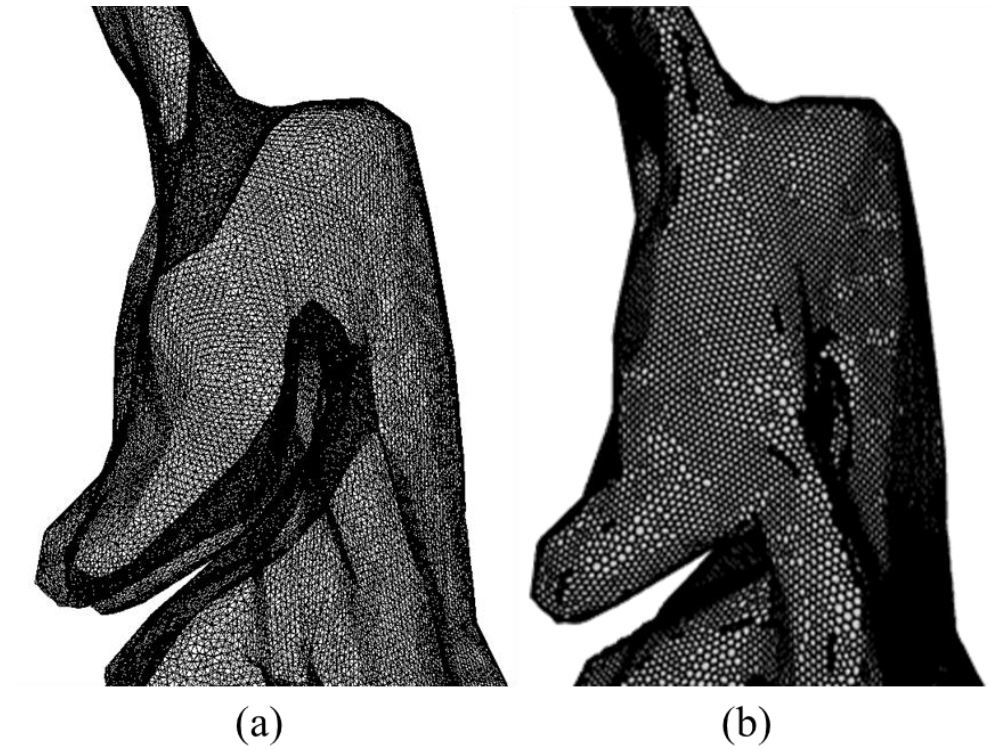

Figure 3. A. 1: Quality of mesh at uvula and epiglottis region (a):Tetrahedral and Hexahedral mesh and (b): Polyhedral mesh.

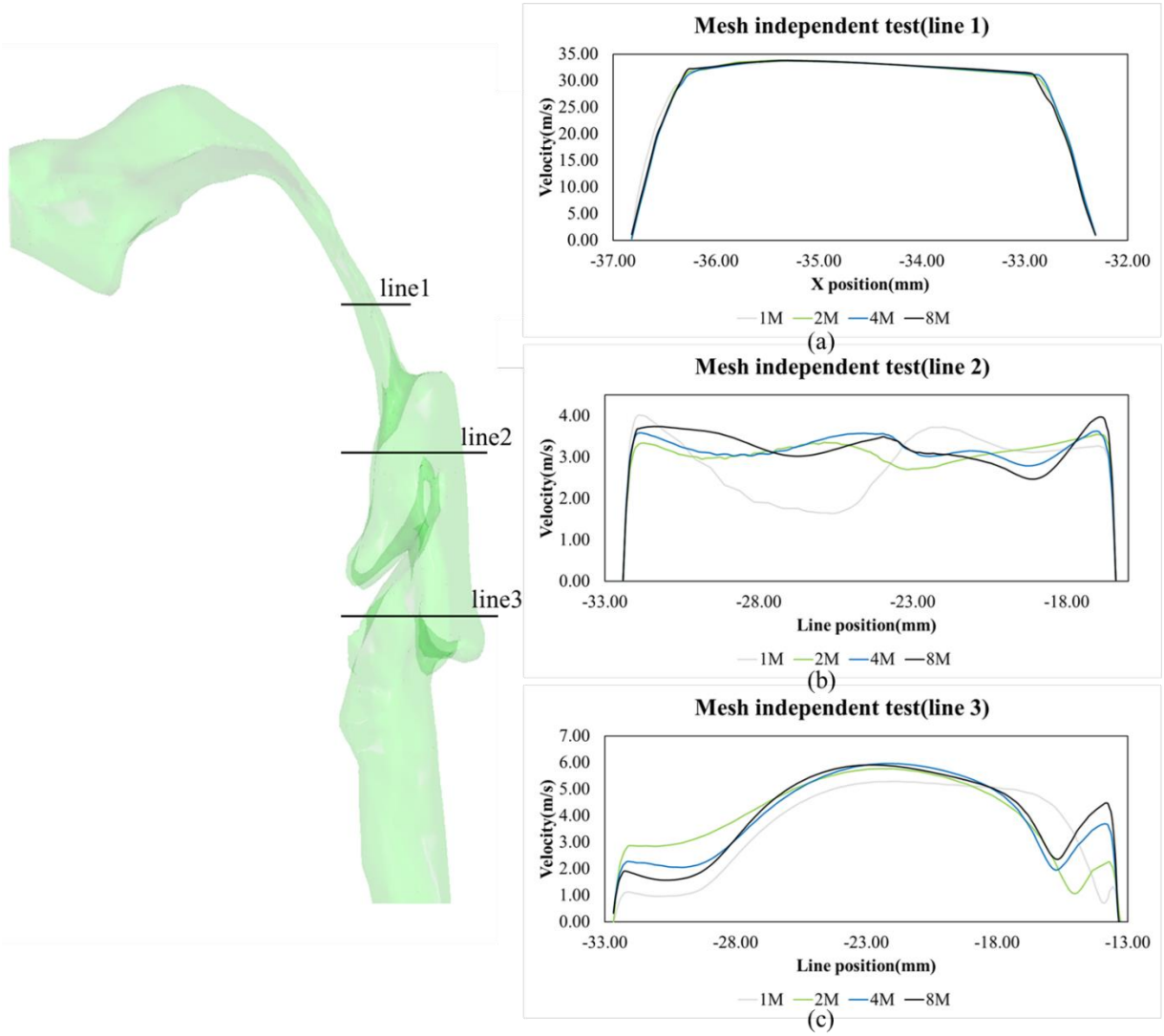

Figure 3. A. 2: Mesh independent test at line 1(a), line 2(b), line 3(c).

3.8 References for Chapter 3

1. Nurmagambetov, T., R. Kuwahara, and P. Garbe, *The economic burden of asthma in the United States, 2008–2013.* Annals of the American Thoracic Society, 2018. **15**(3): p. 348-356.
2. Usmani, O.S., *Choosing the right inhaler for your asthma or COPD patient.* Therapeutics and clinical risk management, 2019. **15**: p. 461.
3. Zhu, B., et al., *Disease burden of COPD in China: a systematic review*. International journal of chronic obstructive pulmonary disease, 2018. **13**: p. 1353.
4. Gayle, A.V., C. Minelli, and J.K. Quint, *Respiratory-related death in individuals with incident asthma and COPD: a competing risk analysis.* BMC Pulmonary Medicine, 2022. **22**(1): p. 28.
5. Dotan, Y., J.Y. So, and V. Kim, *Chronic bronchitis: where are we now?* Chronic Obstructive Pulmonary Diseases: Journal of the COPD Foundation, 2019. **6**(2): p. 178.
6. Manfrin, A., et al., *Better outcomes for everybody evaluates the effectiveness and cost-effectiveness of a pharmacist-led intervention, delivered by community pharmacists in*

collaboration with physicians, in improving disease control, compared with usual care, in asthma and COPD patients during and after COVID-19: A protocol for a pragmatic, parallel randomised controlled trial. Medicine: Case Reports and Study Protocols, 2021. **2**(9).
7. Gutiérrez Villegas, C., et al., *Cost analysis of chronic obstructive pulmonary disease (COPD): a systematic review*. Health Economics Review, 2021. **11**(1): p. 1-12.
8. Newman, S.P., *Delivering drugs to the lungs: The history of repurposing in the treatment of respiratory diseases.* Advanced drug delivery reviews, 2018. **133**: p. 5-18.
9. Cazzola, M., et al., *Advances in pulmonary drug delivery devices for the treatment of chronic obstructive pulmonary disease.* Expert opinion on drug delivery, 2020. **17**(5): p. 635-646.
10. Labiris, N.R. and M.B. Dolovich, *Pulmonary drug delivery. Part II: the role of inhalant delivery devices and drug formulations in therapeutic effectiveness of aerosolized medications.* British journal of clinical pharmacology, 2003. **56**(6): p. 600-612.
11. Newman, S.P., *Drug delivery to the lungs: challenges and opportunities.* Therapeutic delivery, 2017. **8**(8): p. 647-661.
12. Kourmatzis, A., S. Cheng, and H.K. Chan, *Airway geometry, airway flow, and particle measurement methods: implications on pulmonary drug delivery.* Expert opinion on drug delivery, 2018. **15**(3): p. 271-282.
13. Finlay, W.H., *The mechanics of inhaled pharmaceutical aerosols: an introduction*. 2001: Academic press.
14. Burchell, C., et al., *Effects of respiratory rate on the fluid mechanics of a reconstructed upper airway.* Medical Engineering & Physics, 2022. **100**: p. 103746.
15. Cheng, S., et al., *Movement of the tongue during normal breathing in awake healthy humans.* The Journal of physiology, 2008. **586**(17): p. 4283-4294.
16. Wagshul, M.E., et al., *Novel retrospective, respiratory-gating method enables 3D, high resolution, dynamic imaging of the upper airway during tidal breathing.* Magnetic resonance in medicine, 2013. **70**(6): p. 1580-1590.
17. Walsh, J.H., et al., *Evaluation of pharyngeal shape and size using anatomical optical coherence tomography in individuals with and without obstructive sleep apnoea.* Journal of sleep research, 2008. **17**(2): p. 230-238.
18. Tang, P., et al., *Does the United States Pharmacopeia throat introduce de-agglomeration of carrier-free powder from inhalers?* Pharmaceutical research, 2012. **29**(7): p. 1797-1807.
19. Xi, J., et al., *Parametric study on mouth–throat geometrical factors on deposition of orally inhaled aerosols.* Journal of Aerosol Science, 2016. **99**: p. 94-106.
20. Zhang, Y., T.L. Chia, and W.H. Finlay, *Experimental measurement and numerical study of particle deposition in highly idealized mouth-throat models.* Aerosol Science and Technology, 2006. **40**(5): p. 361-372.
21. Newman, S.P. and H.-K. Chan, *In vitro-in vivo correlations (IVIVCs) of deposition for drugs given by oral inhalation.* Advanced Drug Delivery Reviews, 2020. **167**: p. 135-147.
22. Kaviratna, A., et al., *Evaluation of bio-relevant mouth-throat models for characterization of metered dose inhalers.* AAPS PharmSciTech, 2019. **20**(3): p. 1-9.
23. Ung, K.T., et al., *Design of spray dried insulin microparticles to bypass deposition in the extrathoracic region and maximize total lung dose.* International Journal of Pharmaceutics, 2016. **511**(2): p. 1070-1079.
24. Wei, X., P.R. Byron, and P.W. Longest. *Predicting variations in lung dose with different mouth-throat models*.

25. Wei, X., et al., *In vitro tests for aerosol deposition. VI: realistic testing with different mouth–throat models and in vitro—in vivo correlations for a dry powder inhaler, metered dose inhaler, and soft mist inhaler.* Journal of aerosol medicine and pulmonary drug delivery, 2018. **31**(6): p. 358-371.
26. Wei, X. and P. Byron, *Clinically relevant in vitro performance tests for powder inhalers.* Respir. Drug Deliv. Asia, 2016. **1**: p. 111-120.
27. Longest, P.W., et al., *Use of computational fluid dynamics deposition modeling in respiratory drug delivery.* Expert opinion on drug delivery, 2019. **16**(1): p. 7-26.
28. Huang, F., et al., *Role of CFD based in silico modelling in establishing an in vitro-in vivo correlation of aerosol deposition in the respiratory tract.* Advanced Drug Delivery Reviews, 2021. **170**: p. 369-385.
29. Faizal, W.M., et al., *Computational fluid dynamics modelling of human upper airway: A review*. Computer Methods and Programs in Biomedicine, 2020. **196**: p. 105627.
30. Zhang, Z. and C. Kleinstreuer, *Computational analysis of airflow and nanoparticle deposition in a combined nasal–oral–tracheobronchial airway model.* Journal of Aerosol Science, 2011. **42**(3): p. 174-194.
31. Kim, Y.H., et al., *CFD modelling of air and particle flows in different airway models.* Journal of Aerosol Science, 2019. **134**: p. 14-28.
32. Zhang, Y., W.H. Finlay, and E.A. Matida, *Particle deposition measurements and numerical simulation in a highly idealized mouth–throat.* Journal of Aerosol Science, 2004. **35**(7): p. 789-803.
33. Ma, B., et al., *Potential effects of lingual fats on airway flow dynamics and particle deposition.* Aerosol Science and Technology, 2020. **54**(3): p. 321-331.
34. Ariyaratne, W.K.H., et al. *CFD approaches for modeling gas-solids multiphase flows–A review*. Linköping University Electronic Press.
35. Xu, X., et al., *Investigation of inhalation and exhalation flow pattern in a realistic human upper airway model by PIV experiments and CFD simulations.* Biomechanics and Modeling in Mechanobiology, 2020. **19**(5): p. 1679-1695.
36. Heenan, A.F., et al., *Experimental measurements and computational modeling of the flow field in an idealized human oropharynx.* Experiments in fluids, 2003. **35**(1): p. 70-84.
37. Huang, F., et al., *Numerical investigation of deposition mechanism in three mouth–throat models.* Powder Technology, 2021. **378**: p. 724-735.
38. Cheng, S., et al., *Does upper airway deformation affect drug deposition?* International Journal of Pharmaceutics, 2019. **572**: p. 118773.
39. Islam, M.S., et al., *Polydisperse microparticle transport and deposition to the terminal bronchioles in a heterogeneous vasculature tree.* Scientific reports, 2018. **8**(1): p. 1-9.
40. Shrestha, K., et al., *Effect of breathing profiles on nebuliser drug delivery targeting the paranasal sinuses in a post-operative nasal cavity.* Journal of Aerosol Science, 2022. **161**: p. 105913.
41. Zhao, Y., et al., *The effects of upper airway tissue motion on airflow dynamics.* Journal of biomechanics, 2020. **99**: p. 109506.
42. Ruzycki, C.A., et al., *Improved prediction of intersubject variability in extrathoracic aerosol deposition using algebraic correlations.* Aerosol Science and Technology, 2017. **51**(6): p. 667-673.
43. Grgic, B., W.H. Finlay, and A.F. Heenan, *Regional aerosol deposition and flow measurements in an idealized mouth and throat.* Journal of Aerosol Science, 2004. **35**(1): p. 21-32.

44. Yang, M.Y., et al., *Examining the ability of empirical correlations to predict subject specific in vivo extrathoracic aerosol deposition during tidal breathing.* Aerosol Science and Technology, 2017. **51**(3): p. 363-376.
45. Xi, J. and P. Longest, *Transport and deposition of micro-aerosols in realistic and simplified models of the oral airway.* Annals of biomedical engineering, 2007. **35**(4): p. 560-581.
46. Zhang, Z. and C. Kleinstreuer, *Airflow structures and nano-particle deposition in a human upper airway model.* Journal of Computational Physics, 2004. **198**(1): p. 178-210.
47. Koullapis, P.G., et al., *Particle deposition in a realistic geometry of the human conducting airways: Effects of inlet velocity profile, inhalation flowrate and electrostatic charge.* Journal of Biomechanics, 2016. **49**(11): p. 2201-2212.
48. Xi, J., et al., *Modeling the pharyngeal anatomical effects on breathing resistance and aerodynamically generated sound.* Medical & biological engineering & computing, 2014. **52**(7): p. 567-577.
49. Cheng, S., et al., *Healthy humans with a narrow upper airway maintain patency during quiet breathing by dilating the airway during inspiration.* The Journal of physiology, 2014. **592**(21): p. 4763-4774.

Chapter 4 An experimental study of the effect of individual upper airway anatomical features on the deposition of dry powder inhaler formulations

(This chapter has been published in the Journal of Aerosol Science, Volume 177, 106320)

This study aims to investigate the effects of different pharynx anatomical features on the delivery of inhaled aerosols. Six in-vitro upper airway models reconstructed using anatomical images acquired by Magnetic Resonance Imaging (MRI) were used for the experiments. A geometrically accurate airway model was produced, and five other different airway models, each missing one or more specific anatomical features: the uvula, epiglottis, and/or soft palate, were derived from the original model. Hence, the geometrical boundaries of the six models were the same except at regions where specific anatomical structures were removed, and this was done to allow meaningful comparisons between the different geometries to be made using specific measurements. Spray-dried mannitol powder (volume median particle size and span were 3.22 μm and 1.90 μm, respectively) was loaded into a capsule-based dry powder inhaler with different resistance, an Osmohaler™ (low resistance), or Handihaler® (high resistance), attached to the inlet of the airway model, which its outlet was connected to a Next-Generation Impactor (NGI). The studies were performed using flow rates of 30 and 60 LPM. High-performance liquid chromatography (HPLC) was used to quantify the mass deposition of particles in different stages of the NGI and airway replicas. Results from this study show that widening the space between the oral cavity and oropharynx, exemplified by one of the six replicas developed, significantly decreases upper airway deposition as well as increases the fine particle fraction. The case with the highest deposition (63.5%) occurred in the pharynx replica with the soft palate present (at 60 LPM with the Hanihaler), while the lowest deposition (26.0%) occurred in the replica without the soft palate and epiglottis (at 30 LPM with the Osmohaler). This study highlights that in addition to the resistance of the inhalers, their interactions with the human airway anatomical features are likely to play important roles in the subsequent lung dose. Results from this study are novel because while the effects of different inhaler resistance in a given airway replica is known, the effects contributed by specific pharynx anatomical features on particle transport behaviour have not been studied experimentally or reported on in the literature. This study shows that space adjacent to the soft

palate affects particle deposition dramatically but the effect appears to be more significant when using the Handihaler and for the high flow rate cases.

Keywords:

Inhalation drug delivery

Dry powder inhaler

Mouth-throat models

Upper airway deposition

Abbreviations and Symbols for chapter 4 (in alphabetical order)

ACI andersen cascade impactor

AD aerodynamic diameter

AIT alberta Idealized Throat

APSD aerodynamic Particle Size Distribution

CFD computational Fluid Dynamics

CIs cascade Impactors

COPD chronic obstructive pulmonary disease

DPIs dry powder inhalers

DPM discrete Phase Model

D_{10} (µm) volume diameter under which 10% of the particles resides (obtained from laser diffraction)

$D_{15.9}$ (µm) the mass based size distribution that 15.9 % of the volume is contained by particles smaller

D_{50} (µm) volume diameter under which 50% of the particles resides (obtained by laser diffraction)

$D_{84.1}$ (µm) the mass based size distribution that 84.1 % of the volume is contained by particles smaller

D_{90} (µm) volume diameter under which 90% of the particles resides (obtained by laser diffraction)

E removed Epiglottis

FPFem (%) fine particle fraction

FPD (mg) fine particle dose

GSD geometric standard deviation

HPLC high-performance liquid chromatography

LPM liter per minute

MMAD mass median aerodynamic diameter

MT mouth throat

MRI Magnetic Resonance Imaging

NGI next-generation impactor

O original model

OPC Oropharyngeal Consortium

p statistical p-value

SP removed Soft palate

SP+E removed Soft palate and Epiglottis

Stk stokes number

U removed Uvula

U+E removed Uvula and Epiglottis

USP United States Pharmacopeia

VCU Virginia Commonwealth University

3D three-dimensional

4.1 Introduction

Human respiratory diseases, such as asthma (Pate et al., 2021), chronic obstructive pulmonary disease (COPD) (Agustí et al., 2020) and chronic bronchitis (Jarhyan et al., 2022), are well-known diseases that have high mortality rates. Medical and hospitalization costs associated with these diseases remain incredibly high (Gutiérrez Villegas et al., 2021; Stolbrink et al., 2022), and improved treatments and modalities to manage these diseases effectively are warranted. A well-known and common prescription to treat and manage these human respiratory diseases involves targeting inflammation in the airways through aerosolized medications such as dry powder inhalers (DPIs) (N. Islam & Cleary, 2012; A Kourmatzis et al., 2018). DPI-based therapies offer effective approach for alleviating respiratory disease conditions, and they are known to have high therapeutic efficacy (N. Islam & Cleary, 2012), are associated with less drug waste (N. Renee Labiris & Myrna B. Dolovich, 2003) and present rapid disease relief and treatment (Kadota et al., 2020).

Cascade impactors (CIs), including the Andersen cascade impactor (ACI) and the next-generation impactor (NGI), are commonly used for testing inhaled drugs *in-vitro* and specifically in the determination of the aerodynamic particle size distribution (APSD) for a given flow rate and inhalation condition (Mohan et al., 2017). APSD measurements are essential for the evaluation, design and quality assessment of DPIs (Yoshida et al., 2017). Fine particles are typically considered as particles with aerodynamic diameters that are less than 5 microns, and are known to be respirable in the lower airways and they are associated with effective treatment of respiratory disease (Newman, 2022). Fine particle fraction (FPF) measurements obtained from CIs are commonly used to evaluate whether or not a particular device can deliver the associated formulation to the lung (Colthorpe et al., 2013).

Cascade impactors must be used with mouth throat (MT) models to provide the necessary information, and common models include the United States Pharmacopeia (USP) induction port (USP, 2023), the Virginia Commonwealth University (VCU) (Delvadia et al., 2012) model, Alberta Idealized Throat (AIT) (Stapleton et al., 2000), and the Oropharyngeal Consortium (OPC) model (Burnell et al., 2007). Significant geometrical differences exist between these MT models, each representing a human pharynx without one or more of the upper airway anatomical features (Mekonnen et al., 2022). The USP induction port is a simple 90° bent tube (see USP for details on the geometry in (USP, 2023)). Due to its simplicity and published geometry, the USP induction port has been widely used to test inhaled drug delivery and is

useful for establishing a performance benchmark (Y. Zhou et al., 2011). The VCU MT model, whilst more complex, excludes anatomical features such as the uvula, epiglottis and soft palate (a wide oral cavity space that is considered an absent anatomical feature), whereas the AIT MT model consists of the epiglottis and soft palate (a narrow space that may indicate the soft palate) but excludes the uvula (J. Mitchell et al., 2012). While there has been substantial work in this field (Agu & Ugwoke, 2011; Dunbar & Mitchell, 2005; Golshahi et al., 2022; Lizal et al., 2020), knowledge regarding how specific anatomical features in the human pharynx affect regional drug deposition remains limited. And although the simplifications of these features are often found to reasonably replicate deposition of pharmaceutical aerosols well (Delvadia et al., 2012; Stapleton et al., 2000), there is significant potential for improving understanding of the influence of airway geometry.

The above challenge to understand the mechanics underpinning drug delivery using the different airway models has been elucidated in a recent study using a computational model that maintains the pharynx's overall geometry while isolating different anatomical features to understand their impact on particle deposition behaviour. Z. Ma et al. (2022) used *in silico* modelling to systematically remove different features of the human airway and demonstrate that the soft palate plays the most significant role in drug deposition in the mouth-throat region. However, that study did not take into account the effects of inhaler geometry, inhaler airflow resistance, fine particle deposition, or the overall size range of particles exiting the upper airway. This current study aims to a) elucidate the effects of different anatomical features (e.g. the uvula, epiglottis and soft palate) on particle deposition in the MT region of the human airway using NGI and HPLC; b) show how different anatomical features of the human pharynx may affect the fine particle fraction and total "lung dose" as measured in an NGI, based on two different inhaler devices (Handihaler and Osmohaler) at specific flow rates (30and 60 LPM); and c) verify the role the soft palate plays in affecting upper airway drug deposition to create an improved methodology for interpretating CI data used with different MT models.

4.2 Methods:

4.2.1 Airway models casting

MRI images from a healthy human (female, aged 56, with body mass index (BMI) 39.5 kg/m^2 and indicated as overweight) with no history of respiratory diseases were used to reconstruct three-dimensional (3D) upper airway models. The case used in this study involves a High BMI individual, which does not represent the typical airway geometry due to abnormal

oropharynx structure and biomechanical characteristics. Consequently, throat deposition may vary from other geometries. The MRI images were carefully inspected to ensure that anatomical structures, including the uvula, epiglottis and soft palate, were clearly visible and distinguishable. A cube with a voxel size of 0.25 mm was used to generate an image stack (276 voxels*448 voxels*468 voxels) in a computer modelling program (3D Slicer (https://www.slicer.org/)). Specific airway boundaries around the uvula, epiglottis, and soft palate were identified by carefully matching the MRI data to a standard anatomical atlas that defined these structures in detail. The 3D slicer was then used to generate models containing all the detailed anatomical features of the upper airway. Another five models were created with matching upper airway boundaries to those of the original model above, except for specific regions where key anatomical features (uvula, epiglottis and soft palate) were located. These features were systematically removed to create a set of 6 MT variations for use in the study as follows: 1) An Original Model (O) that includes all the anatomical features as described above, 2) Original Model without the uvula (U) 3) Original Model without the epiglottis only (E), 4) Original Model without the uvula and epiglottis (U+E), 5) Original Model without the soft palate (SP), and 6) Original Model without the soft palate and epiglottis (SP+E). The uvula is situated at the distal region of the soft palate and is commonly regarded as an integral part of it (Helwany & Rathee, 2022). Consequently, in the models where the soft palate is removed/widened (i.e. 5 and 6), the uvula is also removed. We note that, when we refer to 'removing' the soft palate in SP and SP+E, in practice the soft palate is only partially removed, resulting in an effective 'widening' of the cavity. For simplicity, and to maintain consistent notation with our previous computational study (Z. Ma et al., 2022), we will describe these cases as having 'removed' the soft palate, which should be considered interchangeable with 'widening' in this context.

All the models were then post-processed using another computer modelling program (Rhino 7, Robert McNeel & Associates, Seattle, Washington) and converted to poly-surfaces. All the six airway models are shown in the Figure 4. 1. The poly-surfaces were imported into SolidWorks (Waltham, MA USA) and used to create casting moulds of the MT geometry suitable for 3D printing. The models are manufactured using combined fabrication techniques of 3D printing and inverse casting. Liquid silicone (Elastosil RT601, Wacker Chemie, Munich, Germany) was prepared, injected into the mould casts, allowed to cure and removed from the cast. The output from this process were high accuracy physical models for each of the six (6) MT models described above and shown in Figure 4. 1. An extended inlet was added to the realistic

geometry to allow the inhalers to be connected via an adapter, while an outlet extension to connect the airway to the NGI. These inlet/outlet extensions, and adapter used to connect the inhalers, are shown in Figure 4. 2.

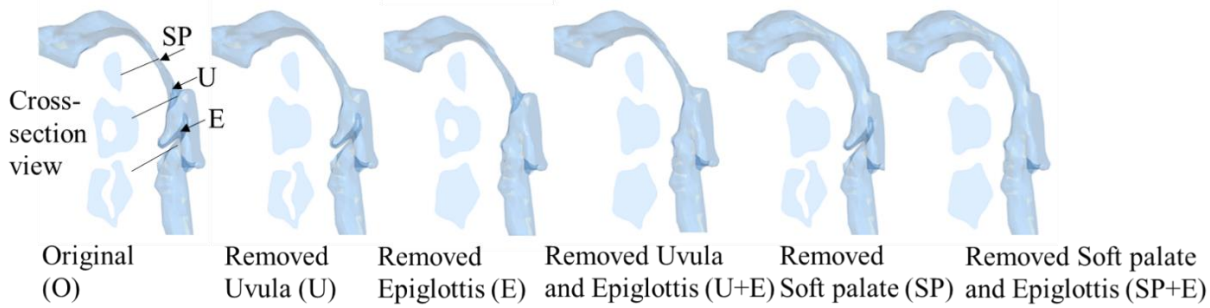

Figure 4. 1: Original model (O)-a basic complete pharynx model that includes all the anatomical features and five other models with specific anatomical features removed from the original model (removed Uvula: U, removed Epiglottis: E, removed Soft palate: SP). The cross-section views were perpendicular to the streamwise velocity.

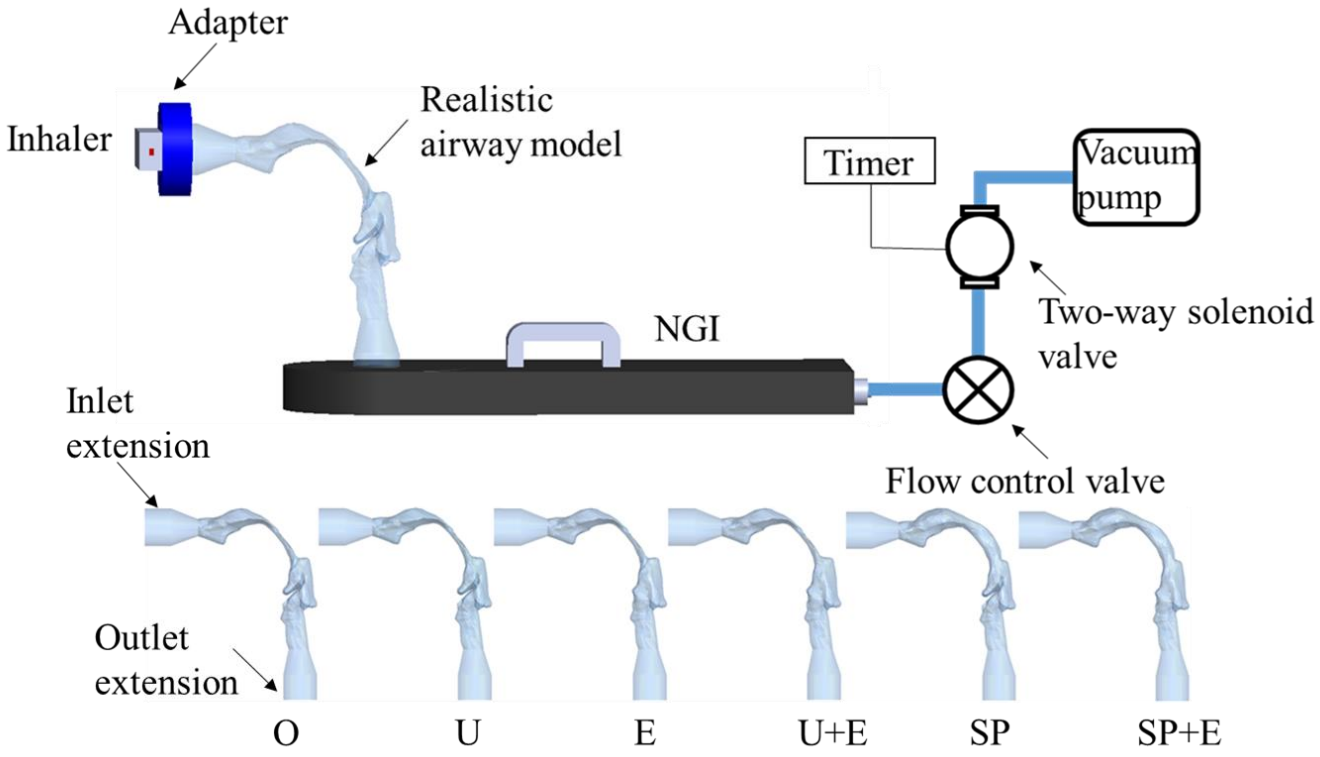

Figure 4. 2: Schematic of the experimental setup using different throat model (Original model: O, removed Uvula: U, removed Epiglottis: E, removed Soft palate: SP). An adapter (shown in blue in top left of the figure) was attached to the extension of the airway in a horizontal orientation. The other models with the inlet/outlet extensions are shown in the bottom row of Figure 4. 2. This extension has the same diameter as the USP throat. The inhalers were inserted

into the adapter as shown in the top left such that the outlet was approximately 40 mm from the start of the realistic geometry. During MRI scans, the patient was lying down with the inhaler inserted perpendicular to their mouth.

4.2.2 Aerosol Powder preparation

Mannitol solutions at 100 mg/mL concentrations were prepared by dissolving the raw material (mannitol powder supplied by Pharmaxis Ltd, Sydney) in deionised water. A spray dryer (Buchi B-290, BUCHI Labortechnik AG, Flawil, Switzerland) was employed to produce spray-dried particles with volume median diameters of 3.2 µm. Process conditions used are shown in Table 4.1.

Table 4. 1: Spray drying condition for mannitol

Feed concentration (mg/mL)	**Inlet temperature** (°C)	**Outlet temperature** (°C)	**Feed rate** (mL/min)	**Aspiration** (m^3/h)	**Atomising airflow** (L/h)
100	140	75	4.2	35	742

4.2.3 Particle size of dry powder

The particle size distributions of spray-dried mannitol were measured by laser diffraction (Mastersizer 3000, Malvern Instruments Ltd., UK). The mannitol sample was loaded into a Scirocco 2000 dry powder feeder (Malvern Instruments, UK) and dispersed in the air with 0.8 bar pressure. The material and absorption refractive indices of mannitol were set at 1.544 and 0.100, respectively. The refractive index (RI) of dispersant was set as 1.0. These RI values were considered accurate, as demonstrated by the low weighted residual values (< 0.61 %) obtained from all measurements. These values indicated a good data fit between the measured scattering data and the data predicted based on the optical properties.

4.2.4 Experimental Protocol, NGI and HPLC Analysis

Mannitol powder with a spray-dried volume median diameter (D_{50}) of 3.22 ± 0.03 µm was used in the experiment. The 20 mg ± 0.15 powder was loaded into a size 3 hydroxypropylmethylcellulose capsule (Capsugel, Sydney, Australia) before loading into the dry powder inhaler. NGI ((Copley Scientific, Nottingham, UK)) was used with the six 6 MT models and two different inhaler devices (Handihaler and Osmohaler), to study particle deposition at flow rates of 30 LPM and 60 LPM, with a fixed 4L volume inhalation, as

recommended by the British Pharmacopoeia (Pharmacopoeia, 2012; Singh et al., 2022). The resistance of the Handihaler and Osmohaler is 0.047 $kPa^{1/2}$/LPM (Jõgi et al., 2021) and 0.021 $kPa^{1/2}$/LPM (Chang et al., 2017), respectively, and these inhalers were chosen because they are well known inhalers that represents the lowest and highest range of inhaler resistance in the market. These flow rates were achieved using a low-pressure drop mass flow meter (TSI 4040 Series Mass Flowmeter) by connecting it to a standard vacuum pump which was attached to the outlet of the NGI. A flow control valve (Airtac ASC300-10) and timer (Omron H3CR-A8, Japan) were installed between the NGI and the vacuum pump to control the flow rate and suction duration to achieve the inhalation volume. All the NGI plates were coated uniformly with silicone grease before each experimental run (Dry Film Silicone Lubricant; LPS, Tucker, GA, USA) to reduce the drug particle bounce.

The experimental protocol entailed delivering the flow and aerosol through the device, realistic airway model and NGI. The experimental setup is shown in Figure 4. 2. The sample collection process involves rinsing the capsule, inhaler, adapter, the upper airway replica, and the eight stages in the NGI with known amounts of Milli-Q water (capsule: 4 mL, inhaler: 10 mL, adapter: 3 mL and each plate of NGI: 2 mL) until the drug concentration of the sample falls within the calibration standards range of 0.03–5.05 mg/mL, to yield 12 samples of drug solution. The individually collected samples were then analysed using HPLC (Model LC-20; Shimadzu, Kyoto, Japan) consisting of a DGU-20A degasser, CBM-20A controller, LC-20AT pump, SIL-20A HT auto-sampler, CTO-20A column oven, and an RID-10A Refractive-Index (RI) detector. A 50 µL volume sample was collected and mixed with mobile phase (Milli-Q water) under a fixed flow rate (0.6 mL/min) through a Hi-Plex Ca2+ column (300 × 7.7 mm, Agilent, Sydney, Australia). The oven temperature was set at 75°C, and each run lasted 10 mins. For all HPLC runs, over 95% mass recovery was obtained. The standard curve for mannitol ranged from 0.03 mg/mL to 5.05 mg/mL, and the coefficient of determination $R^2 \geq 0.997$. The accuracy of the concentration of the prepared known solutions was within ± 5%.

Aerosol performance indices were determined using the following,

$$FPF_{em} = \frac{\text{mass of mannitol} \leq 5\ \mu\text{m in NGI stages}}{\text{mass of mannitol in (1 capsule + inhaler + adaptor + mouth throat model + NGI stages)}} \times 100\%, (1)$$

and FPD is defined as the mass of mannitol ≤ 5 μm in NGI stages. This was calculated using linear interpolation of cumulative doses between the two stages where 5 microns lies, i.e., stages 2 and 3 for 30 LPM; stages 1 and 2 for 60 LPM. The mass median aerodynamic diameter (MMAD) and geometric standard deviation (GSD) were determined in relation to the recovered dose and emitted dose. The MMAD was calculated as the diameter at 50% undersize, obtained through interpolation of the cumulative recovered and emitted doses. The GSD was calculated using equation (2), where $D_{84.1}$ and $D_{15.9}$ are defined similarly to D_{50}, that is, they correspond to the diameters where 84.1% and 15.9% of the volume is contained by particles smaller than these diameters,

$$GSD = \sqrt{\frac{D_{84.1}}{D_{15.9}}}. \quad (2)$$

4.2.5 Statistical Methods

An F-test was first used to examine the equality of variances and two-tailed T-tests. This t-testing was conducted to analyse the differences in throat deposition fraction, deposition between NGI stages, emitted fine particle fraction (FPF), and fine particle dose (FPD), between the original model and each of the other five models under two flow rate conditions. All results in the bar charts are represented as a mean ± standard deviation. A single asterisk in the figures represents $p < 0.05$, two asterisks represent $p < 0.01$, and three asterisks represent $p < 0.001$.

4.3 Results

4.3.1 Deposition fraction in mouth throat model

This section discusses how specific anatomical features in the human pharynx affect particle deposition in the six mouth-throat model replicas with spray dried mannitol (the volumetric

diameters (D_{50}) of spray dried mannitol was = 3.22 µm and the span ((D90 – D10)/D50) was 1.90). Figure 4. 3 shows the experimental results on spray-dried mannitol under 30 LPM and 60 LPM using the Handihaler and Osmohaler.

Significant differences in throat deposition fraction between the original and other airway models with anatomical features removed (uvula, epiglottis and soft palate) can be observed.

For the Handihaler (Figure 4. 3a), the deposition fraction is significantly ($p < 0.05$) lower for SP (22% decrease) and SP+E (25% decrease) relative to the original model at 30 LPM. A significant difference is also observed at 30 LPM for the Osmohaler (Figure 4. 3b), with 35% and 38% decreases for SP and SP+E, relative to the original model. This may be a result of the soft palate significantly narrowing the local airway cavity, which increases the local velocity and, in turn, increases deposition. At 60 LPM, no significant difference was noted for the Handihaler between the original model and the other models, which suggests that at a high flow rate, the effects of Handihaler on particle transport and deposition are likely less susceptible to difference/changes in airway geometries. For the Osmohaler, a statistically significant decrease of approximately 24% is found for both SP and SP+E compared to the original model at 60 LPM, which is smaller than the 35% and 38% relative difference observed at 30 LPM for the same device. This suggests there is a reduced influence of local geometry on deposition with an increase in flow rate, which is consistent with other studies that compare deposition across different geometries (Shaokoon Cheng et al., 2019). The presence of the soft palate reduces the airway cross section in that region, which increases the local Reynolds number (Re) and hence turbulence. While increased turbulence is likely to increase deposition through turbulent dispersion (as seen in the 30 LPM case), this effect need not be linear due to the complexity of the mechanisms behind how particles deposit on the walls. There may therefore be a local Reynolds number where further increases in turbulence do not significantly affect deposition, resulting in the less significant differences seen at 60 LPM. Further research into the precise mechanisms governing deposition, such as attempting to quantify the 'turbulence contribution', would help shed more light on this, and in the discussion section we discuss deposition in greater detail. Throat deposition fraction appears sensitive to the inhaler devices, presumably through their difference in resistance, sensitivity to flow rate, mouthpiece size and differences in their internal geometry (e.g. the presence of a swirl chamber, which could influence powder dispersion).

The trends discussed here, namely that deposition is reduced when the soft pallet is removed, are consistent with our previous CFD study (Z. Ma et al., 2022). However, the relative decreases in the CFD study were much larger (e.g. a 64% decrease for SP+E relative to O at 70 LPM) than in the present study (24% decrease for SP+E relative to O at 60 LPM for the Osmohaler). There are several significant differences between the computational model and the experimental set-up, such as the CFD using monodisperse particles, no inhaler device/adapter, and different flow rates. These, along with limitations in the turbulence modelling could contribute to this difference, but the consistent trends lend support to the present observations.

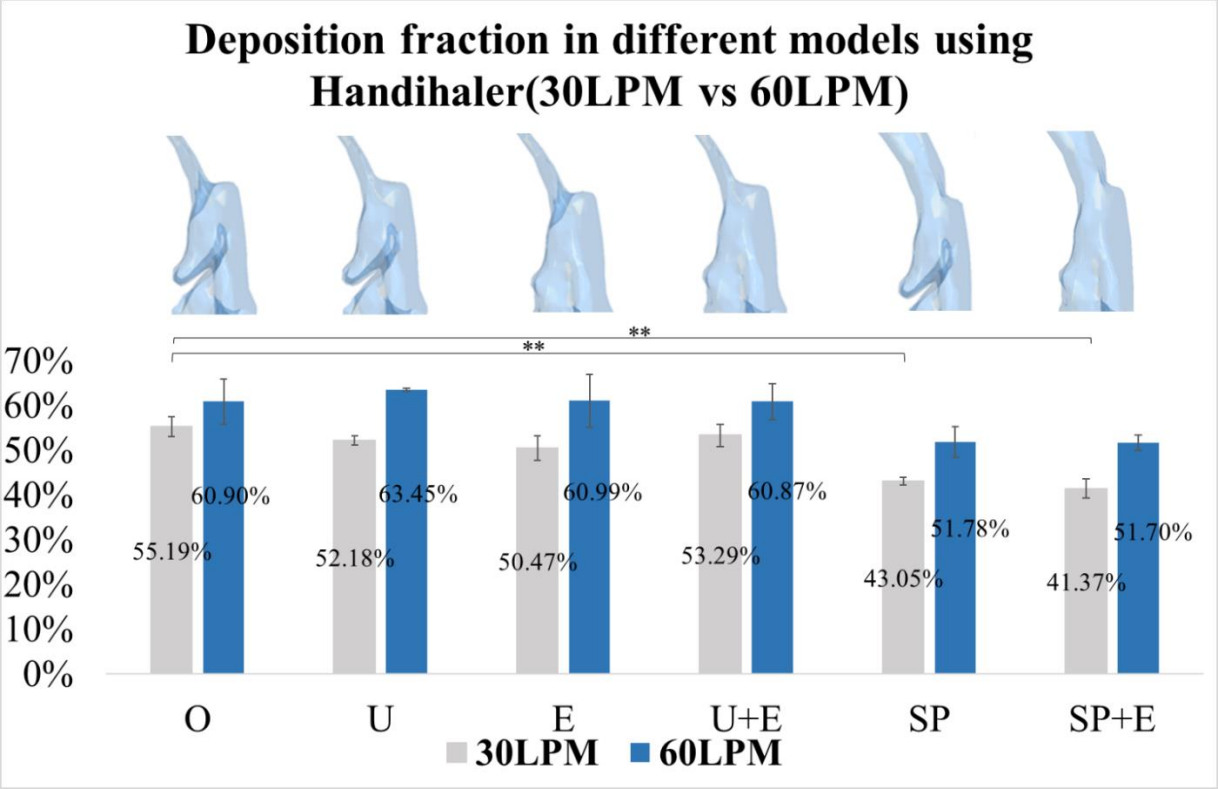

(a)

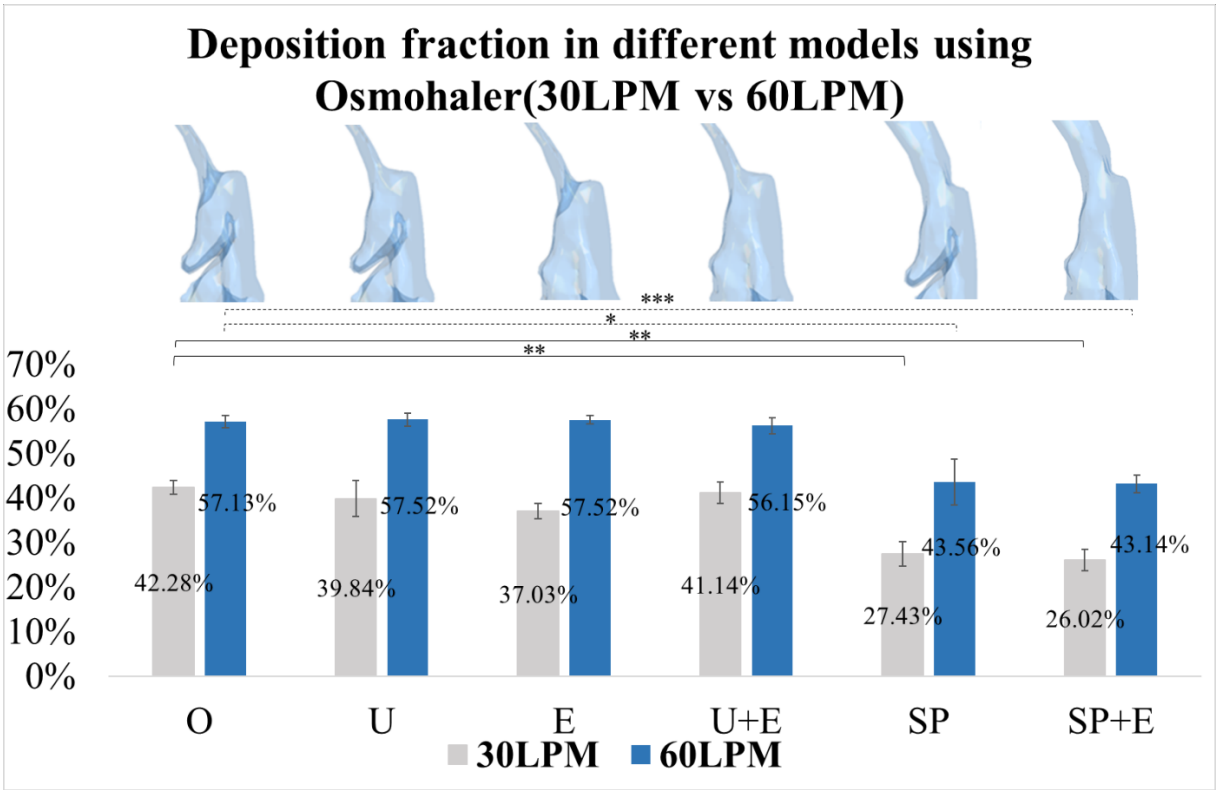

(b)

Figure 4. 3: Different throat model (Original model: O, removed Uvula: U, removed Epiglottis: E, removed Soft palate: SP) deposition fraction comparison under 30 LPM and 60 LPM using two inhalers (a), Handihaler (b), Osmohaler. Asterisks indicate level of significance (* indicates $p < 0.05$, ** indicates $p < 0.01$, *** indicates $p < 0.001$). Error bars refer to standard deviations, n=3.

4.3.2 Deposition in capsule, inhaler devices and adapter

Figure 4. 4 shows the mean deposited mass in the capsule, inhaler devices and adapter for all airway models when using the Handihaler and Osmohaler and based on the 30 LPM and 60 LPM inhalation flow conditions. Results show that there is no significant difference in mannitol deposition in the capsule, inhaler device and adapter, demonstrating that differences in anatomical features in a throat replica are unlikely to change the deposition results upstream. However, consistent with previous work (S. S. Y. Leung et al., 2016), flow rate appears to have an apparent effect on particle deposition in the capsule, device and adapter. Another important observation is that while deposition in the capsule, device and adapter appears unaffected by pharynx anatomical features, the error bars (standard deviations) are relatively large for the

Handihaler at 30 LPM (low flow rate). Given that the experiments were only performed in triplicate, it remains a question whether more data sets would return significant results for deposition in the capsule, device and adapter, which merits further investigations. In general, for the Handihaler, the mass of powder deposited in the capsule and inhaler device is quite variable across different airway models at low flow rate but is much more consistent with the airway models at a higher flow rate. This could be due to insufficient shear generated at lower flow rates to consistently evacuate and disperse powder from the capsule in the Handihaler.

A high mass of deposited particles in the device is noted for the 30 LPM case with the Osmohaler, with the deposition in the Osmohaler experiencing a dramatic reduction with an increase in flow rate. Clearly, the total deposition within the Osmohaler (capsule and device) is considerably higher than the deposition in the Handihaler for all six models, and this is consistent with the study conducted by Leung et al, where the higher deposition was noted in the Osmohaler compared to the Diskhaler (S. S. Y. Leung et al., 2016), which has a similar resistance to that of the Handihaler used in this current work. Finally, deposition in the adapter is insensitive to the flow rate for either the Handihaler or Osmohaler. The results also show that the total deposition in the adapter when using the Osmohaler is less than that of the Handihaler under the same flow rate.

4.3.3 Deposition in NGI stages

Figure 4. 5 shows deposition results in each NGI stage for all the 6 models. There is a significant difference ($p < 0.05$) in stage 1 (Aerodynamic Diameter (AD) > 11.72 µm) between the original model and the model without the soft palate for the case conducted at 30 LPM and with the Handihaler. The average deposition for the model that excludes the soft palate (Model SP and SP+E) increased in stages 3 (3.99 µm <AD < 6.4 µm) and 4 (2.3 µm < AD < 3.99 µm) of the NGI at 30 LPM, such that they are also higher than the original model, and this is not observed in the rest of the airway models. For the cases conducted at 30 LPM when the Osmohaler is in use, removing the soft palate alone leads to a significant increase of drugs in stage 1 ($p < 0.01$, $p < 0.01$, AD > 11.72µm), stage 3 ($p < 0.001$, $p < 0.001$, 3.99µm < AD < 6.4 µm) and stage 4 ($p < 0.01$, $p < 0.01$, 2.3 µm < AD < 3.99 µm). A general observation is that for all the pharynx models, stages 3 and 4 appear to have the most deposition out of the six stages in the NGI for cases conducted at a low flow rate of 30 LPM, and the deposition reduced

dramatically with the increase in flow rate, indicating the decreasing effects of airway anatomical features on deposition in the NGI stages.

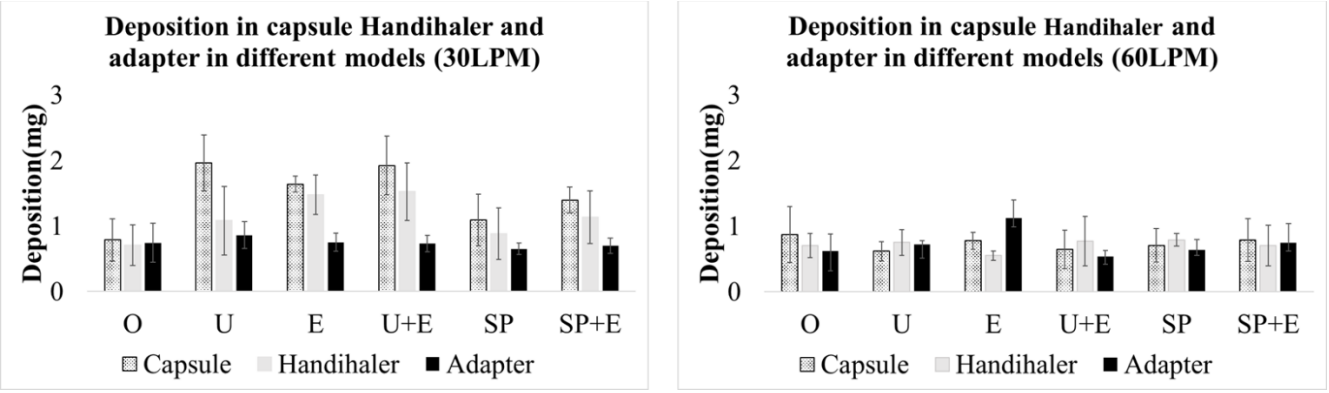

(a)

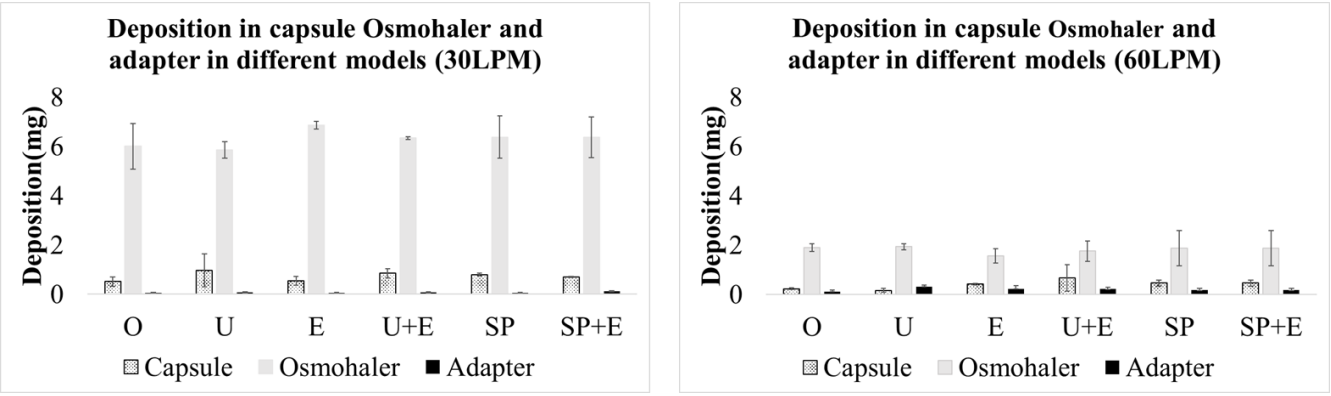

(b)

Figure 4. 4: Drug deposition in capsule, inhaler devices and adapter at 30 LPM and 60 LPM using (a),Handihaler (b), Osmohaler with different throat models (Original model : O, removed Uvula: U, removed Epiglottis: E, removed Soft palate: SP). Error bars refer to standard deviations, n=3.

The aerodynamic cut-off diameter for each NGI stage at 30 LPM and 60 LPM flow rate conditions were calculated and shown in table 4.2. (Marple et al., 2003; Wallin et al., 2019).

Table 4. 2: Cut-off diameter at 30 LPM and 60 LPM

Stage	Cut-off diameter at 30 LPM (µm)	Cut-off diameter at 60 LPM (µm)
1	11.72	8.06
2	6.40	4.46
3	3.99	2.82
4	2.30	1.66
5	1.36	0.94
6	0.83	0.55
7	0.54	0.34
MOC	0.36	0.14

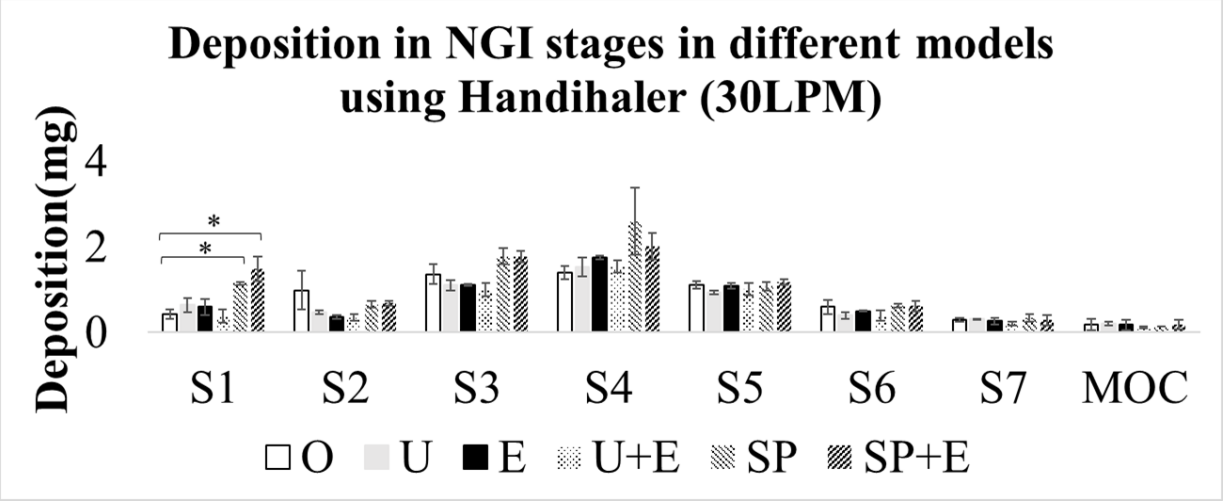

(a)

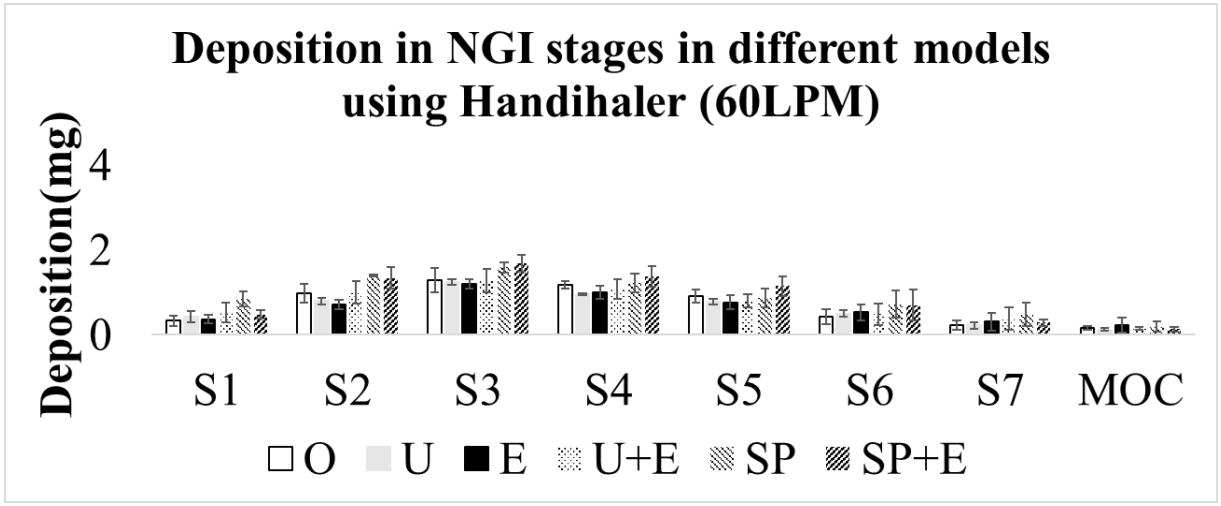
Deposition in NGI stages in different models using Handihaler (60LPM)
Deposition(mg)
4
2
0
S1
S2
S3
S4
S5
S6
S7
MOC
O
U
E
U+E
SP
SP+E

(b)

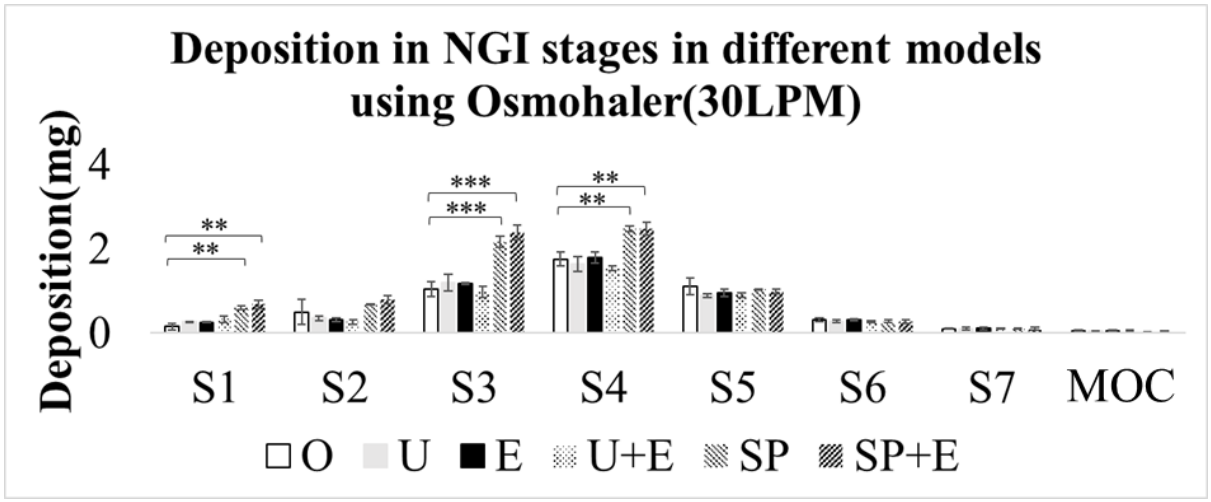
Deposition in NGI stages in different models using Osmohaler(30LPM)
Deposition(mg)
4
2
0
**
**
***
***
**
**
S1
S2
S3
S4
S5
S6
S7
MOC
O
U
E
U+E
SP
SP+E

(c)

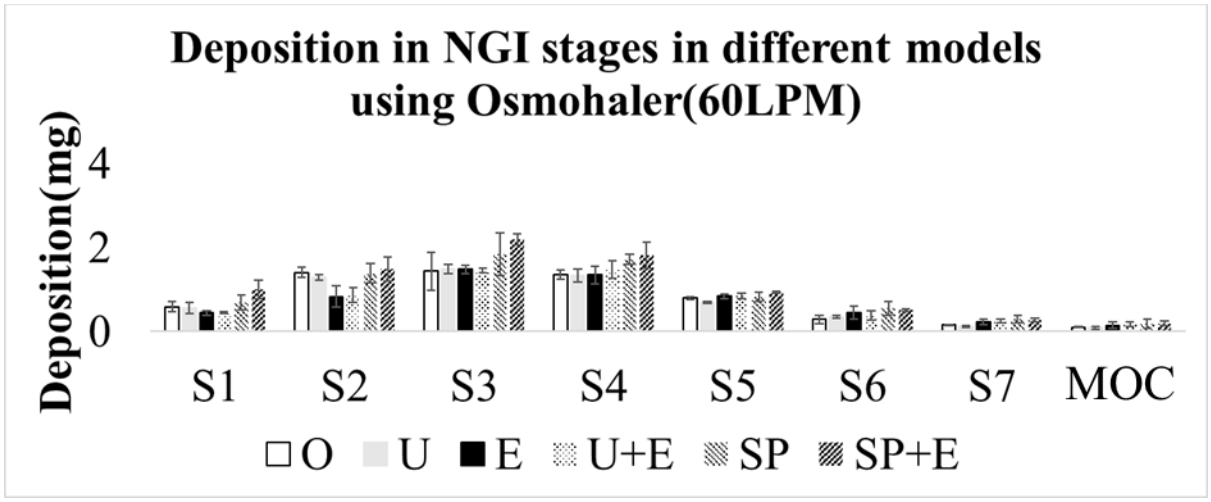
Deposition in NGI stages in different models using Osmohaler(60LPM)
Deposition(mg)
4
2
0
S1
S2
S3
S4
S5
S6
S7
MOC
O
U
E
U+E
SP
SP+E

(d)

Figure 4. 5: Drug deposition in seven NGI stages (stage 1-stage 7: S1-S7) and the Micro-Orifice Collector (MOC) obtained at two flow rates using two inhalers (a),Handihaler with 30 LPM (b), Handihaler with 60 LPM (c), Osmohaler with 60 LPM (d), Osmohaler with 60 LPM with different models (Original model : O, removed Uvula: U, removed Epiglottis: E, removed Soft palate: SP). Error bars refer to standard deviations, n=3.

4.3.4 Fine particle Dose (FPD) and emitted Fine Particle Fraction (FPFem)

The fine particle fraction and dose are critical measures defining a device's efficacy. The fine particle fraction indicates the likelihood of particles entering the lungs Figure 4.6 shows the results of both the fine particle dose (FPD) and emitted fine particle fraction (FPF_{em}) in the different upper airway models, with several statistically significant differences observed between the original model and the SP and SP+E models for both inhalers. For example, a significant difference is found in the FPF_{em} for the Handihaler at 30 LPM between the original model and both SP and SP+E models (37% and 27% increases for SP and SP+E, respectively, relative to O). Significant increases were also observed in both the FPF_{em} and FPD for the Osmohaler between the original model and SP (34% and 28% for FPF_{em} and FPD, respectively) and SP+E (34% and 29% for FPF_{em} and FPD, respectively). Interestingly, despite the statistically significant difference in emitted FPF, no statistically significant difference in the fine particle dose is noted for the Handihaler due to the change of the emitted dose.

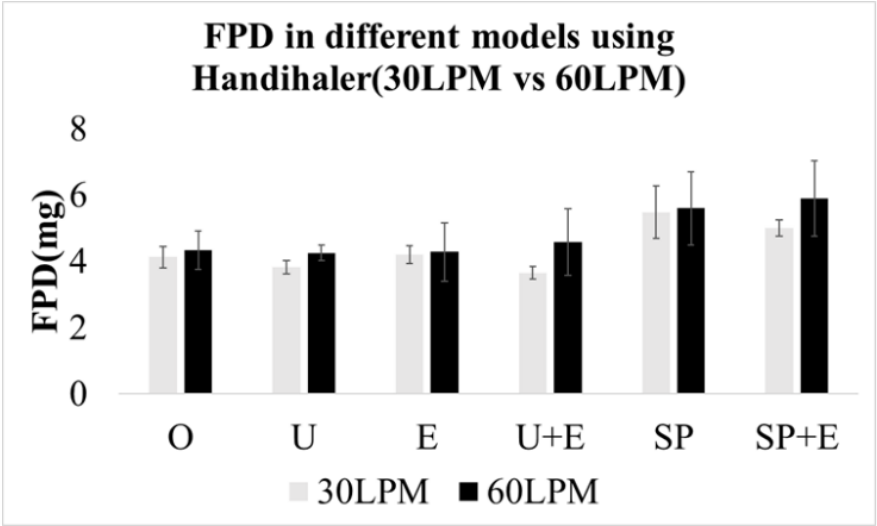
FPD in different models using Handihaler(30LPM vs 60LPM)
FPD(mg)
8
6
4
2
0
O
U
E
U+E
SP
SP+E
30LPM
60LPM

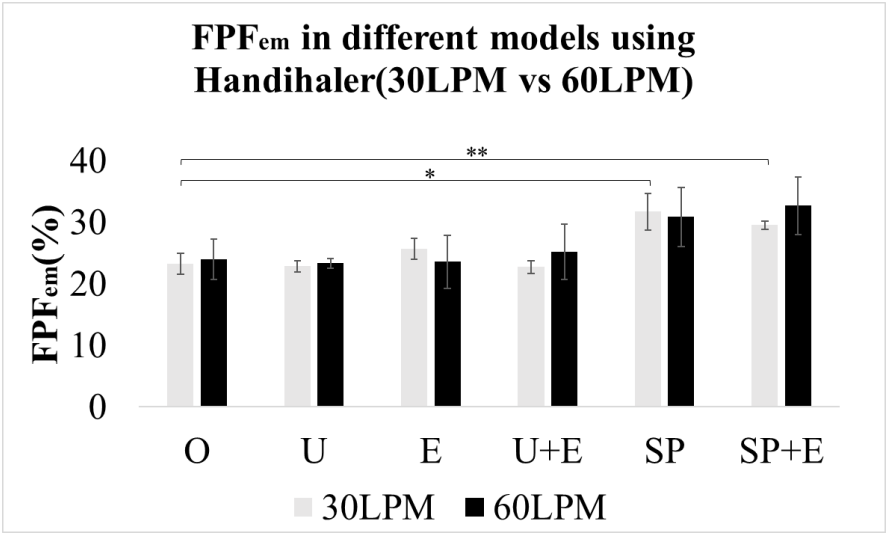
FPFem in different models using Handihaler(30LPM vs 60LPM)
FPFem(%)
40
30
20
10
0
**
*
O
U
E
U+E
SP
SP+E
30LPM
60LPM

(a)

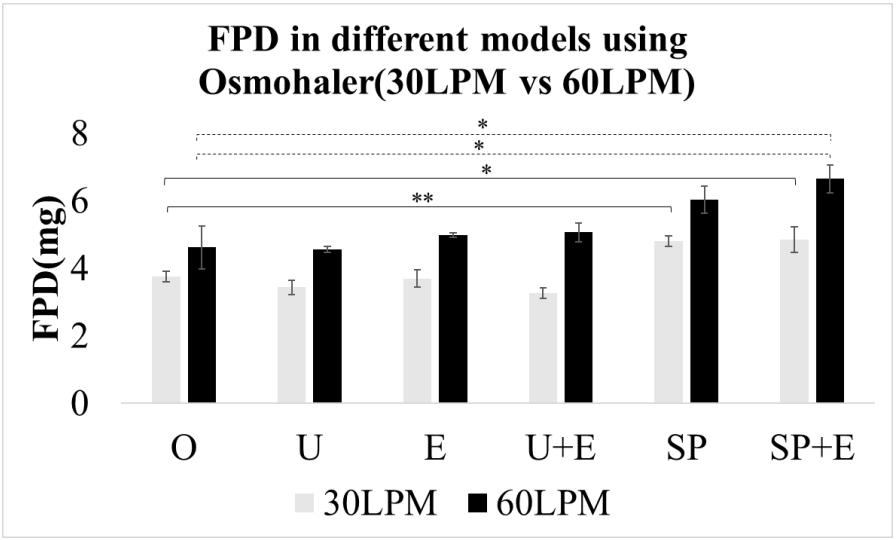

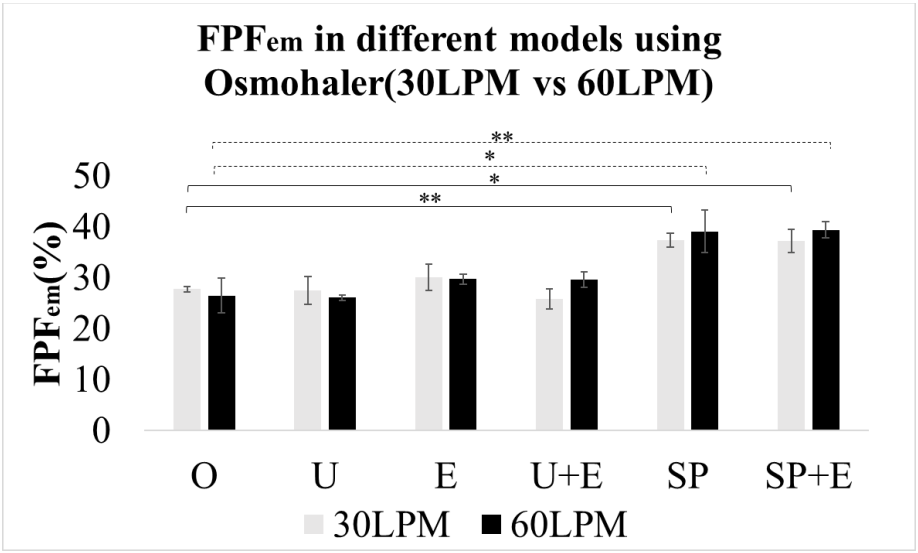

(b)

Figure 4. 6: FPD and emitted FPF in different models (Original model: O, removed Uvula: U, removed Epiglottis: E, removed Soft palate: SP) at 30 LPM and 60 LPM using (a), Handihaler (b), Osmohaler. Error bars refer to standard deviations, n=3.

4.3.5 Mass median aerodynamic diameter (MMAD) and geometric standard deviation (GSD)

Figure 4. 7 shows the mass median aerodynamic diameter (MMAD) and GSD for all airway models at both flow rates using the two inhalers. There is a significant increase in MMAD when the soft palate is removed for 30 LPM with the Osmohaler, which is consistent with the

previous finding of upper airway deposition decreasing when this feature is removed. At 60 LPM, the impact of anatomical features on MMAD decreases and the differences are less significant. This is also consistent with the previously discussed finding that anatomical differences become less important at higher Reynolds numbers.

We generally observe some decrease in MMAD with increasing flow rate across all models, but this is most significant for the case without the soft palate and epiglottis. There is also an increase in the GSD with flow rate, which could potentially be attributed to the loss of larger particles in the upper airway (W. H. Finlay, 2001), leading to leftward shift in the particle size distribution (Marple et al., 2003).

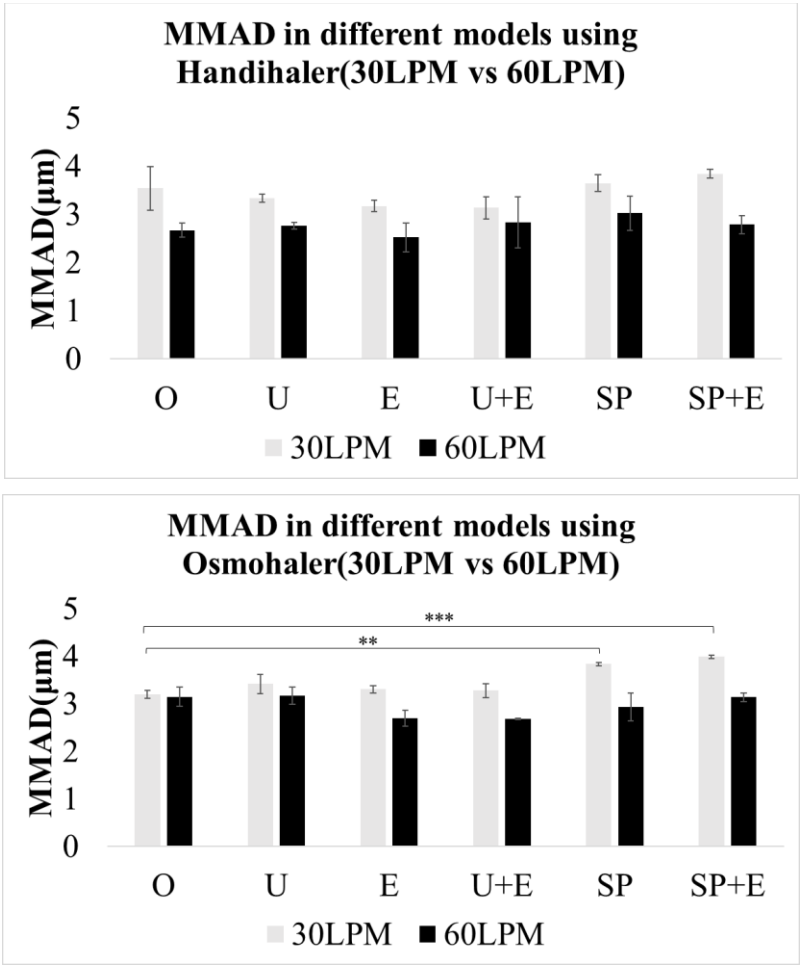

(a)

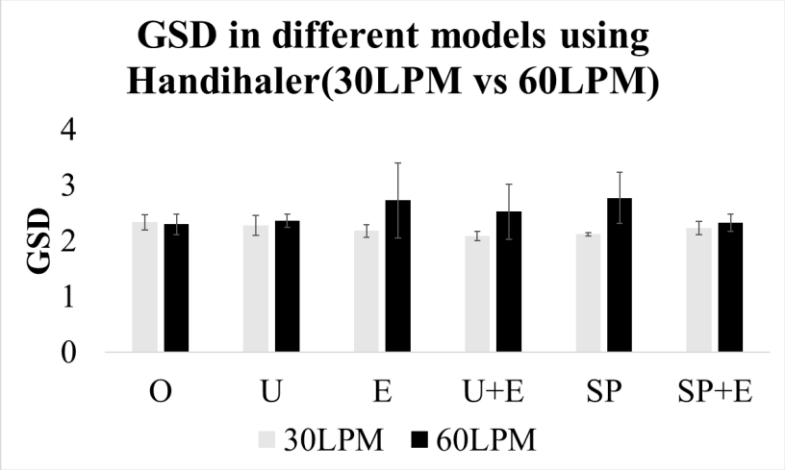

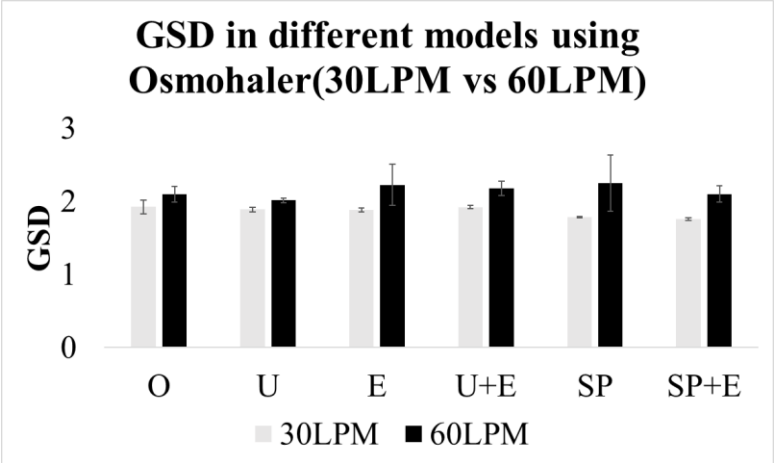

(b)

Figure 4. 7: MMAD and GSD in different models (Original model: O, removed Uvula: U, removed Epiglottis: E, removed Soft palate: SP) under 30 LPM and 60 LPM applying two inhalers (a), Handihaler (b), Osmohaler. Error bars refer to standard deviations, n=3.

4.5 Discussion

There is a lack of research studies focusing on the role of human extrathoracic anatomical features in particle deposition and downstream dose delivery. To the best of authors' knowledge, this is one of few experimental works that has demonstrated the effect of anatomical features on drug deposition and how these features will affect the drug particle aerodynamic size distribution entering the lung. The main finding of this study is that the space where the soft palate is located is likely one of the most vital anatomical features that affect fine particle transport and deposition. These results are supported by (Golshahi et al., 2013), who also identified the importance of this region for deposition. They found that, by using a

characteristic diameter based on a region defined similarly to SP as indicated in Figure 4. 1, they could reduce the scatter in their deposition data when considering an empirical relation involving Re and Stk.

While the uvula and epiglottis are both somewhat protruding anatomical structures of the human airway and have been demonstrated to affect the flow dynamics and velocity field in the pharynx dramatically (Bingjie Ma et al., 2020; Zhao et al., 2020), it is interesting to note that both these features appear to have little effects on particle transport behaviour. According to the finding of this current work, removing the soft palate leads to very low deposition in the upper airway and high FPF in the NGI, which is in essence, a representation of the USP throat model where there is an absence of change in pharynx cross-section along the airway, and unlike the AIT.

Results in this current work provide further evidence that the soft palate has a major effect on the overall deposition in the mouth-throat region compared to the other anatomical features, which is consistent with our previous computational modelling study (Z. Ma et al., 2022). A significant difference ($p < 0.05$) in throat deposition between the original model and the models without the soft palate was observed when the Osmohaler was used, and this was determined for both the 30 LPM and 60 LPM experimental cases. However, the relative difference with respect to the full model was lower at 60 LPM (24% decrease from O to SP) than at 30 LPM (35% decrease from O to SP). As for the Handihaler, while there is a significant decrease ($p < 0.05$) in pharynx deposition between the original airway model and the models without the soft palate, the observation was only made for the 30 LPM case. It is worth noting that while the deposition fraction measured is different from the previous computational study (Ma et al., 2022), which simulated the deposition fraction using a Computational Fluid Dynamics-Discrete Phase Model (CFD-DPM) approach, without modelling the inhaler, the adapters, and the size band of the particles; the general trends in pharynx particle deposition as depicted by (Z. Ma et al., 2022) adequately captured the key behaviours in terms of the effects between different geometries measured here, and specifically the central role of the soft palate as opposed to other anatomical features.

The deposition results in the inhaler and adapter (Figure 4. 4) show that the deposition in the Osmohaler is higher than in the Handihaler, which is generally consistent with previous work, where the higher deposition was noted in the Osmohaler compared to the Diskhaler (S. S. Y. Leung et al., 2016). In Leung et al. 2016, the Osmohaler has higher aerosol retention than the

Diskhaler. The difference in inhaler deposition is likely due to the difference in working mechanisms and principles between the inhaler devices (Almeida et al., 2022; Huang et al., 2022; Singh et al., 2022). For example, the powder in the Osmohaler will first impact the wall before the powder leaves the device, increasing the deposition in the device (Almeida et al., 2022). Meanwhile, the Handihaler shows a relatively higher deposition fraction downstream of the device. A plausible reason why deposition is higher in the adapter when using the Handihaler is that the Handihalers mouthpiece is much smaller than the Osmohalers mouthpiece, and therefore the higher velocity in the central area near the outlet of the Handihaler may lead to a more turbulent jet flow (Huang et al., 2022). The jet flow will lead to the impaction of particles on the airway wall and trap the particles, which makes the airway geometry less important.

The deposition in the NGI stages shows the implications of removing various anatomical features of the pharynx. According to Figure 4. 5, removing the soft palate not only affects the throat deposition fraction but also significantly affects the particle size distribution in experiments conducted at 30 LPM. Removing the soft palate can considerably increase the deposition in stages 3 and 4 of the NGI. However, with the increase in flow rate, this dependence becomes weak. This is likely due to the increase in Reynolds number associated with the high flow rate condition. At the mouthpiece region, the Reynolds number for Handihaler under 30 LPM and 60 LPM are 8546 and 17093 respectively; and 3885 and 7769 for the Osmohaler respectively. Under 60 LPM, the flow becomes more turbulent in the airway model, which may have led to a dominance of aerodynamic forces early in the airway model that encourages deposition close to the mouth. This makes the presence of unique anatomical features less important since there is now less powder downstream of the near-mouth region that may be influenced by anatomical variations. Such findings are consistent with previous work in more simplified geometries, which demonstrated the dominant role of aerodynamic forces at higher Reynolds numbers (Elserfy et al., 2020).

In addition to the previously discussed influence of Reynolds number on deposition, the Stokes number, Stk, also plays a role,

$$Stk = \frac{\rho_p d_p^2 \, \widehat{U}}{18 \, \mu_f \widehat{D}}, \tag{3}$$

where ρ_p is the particle density (mannitol), d_p is the particle diameter (D_{50}), μ_f is the fluid's dynamic viscosity (air), $\widehat{U}$ is the fluid's velocity and $\widehat{D}$ is a length scale, or 'effective

diameter', that characterises the overall airway geometry. These characteristic scales are defined in the same way as in (Grgic, Finlay, Burnell, et al., 2004), which are based on the total volume of the airway, V, and the path length of the sagittal axis, L,

$$V = \hat{A}L\ , \tag{4}$$

$$\hat{U} = \frac{Q}{\hat{A}}\ , \tag{5}$$

where Q is the flow rate and $\hat{A} = \pi\hat{D}^2/4$.

The Stokes and Reynolds number, $Re = \hat{U}\hat{D}/\nu_f$, where ν_f is the kinematic viscosity of air, are listed in table 4.3 for each variation of the model at both flow rates. Low Stokes numbers (Stk<<1) imply the particles follow the fluid flow closely, while a larger Stk indicates the particles have more inertia and, for example, may be more likely to collide with the airway walls when the flow changes direction. While Stk is low in each model variation, it, like the Reynolds number, decreases when anatomical features are removed since this tends to increase the effective diameter and reduce the local velocity. (Grgic, Finlay, Burnell, et al., 2004; Grgic, Finlay, et al., 2004a) proposed the empirical correlation $Stk \cdot Re^{0.37}$, to relate deposition efficiency (%), which was found collapsed their data well along an 's-shaped' curve (on a logarithmic scale) in a later study (Grgic, Finlay, Burnell, et al., 2004). This empirical quantity has been computed for the current data and presented in Figure 4. 8, where it is shown alongside the best fit curve from (Grgic, Finlay, Burnell, et al., 2004), who gathered data from several airway models and did not use a commercial DPI (instead delivering the flow from an aerosol generator).

At 60 LPM, the present data from both inhalers agrees very well with (Grgic, Finlay, Burnell, et al., 2004), despite the very different source conditions. Here the Reynolds number is high, and thus the influence of inlet conditions (such as inhaler geometry) on deposition are likely to be diminished. There is less agreement at lower $Stk \cdot Re^{0.37}$ (30 LPM), where there is a clear difference between the two inhalers, and both are somewhat higher than the best fit line from (Grgic, Finlay, Burnell, et al., 2004). Despite differences across devices (Handihaler vs Osmohaler in this study), and across different airway models (this study vs (Grgic, Finlay, Burnell, et al., 2004; Grgic, Finlay, et al., 2004a)), being more prevalent at lower Stokes/Reynolds numbers, a consistent trend of increasing deposition with $Stk \cdot Re^{0.37}$ is observed in the present data as airway features are modified for a given device/flow rate. This suggests that changes in deposition fraction due to local variation in anatomical features can

still be categorized using bulk quantities such as Re and Stk with respect to their influence on deposition, and supports the idea that these differences are less significant at higher Reynolds numbers when the flow is more turbulent.

Table 4. 3: Reynolds and Stokes numbers.

	$\hat{D}$ (mm)	Reynolds number		Stokes number	
		30 LPM	**60 LPM**	**30 LPM**	**60 LPM**
Original model (O)	15.39	2777	5555	0.0084	0.0168
Removed Uvula (U)	15.45	2765	5530	0.0083	0.0165
Removed Epiglottis (E)	16.21	2636	5272	0.0072	0.0143
Removed Uvula + Epiglottis (U+E)	16.27	2626	5252	0.0071	0.0142
Removed Soft Palate (SP)	16.97	2518	5037	0.0063	0.0125
Removed Soft Palate + Epiglottis (SP+E)	17.79	2402	4805	0.0054	0.0109

Data is also shown in Figure 4. 8 from our previous CFD study using the same airway geometries, but without an inhaler device, at different flow rates of 40 and 70 LPM, and for monodisperse (3 μm) particles (Z. Ma et al., 2022). The simulation data for 40 LPM in reasonably good agreement with present experimental data and best fit line in (Grgic, Finlay, Burnell, et al., 2004). The CFD data at 70 LPM is somewhat lower than the present data and best fit line at lower $Stk \cdot Re^{0.37}$, and vice versa at higher $Stk \cdot Re^{0.37}$. However, the increasing trend with $Stk \cdot Re^{0.37}$ is still observed despite the aforementioned differences between the CFD conditions and experiments.

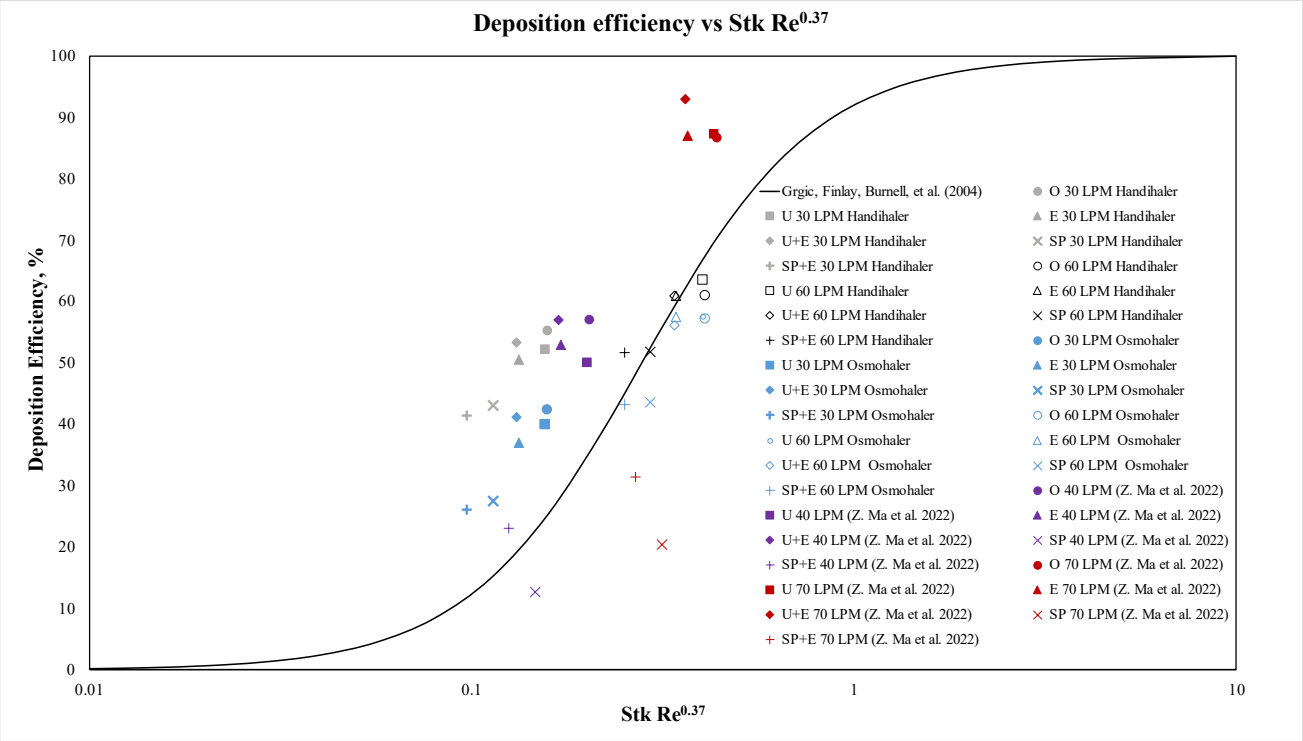

Figure 4. 8: Deposition efficiency vs. the non-dimensional quantity StkRe0.37 for all model variations at 30 LPM and 60 LPM for the Handihaler (grey/black) and Osmohaler (blue).

Results from the current experimental study confirmed the conclusion from a previous CFD study (Z. Ma et al., 2022) that the space adjacent to the soft palate plays a critical role in drug deposition in the upper airway and also indicate that larger space at this pharynx region will increase the fine particle dose significantly. These findings may provide insights into the body mass index (BMI) effects on aerosol delivery in the human airway. Previous work has shown that high BMI leads to a more constricted airway lumen, suggesting that high BMI may lead to more drug waste in the upper airway region due to the narrow region in the oropharynx known to dominate in high BMI population groups (Cai et al., 2022; Bingjie Ma et al., 2020; Mohsenin, 2001).

4.6 Limitations

The experiment was originally designed to use the Handihaler. A mock-up of the Handihaler was imaged with MRI, when the patient did the scan. To mimic the real situation, a Handihaler was set as a reference inhaler, which has a valid flow rate from 20 LPM to 60 LPM due to the high resistance of the device. Since a 30 LPM condition was used for the Handihaler, we ran the experiment for the Osmohaler under the same flow rate for comparative purposes. The

Osmohaler device is not designed for treatment at 30 LPM, but for a direct comparison, the above condition was adopted in the current study.

An alternative approach would be to fix the pressure drop across the two inhalers, which requires appropriately modifying the flow rate for each device. This, however, would change the Reynolds number once the flow enters the airway, and could significantly alter the flow dynamics. Table 4.4 shows the Reynolds numbers at the outlet of the inhalers, and a 'bulk' value for the original-model airway (based on the equivalent diameter defined by equation (4). For example, if the pressure drop was fixed at 1 kPa, this results in airway Reynolds numbers of 1815 and 4408 for the Handihaler and Osmohaler, respectively. This crosses the turbulent flow threshold and so results in completely different flow regimes in the airway for the two inhalers cases. When the flow rate is fixed, the same Reynolds number in the airway is obtained since the airway equivalent-diameter is unchanged. It may be noted that, for this particular pair of devices, the Reynolds number at the inhaler is more similar across the two devices when the pressure drop is fixed than when the flow rate is. However, the primary aim of the present study is to investigate the effect of changing anatomical features in the airway, and whether similar differences are observed when using the two inhaler devices. Since the influence of specific anatomical features on the flow is more closely related to the airway Reynolds number, as opposed to the inhaler Reynolds number, fixing the former by keeping the flow rate constant was considered more appropriate for the present investigation.

Table 4. 4: Fixing pressure drop vs flow rate.

	Handihaler		**Osmohaler**	
Resistance ($kPa^{0.5}$/LPM)	0.051		0.021	
Fixing flow rate:				
Flow rate (LPM)	30	60	30	60
Pressure drop (kPa)	2.34	9.36	0.40	1.59
Reynolds number (inhaler)	8546	17093	3885	7769
Reynolds number (airway)	2777	5555	2777	5555
Fixing pressure drop:				
Flow rate (LPM)	19.61	27.73	47.62	67.34
Pressure drop (kPa)	1	2	1	2
Reynolds number (inhaler)	5586	7900	6166	8720
Reynolds number (airway)	1815	2567	4408	6234

During the MRI scans, patients were lying down with the inhaler inserted into their mouth. During experiments, however, an adapter and inlet extension was necessary to link the inhaler device to the airway model. This is shown in Figure 4. 2, where the inhaler is inserted into the adapter horizontally such that the outlet is approximately 40 mm from the start of the realistic geometry. This presents an unphysiological feature of the experimental protocol. The impact of this was controlled by constructing all of the inlet/outlet extensions to be the same in the different airway models so that they have the same diameter as the USP induction port. This enables easier benchmarking between airway models.

A fixed flow rate was adopted in the experiment to collect an accurate APSD and to simplify the experimental protocol to isolate the impact of anatomical features. Given that the physiologically realistic inhalation has a time-varying profile, the implications of such transient flow may reveal more insights into the effects of anatomical features on drug particle transport, which merits further investigations. Nonetheless, comparing results obtained based on the two inhalers at similar flow rates and cross-referencing them to previous CFD and experimental work has suggested that the results presented in this current work are likely accurate.

Finally, in order to keep the study feasible, we have only considered airway models based on a single subject, and so an obvious question is whether the conclusions will generalise to other subjects. Additionally, the subject had high BMI (39.5 kg/m^2), and so the geometry studied is not necessarily representative of the average patient. However, provided the soft palate has a similar influence on the airway geometry between subjects (i.e. narrowing the region and increasing the Reynolds number), it is reasonable hypothesis that at least some results will generalise. However, this should not be overstated, and additional research is required to confirm this, presenting an opportunity for future studies into different airways (e.g. from subjects with a different BMI or sex).

4.7 Conclusions

The effect of certain anatomical features in the upper airway has been studied using realistic airway replicas. Expansion of the soft palate allows more drug particles entering the NGI and significantly increases the FPF. Removing/widening the soft palate also results in significantly reduced deposition, since it increases the local airway cross-section and reduces the Reynolds number, making the flow less turbulent. The effect of the soft palate is more apparent when using the Osmohaler than the Handihaler, potentially due to the smaller mouthpiece of the

Handihaler, which increases the inlet velocity leading to more turbulence at the inlet. At a higher flow rate, the impact of anatomical features on drug particle transport and deposition after the mouth-throat region is reduced. This may be due to increased deposition in the near mouth region at higher Re, resulting in less mass being available at the pharynx that may be influenced by the local geometry.

Like the Reynolds number, the removal of these anatomical features also act to decrease the Stokes number, both of which influence deposition. This was shown in Figure 4. 8 through an empirical relationship, $Stk \cdot Re^{0.37}$, where at higher Stokes and Reynolds numbers, we see similar deposition fractions to (Grgic, Finlay, Burnell, et al., 2004). At lower $Stk \cdot Re^{0.37}$, the trends are consistent but there is a larger difference between the two inhalers, suggesting that the effect of source conditions is more significant at lower Reynolds numbers.

4.8 References for Chapter 4

1. Agu, R. U., & Ugwoke, M. I. (2011). In vitro and in vivo testing methods for respiratory drug delivery. *Expert opinion on drug delivery, 8*(1), 57-69.
2. Agustí, A., Vogelmeier, C., & Faner, R. (2020). COPD 2020: changes and challenges. In (Vol. 319, pp. L879-L883): American Physiological Society Bethesda, MD.
3. Almeida, L. C., Bharadwaj, R., Eliahu, A., Wassgren, C. R., Nagapudi, K., & Muliadi, A. R. (2022). Capsule-based dry powder inhaler evaluation using CFD-DEM simulations and next generation impactor data. *European Journal of Pharmaceutical Sciences, 175*, 106226.
4. Burnell, P. K., Asking, L., Borgström, L., Nichols, S. C., Olsson, B., Prime, D., & Shrubb, I. (2007). Studies of the human oropharyngeal airspaces using magnetic resonance imaging IV—the oropharyngeal retention effect for four inhalation delivery systems. *Journal of aerosol medicine, 20*(3), 269-281.
5. Cai, X., Ma, B., Kourmatzis, A., Salehi, F., Lee, A., Farina, D., Chan, K., & Cheng, S. (2022). Potential effects of inhaler mouthpiece size on particle deposition in the human upper airway. *Aerosol Science and Technology, 56*(9), 802-818.
6. Chang, R. Y., Wong, J., Mathai, A., Morales, S., Kutter, E., Britton, W., Li, J., & Chan, H.-K. (2017). Production of highly stable spray dried phage formulations for treatment of Pseudomonas aeruginosa lung infection. *European Journal of Pharmaceutics and Biopharmaceutics, 121*, 1-13.
7. Cheng, S., Kourmatzis, A., Mekonnen, T., Gholizadeh, H., Raco, J., Chen, L., Tang, P., & Chan, H.-K. (2019). Does upper airway deformation affect drug deposition? *International Journal of Pharmaceutics, 572*, 118773.
8. Colthorpe, P., Voshaar, T., Kieckbusch, T., Cuoghi, E., & Jauernig, J. (2013). Delivery characteristics of a low-resistance dry-powder inhaler used to deliver the long-acting muscarinic antagonist glycopyrronium. *Journal of drug assessment, 2*(1), 11-16.
9. Delvadia, R. R., Longest, P. W., & Byron, P. R. (2012). In vitro tests for aerosol deposition. I: Scaling a physical model of the upper airways to predict drug deposition

variation in normal humans. *Journal of aerosol medicine and pulmonary drug delivery, 25*(1), 32-40.
10. Dunbar, C., & Mitchell, J. (2005). Analysis of cascade impactor mass distributions. *Journal of aerosol medicine, 18*(4), 439-451.
11. Elserfy, K., Kourmatzis, A., Chan, H.-K., Walenga, R., & Cheng, S. (2020). Effect of an upstream grid on the fluidization of pharmaceutical carrier powders. *International Journal of Pharmaceutics, 578*, 119079.
12. Finlay, W. H. (2001). *The mechanics of inhaled pharmaceutical aerosols: an introduction*: Elsevier.
13. Golshahi, L., Finlay, W. H., & Wachtel, H. (2022). Use of airway replicas in lung delivery applications. *Journal of aerosol medicine and pulmonary drug delivery, 35*(2), 61-72.
14. Golshahi, L., Noga, M. L., Vehring, R., & Finlay, W. H. (2013). An in vitro study on the deposition of micrometer-sized particles in the extrathoracic airways of adults during tidal oral breathing. *Annals of biomedical engineering, 41*(5), 979-989.
15. Grgic, B., Finlay, W. H., Burnell, P. K., & Heenan, A. F. (2004). In vitro intersubject and intrasubject deposition measurements in realistic mouth–throat geometries. *Journal of Aerosol Science, 35*(8), 1025-1040.
16. Grgic, B., Finlay, W. H., & Heenan, A. (2004). Regional aerosol deposition and flow measurements in an idealized mouth and throat. *Journal of Aerosol Science, 35*(1), 21-32.
17. Gutiérrez Villegas, C., Paz-Zulueta, M., Herrero-Montes, M., Parás-Bravo, P., & Madrazo Pérez, M. (2021). Cost analysis of chronic obstructive pulmonary disease (COPD): a systematic review. *Health Economics Review, 11*(1), 1-12.
18. Helwany, M., & Rathee, M. (2022). Anatomy, head and neck, palate. In *StatPearls [Internet]*: StatPearls Publishing.
19. Huang, F., Zhou, X., Dai, W., Yu, J., Zhou, Z., Tong, Z., & Yu, A. (2022). In Vitro and In Silico Investigations on Drug Delivery in the Mouth-Throat Models with Handihaler®. *Pharmaceutical research, 39*(11), 3005-3019.
20. Islam, N., & Cleary, M. J. (2012). Developing an efficient and reliable dry powder inhaler for pulmonary drug delivery–a review for multidisciplinary researchers. *Medical engineering & physics, 34*(4), 409-427.
21. Jarhyan, P., Hutchinson, A., Khaw, D., Prabhakaran, D., & Mohan, S. (2022). Prevalence of chronic obstructive pulmonary disease and chronic bronchitis in eight countries: a systematic review and meta-analysis. *Bulletin of the World Health Organization, 100*(3), 216.
22. Jõgi, R., Mattila, L., Vahteristo, M., Takala, A., Lähelmä, S., Vartiainen, V. A., & Lindqvist, A. (2021). Inspiratory flow parameters through dry powder inhalers in healthy volunteers and patients with chronic obstructive pulmonary disease (COPD): device resistance does not limit use in COPD. *International Journal of Chronic Obstructive Pulmonary Disease*, 1193-1201.
23. Kadota, K., Sosnowski, T. R., Tobita, S., Tachibana, I., Tse, J. Y., Uchiyama, H., & Tozuka, Y. (2020). A particle technology approach toward designing dry-powder inhaler formulations for personalized medicine in respiratory diseases. *Advanced Powder Technology, 31*(1), 219-226.
24. Kourmatzis, A., Cheng, S., & Chan, H.-K. (2018). Airway geometry, airway flow, and particle measurement methods: implications on pulmonary drug delivery. *Expert opinion on drug delivery, 15*(3), 271-282.

25. Labiris, N. R., & Dolovich, M. B. (2003). Pulmonary drug delivery. Part II: the role of inhalant delivery devices and drug formulations in therapeutic effectiveness of aerosolized medications. *British journal of clinical pharmacology*, *56*(6), 600-612.
26. Leung, S. S. Y., Parumasivam, T., Tang, P., & Chan, H.-K. (2016). A proof-of-principle setup for delivery of Relenza®(Zanamivir) inhalation powder to intubated patients. *Journal of aerosol medicine and pulmonary drug delivery*, *29*(1), 30-35.
27. Lizal, F., Elcner, J., Jedelsky, J., Maly, M., Jicha, M., Farkas, Á., Belka, M., Rehak, Z., Adam, J., & Brinek, A. (2020). The effect of oral and nasal breathing on the deposition of inhaled particles in upper and tracheobronchial airways. *Journal of Aerosol Science*, *150*, 105649.
28. Ma, B., Kourmatzis, A., Zhao, Y., Yang, R., Chan, H.-K., Salehi, F., & Cheng, S. (2020). Potential effects of lingual fats on airway flow dynamics and particle deposition. *Aerosol Science and Technology*, *54*(3), 321-331.
29. Ma, Z., Kourmatzis, A., Milton-McGurk, L., Chan, H.-K., Farina, D., & Cheng, S. (2022). Simulating the effect of individual upper airway anatomical features on drug deposition. *International Journal of Pharmaceutics*, *628*, 122219.
30. Marple, V. A., Olson, B. A., Santhanakrishnan, K., Mitchell, J. P., Murray, S. C., & Hudson-Curtis, B. L. (2003). Next generation pharmaceutical impactor (a new impactor for pharmaceutical inhaler testing). Part II: Archival calibration. *Journal of aerosol medicine*, *16*(3), 301-324.
31. Mekonnen, T., Cai, X., Burchell, C., Gholizadeh, H., & Cheng, S. (2022). A review of upper airway physiology relevant to the delivery and deposition of inhalation aerosols. *Advanced Drug Delivery Reviews*, 114530.
32. Mitchell, J., Copley, M., Sizer, Y., Russell, T., & Solomon, D. (2012). Adapting the Abbreviated Impactor Measurement (AIM) concept to make appropriate inhaler aerosol measurements to compare with clinical data: a scoping study with the "Alberta" Idealized Throat (AIT) inlet. *Journal of aerosol medicine and pulmonary drug delivery*, *25*(4), 188-197.
33. Mohan, M., Lee, S., Guo, C., Peri, S. P., & Doub, W. H. (2017). Evaluation of abbreviated impactor measurements (AIM) and efficient data analysis (EDA) for dry powder inhalers (DPIs) against the full-resolution next generation impactor (NGI). *AAPS PharmSciTech*, *18*, 1585-1594.
34. Mohsenin, V. (2001). Gender differences in the expression of sleep-disordered breathing: role of upper airway dimensions. *Chest*, *120*(5), 1442-1447.
35. Newman, S. P. (2022). Fine particle fraction: The good and the bad. *Journal of aerosol medicine and pulmonary drug delivery*, *35*(1), 2-10.
36. Pate, C. A., Zahran, H. S., Qin, X., Johnson, C., Hummelman, E., & Malilay, J. (2021). Asthma surveillance—United States, 2006–2018. *MMWR Surveillance Summaries*, *70*(5), 1.
37. Pharmacopoeia, B. (2012). Appendix XII C: Consistency of formulated preparations. *Her Majesty's Stationary Office, London, UK*.
38. Singh, G., Tang, P., Cheng, S., Chan, H.-K., & Kourmatzis, A. (2022). From laminar to turbulent flow in a dry powder inhaler: The effect of simple design modifications. *International Journal of Pharmaceutics*, *616*, 121556.
39. Stapleton, K. W., Guentsch, E., Hoskinson, M., & Finlay, W. H. (2000). On the suitability of k–ε turbulence modeling for aerosol deposition in the mouth and throat: a comparison with experiment. *Journal of Aerosol Science*, *31*(6), 739-749.
40. Stolbrink, M., Thomson, H., Hadfield, R. M., Ozoh, O. B., Nantanda, R., Jayasooriya, S., Allwood, B., Halpin, D. M., Salvi, S., & de Oca, M. M. (2022). The availability, cost, and affordability of essential medicines for asthma and COPD in low-income and

middle-income countries: a systematic review. *The Lancet Global Health, 10*(10), e1423-e1442.
41. USP. (2023). General Chapter, ⟨601⟩ Inhalation and Nasal Drug Products: Aerosols, Sprays, and Powders—Performance Quality Tests. In. Rockville, MD: United States Pharmacopeia.
42. Wallin, M., Tang, P., Chang, R. Y. K., Yang, M., Finlay, W. H., & Chan, H.-K. (2019). Aerosol drug delivery to the lungs during nasal high flow therapy: an in vitro study. *BMC pulmonary medicine, 19*, 1-11.
43. Yoshida, H., Kuwana, A., Shibata, H., Izutsu, K.-i., & Goda, Y. (2017). Comparison of aerodynamic particle size distribution between a next generation impactor and a cascade impactor at a range of flow rates. *AAPS PharmSciTech, 18*, 646-653.
44. Zhao, Y., Raco, J., Kourmatzis, A., Diasinos, S., Chan, H.-K., Yang, R., & Cheng, S. (2020). The effects of upper airway tissue motion on airflow dynamics. *Journal of biomechanics, 99*, 109506.
45. Zhou, Y., Sun, J., & Cheng, Y.-S. (2011). Comparison of deposition in the USP and physical mouth–throat models with solid and liquid particles. *Journal of aerosol medicine and pulmonary drug delivery, 24*(6), 277-284.

Chapter 5 Measurement of particle deposition and velocity in a human upper airway model using laser attenuation

(This chapter will be submitted very shortly to the International Journal of Pharmaceutics)

Building upon previous computational (CFD) and in-vitro deposition studies, this chapter introduces an experimental approach that provides real-time insights into aerosol transport in the human upper airway. While in-vitro experiments offer valuable data on deposition patterns, they do not capture the transient behavior of drug particles during inhalation. To bridge this gap, this study integrates a laser-based measurement technique to track particle motion dynamically, offering a more comprehensive understanding of drug aerosol behavior.

This study aims to demonstrate a novel methodology for analyzing drug particle flow in a realistic model of the human upper airway. A realistic airway model was reconstructed based on MRI data using 3D printing techniques. Two spray dried mannitol powder types with volume median sizes of 3.22 µm and 6 µm, with a span of 1.90 µm and 2.12 µm, were loaded into an Osmohaler inhaler. The osmohaler was attached to the inlet of the airway model and the experiments were performed under 3 different flow rates (20 LPM, 40 LPM and 60 LPM). Four pairs of observation windows were installed at four different regions of the upper airway model (mouth, uvula, epiglottis and trachea). Laser and photodiode techniques were employed to investigate the transient flow behavior in a realistic human upper airway model. Signal analysis was utilized to examine average drug particle velocity, escape time, and regional deposition at various locations along the airway. Results from this study suggest that a simple laser attenuation method offer substantial insight into the in-airway dynamics of transient drug particle flow.

5.1 Introduction

The prevalence of respiratory disorders, such as asthma and chronic obstructive pulmonary disease (COPD), which are characterized by persistent airway inflammation and bronchial obstruction (Caramori & Adcock, 2003; Fabbri et al., 2003), remain a significant global health

concern. According to a 2019 estimation by the World Health Organization, COPD ranks as the third leading cause of mortality worldwide, resulting in an annual death toll of 3.2 million individuals (WHO, 2023; X. Yang et al., 2021), while asthma affects a staggering 262 million people globally (Vos et al., 2020). The inhalation of an aerosol formulation is the preferred route for treating these pulmonary diseases due to reduced drug wastage (Hoppentocht et al., 2014), minimal systemic side effects, and higher concentration of medication at the targeted site of action (Nancy Renee Labiris & Myrna B Dolovich, 2003; Scichilone et al., 2015). Attributed to the ability to provide convenient and user-friendly formulations for patients, pressurized metered dose inhalers (pMDI) and dry powder inhalers (DPI) are widely used (Haidl et al., 2016; Khanal et al., 2020). In recent years, dry powder inhalers have been the subject of substantial research studies aimed towards understanding the intricate interplay between anatomical geometry (Shaokoon Cheng et al., 2019; Delvadia et al., 2012; Wei et al., 2018), inhaler device, inhalation flow rate, and drug particle size (Cai et al., 2022; Chew et al., 2000; Chew & Chan, 1999; Weers & Clark, 2017) in determining the effectiveness of dry powder aerosol medication delivery to the respiratory system.

The human airway can be considered to be composed of three major anatomical sections, namely the extrathoracic region, the tracheobronchial region, and the alveolar region (Ahookhosh et al., 2020). Investigation of particle transportation mechanisms in the extrathoracic region is commonly analyzed separately due to the substantial deposition of undesired drug particles in the upper airway (W. H. Finlay, 2001; Grgic, Finlay, Burnell, et al., 2004) and limitations associated with imaging technologies (A Kourmatzis et al., 2018). Standard nuclear imaging, including two-dimensional (2D) gamma scintigraphy, X-ray computerized tomography (CT), Positron Emission Tomography (PET), single Photon Emission Computed Tomography (SPECT), and magnetic resonance imaging (MRI) are critically important in pulmonary drug delivery by measuring anatomical features, but can only measure the drug deposition by using radiolabelled drug particles (Conway, 2012; Milne & King, 2014; Venegas et al., 2013) at relatively low resolution, and typically only post deposition. Details such as extrathoracic airflow mechanics or particle trajectories, cannot be accurately obtained during inhalation due to the lack of both temporal and spatial resolution (A Kourmatzis et al., 2018).

Numerous in-vivo and in-vitro correlation (IVIVC) (Byron et al., 2010; Grgic, Finlay, Burnell, et al., 2004; Newman & Chan, 2020; Wei et al., 2018) studies have been conducted in pulmonary drug delivery to investigate the flow behavior of drug particles within the human

upper airway. Cascade impactors (S. S. Y. Leung et al., 2015; X. Yang et al., 2021) remain a standard measurement in the pharmaceutical industry for conducting in vitro testing of inhaled drugs and determining the aerodynamic particle size distribution under specific flow rates and inhalation conditions(J. P. Mitchell & Nagel, 2003). The combination of idealized mouth throat models with cascade impactors is commonly employed to obtain an overall deposition in the extrathoracic region (Shaokoon Cheng et al., 2019; Chrystyn et al., 2015), with the advancement of 3D printing having facilitated the utilization of realistic airway models in this field (A. R. Martin et al., 2018). However, despite the usefulness of impactors in measuring aerodynamic particle size, their limitations of are widely recognized, being poor flow rate sensitivity (J. P. Mitchell & Nagel, 2003) and also high labour intensity. Furthermore, similar to medical imaging techniques, cascade impactors cannot provide drug particle flow behavior and deposition information simultaneously (J. P. Mitchell & Nagel, 2003).

In vitro laser imaging techniques, such as Particle Image Velocimetry (PIV) (Schröder & Willert, 2008; Soodt et al., 2012) and Laser/phase Doppler anemometry (Kakade et al., 2007), have been extensively employed in the field of fluid mechanics to investigate flow behavior in pulmonary drug delivery. However, these techniques are generally incapable of quantifying deposition in airway models (Schröder & Willert, 2008). Additionally, the necessary experimental equipment for PIV, such as a laser with a short pulse width and a high-speed camera, incurs significant costs (A Kourmatzis et al., 2018). The technique of laser diffraction is extensively used for volume particle size distribution measurement, with commonly recognized commercial variants being the Malvern Mastersizer (Liang et al., 2014) and Malvern Sparytec (Tang et al., 2023). Complementing laser based particle velocity and size measurements is computational fluid dynamics (CFD) which plays a vital role in the field by providing simulated flow field results and deposition in the human upper airway simultaneously where experimental methods are more challenging to implement (Bingjie Ma et al., 2020; Z. Ma et al., 2022). However, the validation of computational results necessitates the incorporation of experimental studies, and a further issue is that certain computational models, such as large eddy simulation (LES), require substantial computational resources (W. Faizal et al., 2020). Therefore, despite significant progress made in in-vitro and in-silico methods there still remains a need to provide quantitative measurements of particle dynamics, as they relate to in pulmonary drug delivery which provide insight into both particle velocity as well as deposition information, simultaneously.

The laser attenuation method is one experimental method that has been extensively employed in the past for investigating powders and sprays. A recent study conducted by (Mahmoudi et al., 2019) employed a two-beam line of sight attenuation method, and revealed fundamental characteristics of fluidization behavior exhibited by lactose powders within a simple channel flow. An earlier study by (Ju et al., 2010) investigated the characteristics of propellant mass fraction from pressurized metered dose inhalers using a similar method which followed from earlier work by (Kourmatzis, 2007). The above studies were all inspired by an earlier low-cost photo-transistor-based method which was proposed to accurately measure the velocity distribution of suspended particles in a gas-solid flow within a vertical channel, contributing to advancements in the field of dilute pneumatic conveying research (Dyakowski & Williams, 1993). Despite the wide use of laser extinction method in the existing research for studying powders and sprays, there remains a lack of application of this method to the study of drug particle dynamics within the human airways.

In this paper, we propose a simple approach using multiple laser diodes and photodiode sensors to simultaneously measure regional deposition and particle cluster velocity in a realistic human upper airway model. This approach enables a real-time measurement of the dynamics of particles within realistic airway geometries non-intrusively, and we also demonstrate that the results obtained provide physically meaningful data that can be interpreted alongside CFD model data. Spray-dried pharmaceutical particles delivered through an Osmohaler are investigated in this research. The discussion includes analysis of the regional deposition in the human upper airway, particle cluster transport velocity, and evaluation of inhaler evacuation time using different particle sizes (D50 = 3um, 6um) under three distinct flow rate conditions (20 LPM, 40 LPM, and 60 LPM).

5.2 Methods

5.2.1 Airway reconstruction

MRI images from a healthy human subject, with a body mass index (BMI) of 39.5 kg/m^2 indicating overweight but no history of respiratory diseases, were utilized for the reconstruction of three-dimensional (3D) models of the upper airway. The image stack (276 voxels * 448 voxels * 468 voxels) was generated in a computer modelling program (3D Slicer (https://www.slicer.org/)), using a cube with a voxel size of 0.25 mm. The MRI images were

meticulously examined to ensure the integrity of anatomical structures, prior to being subjected to post-processing using the computer modelling program Rhino 7 (Rhino 7, Robert McNeel & Associates, Seattle, Washington). The resulting data was subsequently transformed into poly-surfaces and imported into 3D modelling software to generate models by subtracting the airway structure from the mold, thereby creating the inner lumen. The mold was then saved in STL file format for 3D printing. Manufacturing of the mold was done using a 3D printer (UP Box). PrusaSlicer software (PrusaSlicer 2.5.0, Prusa Research, Prague, Czech Republic) was used for the slicing process. The airway mold was fabricated using Fused Deposition Manufacturing (FDM) with the 3D printer. PolyLactic Acid (PLA) based filament was used for the airway fabrication in a 1.75 mm filament diameter. The Extruder temperature and bed temperature was set as 210 °C and 60 °C, respectively. The nozzle diameter is 0.4 mm, in combination with a print speed of 60mm/s and an infill density of 20%. The 3D model of the airway is provided in the appendix.

5.2.2 Mannitol powder preparation

The administration of inhaled dry powder Mannitol enhances mucociliary clearance (Chan et al., 2011) and has been utilized for the diagnosis of asthma as well as the treatment of cystic fibrosis (S. D. Anderson et al., 2018). Due to the narrow size distribution, well characterized dispersion behavior through previous studies of the authors', and cost-effectiveness, spray-dried mannitol was selected to be used in current study. The raw material mannitol powder (supplied by Pharmaxis Ltd, Sydney) was dissolved in deionised water to prepare mannitol solutions at a concentration of 100 mg/mL. A spray dryer (Buchi B-290, BUCHI Labortechnik AG, Flawil, Switzerland) was utilized to generate different sizes of spray-dried particles with a volume median diameter of 3.2 µm and 6.5 µm. The spray dry conditions employed are detailed in Table 5.1.

Table 5. 1: Spray drying condition for mannitol.

Feed concentration (mg/mL)	Inlet temperature (°C)	Outlet temperature (°C)	Feed rate (mL/min)	Aspiration (m3/h)	Atomising airflow (L/h)
100	140	75	4.2	35	742
100	175	84	4.5	35	742

5.2.3 Particle size of dry powder

The particle size distributions of spray-dried mannitol were determined using laser diffraction analysis (Mastersizer 3000, Malvern Instruments Ltd., UK). The mannitol sample was loaded into a Scirocco 2000 dry powder feeder (Malvern Instruments, UK) and dispersed in air under a pressure of 0.8 bar. The refractive indices for material and absorption of mannitol were set at 1.544 and 0.100 respectively. The refractive index (RI) of the dispersant was set to 1.0, which was considered accurate based on the low weighted residual values (< 0.61%) obtained from all measurements. These values indicate a strong correlation between the measured scattering data and the predicted data derived from optical properties. The volumetric diameters (D50) of two spray-dried mannitols were determined to be 3.22 μm and 6.5 μm, with a span ((D90 − D10)/D50) of 1.90 and 2.12, respectively.

5.2.4 Experimental setup

5.2.4.1 Laser integrated airway model

A schematic of the experimental setup is shown in Figure 5. 1. Four pairs of windows were located at four representative positions in the human upper airway: position 1 - mouth region; position 2 - sub uvula; position 3 – sub-epiglottis region; position 4 - trachea region. The windows were created using laser cutting techniques (Epilog Fusion M2 75W CO2 Laser Cutter), employing acrylic material with dimensions of 3.2 × 2.8 mm to precisely match the size of the photodiode. The laser diodes (VLM-520-01) and Si PIN photodiodes (S1223-01) are positioned on opposite sides of the pair of windows on the airway model to ensure that the laser passes through the airway inner lumen across the transparent window and accurately hits the detection area of the photo diode. The laser diodes were all connected to a direct current (DC) power supply, while the photodiodes were connected to the data acquisition card (DAQ NI 9215) in parallel with an amplified circuit for photodiode signal data acquisition. The computer also established a connection with the DAQ card to facilitate system control, data collection, and visualization using a computer software Labview. The subsequent signal analysis and processing was conducted using MATLAB.

The experiment utilized two different mannitol powders with a spray-dried volume median diameter (D50) of 3.22 ± 0.03 μm and 6.52 ± 0.02 μm, respectively. These particle sizes were chosen to represent typical ranges found in dry powder inhalers, balancing between those

capable of reaching the lower airways and those more likely to deposit in the upper airway. The 20 mg ± 0.20 powder was filled into a size 3 hydroxypropylmethylcellulose capsule (Capsugel, Sydney, Australia) prior to being loaded into a dry powder inhaler (Osmohaler). The low-pressure drop mass flow meter (TSI 4040 Series Mass Flowmeter) was connected to a vacuum source which was attached to the outlet of the airway model, allowing for the attainment of three distinct fixed flow rates (20 LPM, 40 LPM, and 60 LPM) at the inlet of the airway model when Osmohaler was used. The vacuum source is controlled by a two-way solenoid valve and pressure regulator. The 10s duration and data acquisition time from each experiment was controlled by the computer. All the experiments were done in triplicate.

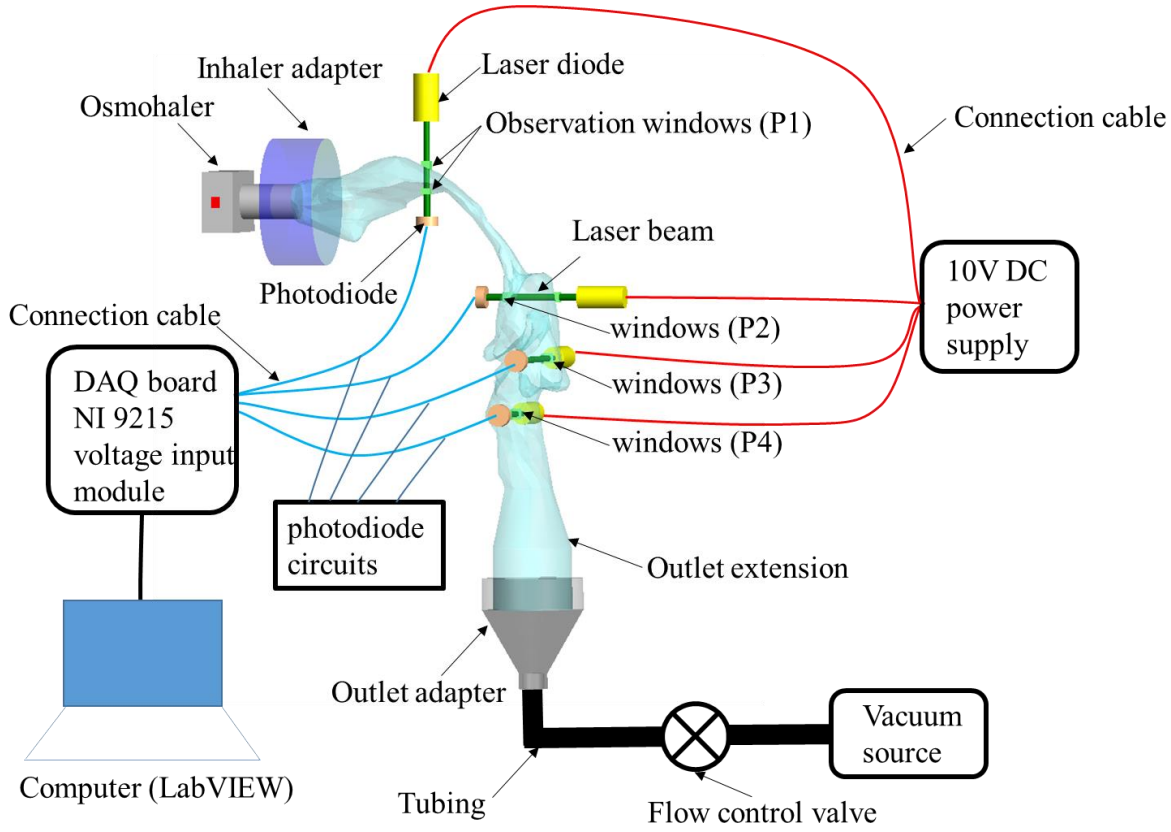

Figure 5. 1: Schematic of the experiment.

5.2.4.2 Calibration experiment

A calibration experiment was designed to quantify the relationship between laser signal transmittance variation and regional deposition. A 3D printed United States Pharmacopeia

(USP) induction port (USP, 2023) with portable window on was used in the experiment. All experimental procedures were identical to those employed in the main experiment in terms of laser power and acquisition settings.

After each experimental run, the window was weighed on a mass balance to verify changes in mass due to the deposition of drug particles on the window wall. Laser power measurements were taken before and after the experiment across the window to assess variations in transmittance which combined with mass change, were then plotted as a linear relationship relating total deposition on an imaging window vs. transmittance. This process is demonstrated in Figure 5. 2.

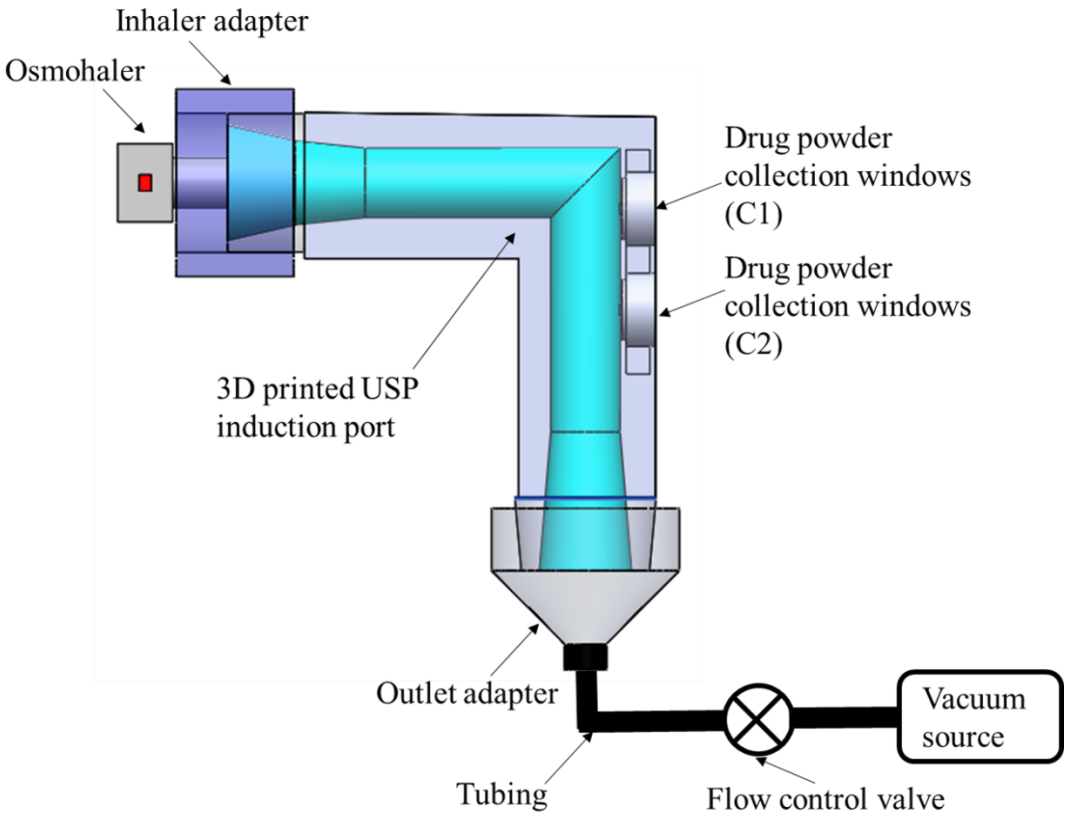
Inhaler adapter
Osmohaler
Drug powder collection windows (C1)
Drug powder collection windows (C2)
3D printed USP induction port
Outlet adapter
Vacuum source
Tubing
Flow control valve

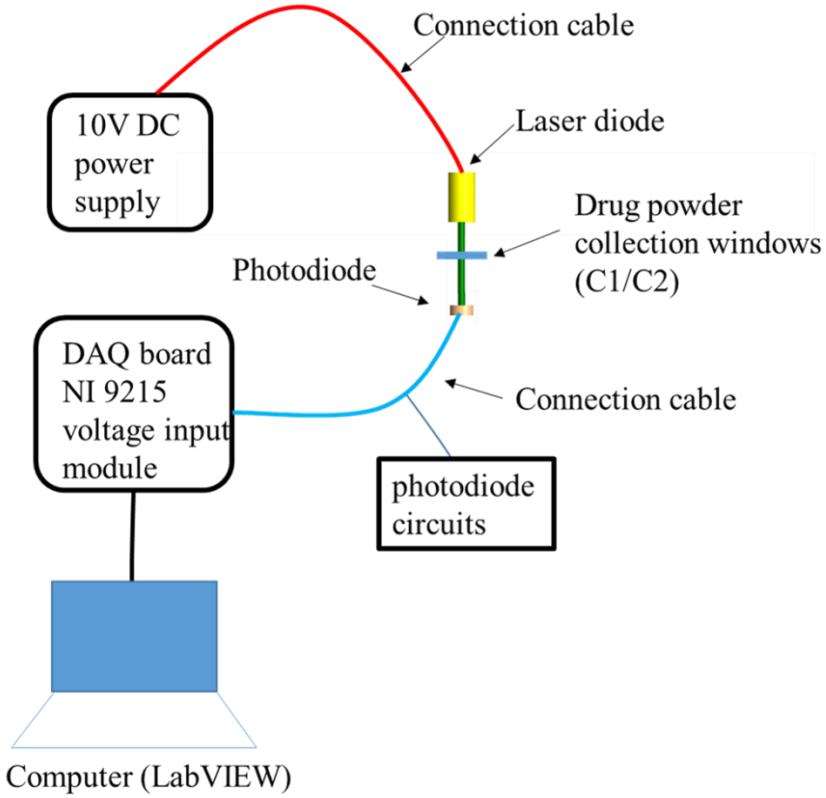
Connection cable
10V DC power supply
Laser diode
Drug powder collection windows (C1/C2)
Photodiode
DAQ board NI 9215 voltage input module
Connection cable
photodiode circuits
Computer (LabVIEW)

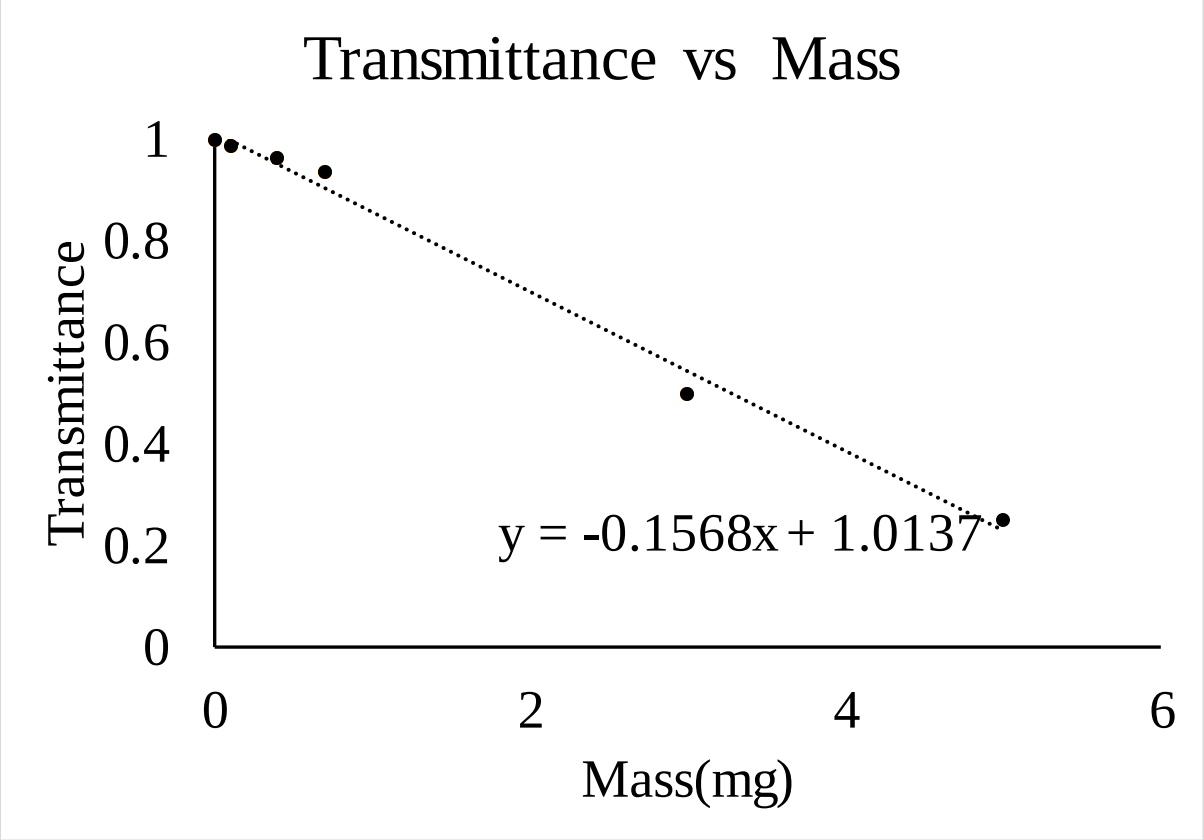

Figure 5. 2: Calibration experiment setup(a) and transmittance and mass relationship obtained from the experiment

5.2.5 Signal analysis and calculation method

The raw signal obtained from the experiment schematically shown in Figure 5. 1 was imported into MATLAB for analysis. Specifically, other than observations of the overall morphology of the signal, the frequency of the signal, the total period of the signal (i.e. escape time 'T') and the time delay between signals at different locations, were extracted. The frequency was computed using a standard Fast Fourier transform with a low pass filter used to eliminate background noise. The total escape time 'T', was determined by measuring the duration of the signal from the start-time: when the signal intensity began to drop below its background threshold to the end-time: when the signal intensity increased back to a value with a constant moving average. The time delay between two signals is computed using a standard signal cross-correlation with the delay time being computed as the lag time with the strongest normalized cross-correlation coefficient.

Throughout the results, the Reynolds number is used, where relevant, to categorize different flow conditions across airway models. In this study, the Reynolds number was defined and

calculated based on the flow rate, cross-sectional area, and airway diameter to estimate the average velocity.

$$Re = \frac{uD_T}{v}$$

Where u is the mean inflow velocity in the human airway, v is the kinematic viscosity of air (1.46×10^{-5} m2/s) (List, 1951), D_T is the hydraulic diameter, defined as:

$$D_T = \frac{4A}{P}$$

In which, A is the cross-sectional area of the airway perpendicular to the inflow, and P is the wetted perimeter.

5.3 Results and discussion

In this section, signal data obtained from different locations in the human upper airway will be presented and analyzed, allowing for quantifying the effect of turbulent flow in the human upper airway on regional particle velocity, deposition, drug particle escape time, and transient behavior of aerosols in the human respiratory tract. Measurements which help to define the nature of the transient drug particle flow within realistic human airway models are rare in the literature.

5.3.1 General features

General characteristics of the measured signals at different locations in the airway at flow rates of 20 LPM, 40 LPM, and 60 LPM with two different sizes of spray-dried particles are presented in this section. The signal collection positions (four representative positions in the human upper airway: position 1 (P1) - mouth region; position 2 (P2) - below the uvula; position 3 (P3) - below epiglottis; position 4 (P4) - trachea region) are shown in Figure 5. 3. The normalized discrete signal fluctuation in Figure 5. 4 represents the drug particle flow related light intensity variation detected by the optical sensor in the time domain, which illustrates the temporal behavior of dry powder dynamics in the human upper airway. The signal typically originates from a statistically stationary voltage before entering a transient state, which is induced by the movement of drug particles in the human airway, and then returns to a different statistically stationary voltage after the drug fully evacuations following inhaler activation.

In Figure 5. 4, at a lower flow rate of 20 LPM, particularly for the 6um particles the signals show signals with a gradual decline and significant similarity across positions 1 to 4. This is due to the inhaler gradually releasing fewer drug particles into the airway, resulting in an extended-release duration behavior which is captured through the signal. However, as the flow rate increases, a noticeable discrepancy arises between position 1 and the remaining three positions. The signals demonstrate a consistent strong attenuation followed by a recovery in the signal across all cases at position 1 whereas a significant and consistent decrease in signal transmittance is noted across positions 2 to 4 when the flow rate is increased to 40 LPM and 60 LPM. This is due to the increased strength of the air-flow at higher flow rate, resulting in the formation of a denser particle cloud within a short period, leading to a significant rise in light obstruction which results in the signal remaining attenuated, due to wall deposition. Regional deposition information can be obtained by comparing the start point and end point of the signal at different window positions. It is worth noting that the main features of different signals are generally consistent between different particle sizes, especially the two different particles used in the current study, which will be further analyzed in section 5.3.4.

The general features of the signals demonstrate overall temporal information regarding drug particle fluidization in the human upper airway, along with transient flow data and inhaler-related information, as well as information on regional deposition. To the best of the authors' knowledge, despite this method being simple, it is one of few studies demonstrating temporal and spatial information simultaneously in the context of drug particle fluidization and deposition in the human upper airway.

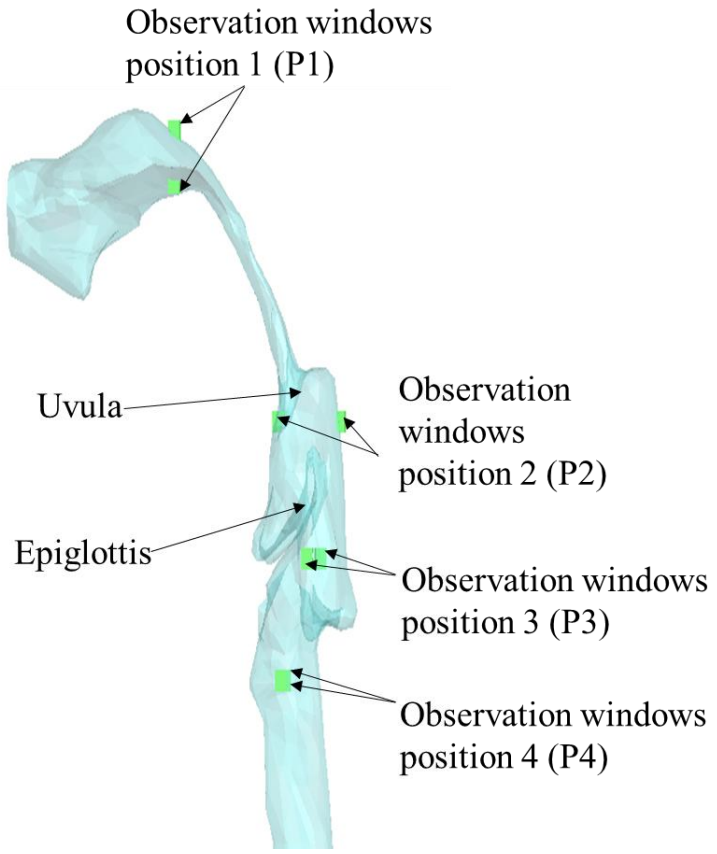

Figure 5. 3: Measurement positions in the human upper airway

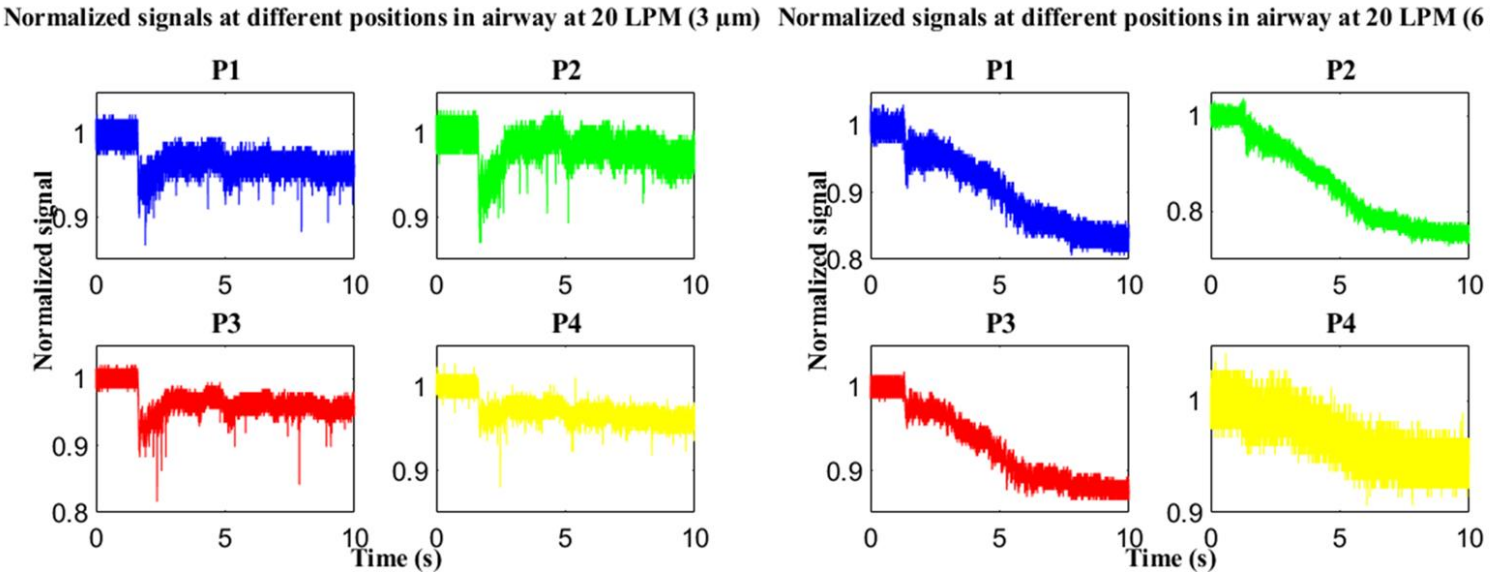

(a)

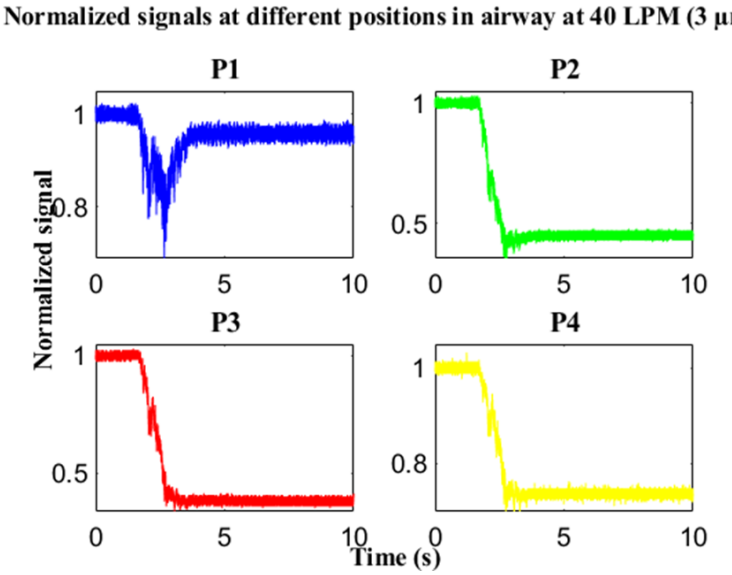

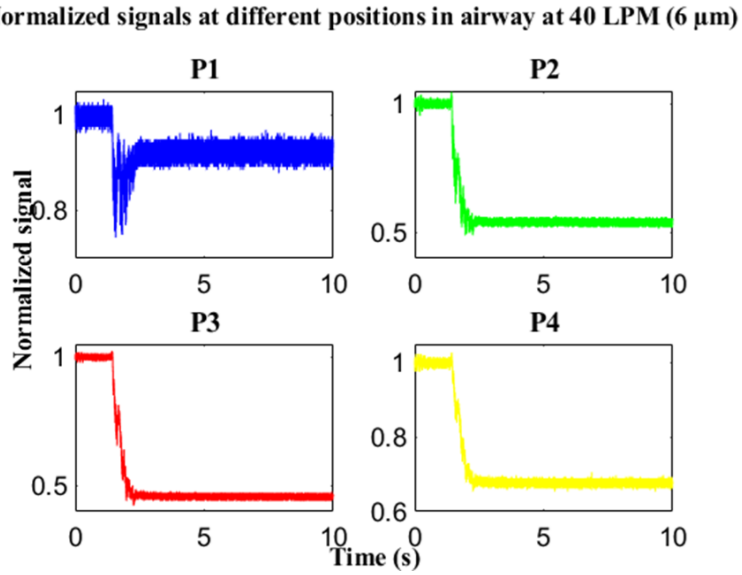

(b)

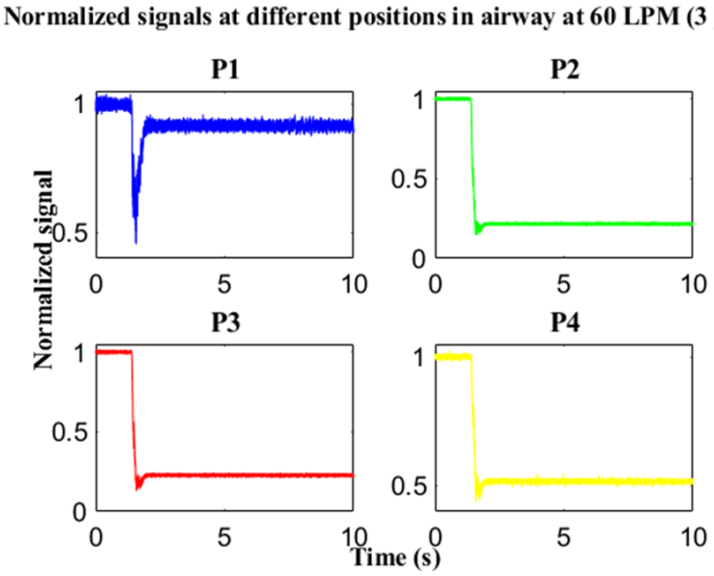

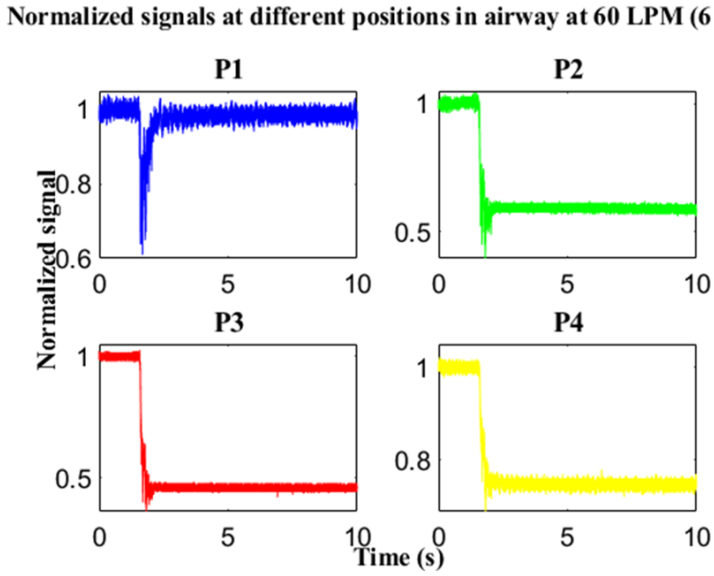

(c)

Figure 5. 4: Raw signal under three different flow rates with two drug particles (3 µm and 6 µm), (a): 20 LPM, (a): 40 LPM, (a): 60 LPM

5.3.2 Particle velocity

Figure 5. 5(a) shows the mean particle velocity magnitude, computed through the measured time delay from cross correlation and the distance between each sensor and shown at various locations under inhalation flow conditions of 20 LPM, 40 LPM, and 60 LPM using drug particles with sizes of 3 µm and 6 µm. The results show that the maximum particle velocity occurs under 60 LPM between position 1 and position 2 (soft palate region), which has the narrowest cross section area between the two measurement positions. In contrast, a different phenomenon is observed from position 1 to position 2 (soft palate region) under 20 LPM and 40 LPM conditions, which shows that the mean particle velocity is approximately 6 m/s, which is significantly lower than the velocity under 60 LPM. This might relate to the sub-optimal flowrate use of Osmohaler and the potential for reduced aerosolization efficiency of the powder. Our previous simulations, shown in Figure 5.5(b), support this finding, showing a similar trend in airflow velocity at 60 LPM.

The mean particle velocity from position 1 to position 4 (mouth-trachea) increases proportionally with the increase of flow rate from 20 LPM to 60 LPM. This observation validates the efficacy of our methodology in accurately capturing particle velocities across varying flow rates within the realistic human upper airway. The mean particle velocity is insensitive to the flow rate in the position 2 – position 3 region (uvula-epiglottis region) and the position 3 - position 4 regions (epiglottis-trachea region). This may be attributed to the turbulent flow generated by the complex anatomical features (uvula and epiglottis) in that region which results in multi-directional flow that can make cross-correlation along a line far less accurate. The reader is reminder that the measurement provided at a particular position along the airway is an integrated measurement across the lumen and therefore not spatially resolved.

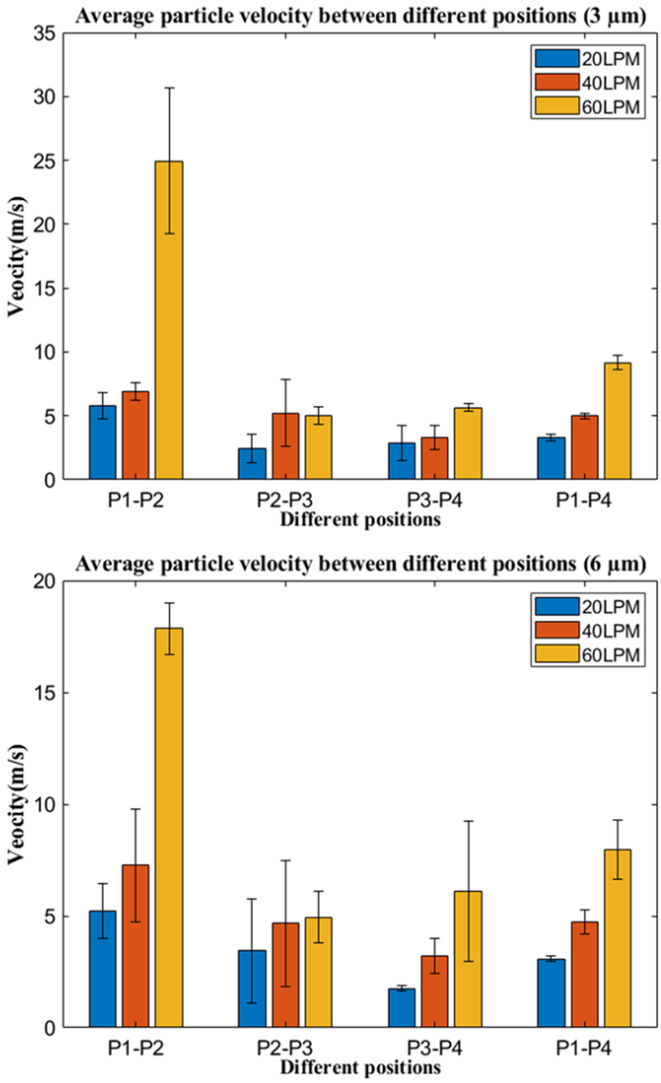
Average particle velocity between different positions (3 µm)
Veocity(m/s)
Different positions
20LPM
40LPM
60LPM
P1-P2
P2-P3
P3-P4
P1-P4
Average particle velocity between different positions (6 µm)
Veocity(m/s)
Different positions
20LPM
40LPM
60LPM
P1-P2
P2-P3
P3-P4
P1-P4

(a)

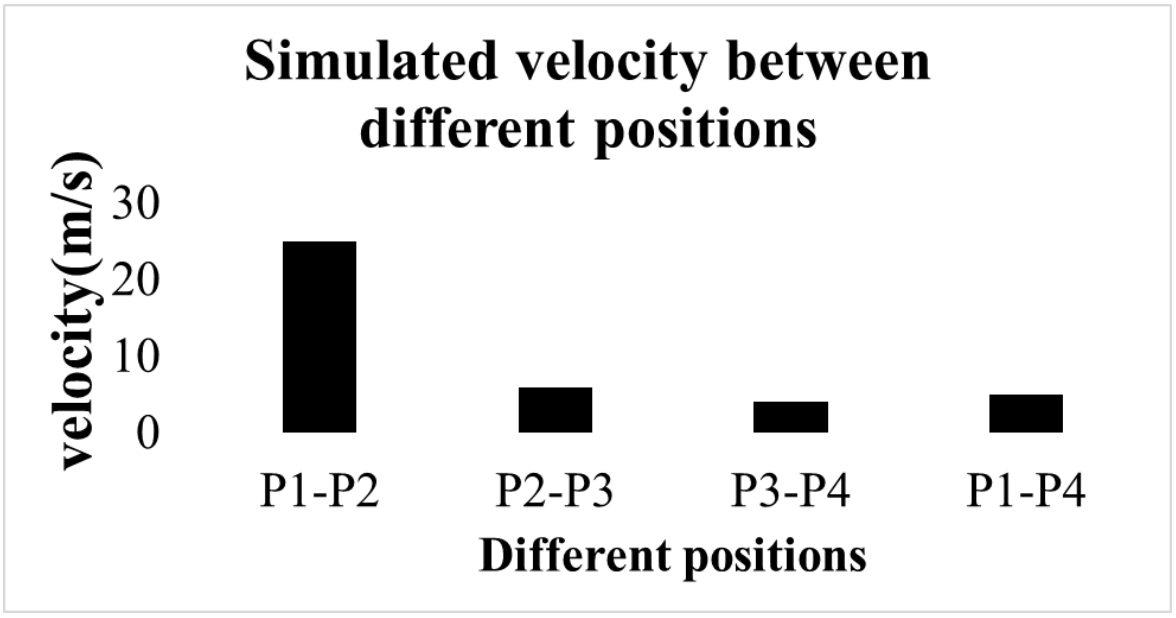
Simulated velocity between different positions
velocity(m/s)
Different positions
P1-P2
P2-P3
P3-P4
P1-P4

(b)

Figure 5. 5: (a) Particle velocity between different positions under different flow rate using two sizes of mannitol. Error bars refer to standard deviations, n=3. (b) Simulated velocity between different positions (normalized to 60 LPM).

Figure 5. 6 demonstrates the drug particle travelling time passing one single laser beam, indicating the aerosol escape time for inhalers. The escape time shows a consistency using powder with different particle sizes. The escape time is approximately seven seconds under 20 LPM conditions, representing a six-fold increase compared to the escape time of one second at 60 LPM. This is due to the suboptimal utilization of the Osmohaler, resulting in a gradual release of powder from the inhaler. When the flow rate increased to 40 LPM, which is the minimum effective working flow rate for Osmohaler, the escape time was reduced by 75%, from approximately 8 s to 2 s. Interestingly, the escape time for the large particle (6 μm) under 40LPM is observed to be shorter, which could be attributed to the reduced particle numbers at the same mass or improved particle lift behaviour. However, when increasing the flow rate to 60 LPM, the turbulent flow and rapid release of drug particles counteract this effect. The attainment of optimal therapeutic efficacy for inhalation aerosols often requires proper training in the correct use of inhalers(Haidl et al., 2016). The challenge faced by patients using inhalers lies in the difficulty of determining when the inhaler is depleted, as well as accurately measuring the dosage and duration required for effective airway administration. Analyzing escape time can offer valuable insights into inhalation duration and potentially serve as a guide and when combined with inhalation profile, this information can be valuable for evaluating the transient behavior of inhalers.

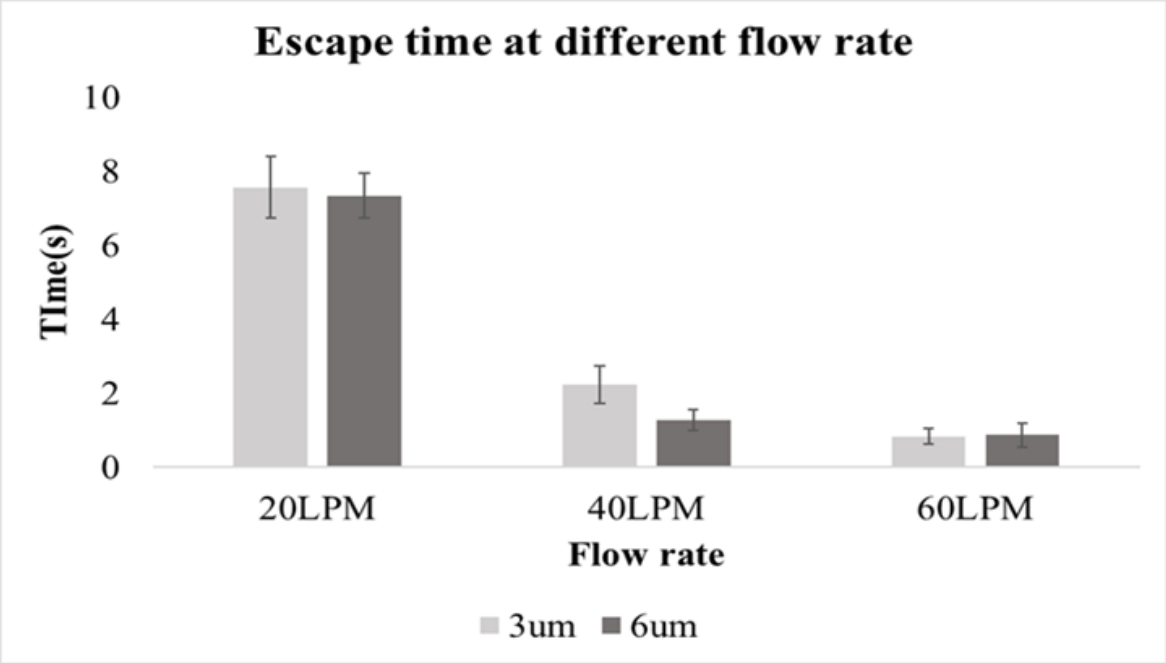

Figure 5. 6: Escape time at different flow rate. Error bars refer to standard deviations, n=3.

5.3.3 Regional deposition

Analysis of the signals can also shed light on regional deposition at different locations in the realistic human airway. Regional deposition plays a crucial role in enhancing our understanding of particle dynamics within different geometries, and also crucially, in acting as a source of data for CFD model validation.

Figure 5. 7(a) presents the results of the quantitative evaluation of regional deposition at four different locations in the human upper airway measured by using laser-optical sensor method based on 3 µm and 6 µm sized mannitol and at flow rates of 20 LPM, 40 LPM and 60 LPM.

The deposition increases from position 1 (mouth region) to position 2 (uvula region) and position 3 (epiglottis region), followed by a subsequent decrease from position 3 to position 4 (epiglottis-trachea region) under three different flow rates using two different sizes of particles. This is attributed to the different regional deposition affected by distinct anatomical features in the human upper airway. The deposition at positions 2, 3 and 4 using 3 µm particles significantly increases as the flow rate is increased from 20 LPM to 60 LPM. This observation aligns with numerous previous studies that have consistently shown a direct relationship between higher flow rates and increased deposition in the extrathoracic region. In contrast, the deposition in the mouth region (position 1) shows insensitivity to the flow rate, possibly related to reduced deposition in that area caused by the jet flow generated from the inhaler. Additionally, an interesting phenomenon was observed in the airway at four different positions.

The regional deposition fraction using 6 µm particles is similar to the regional deposition fraction using 3 µm particles, ranging from 20LPM to 40LPM. However, there is a decrease in deposition at different locations when the flow rate further increases from 40 LPM to 60 LPM. The reason may be attributed to the smooth surface of the acrylic window, which facilitates the detachment of larger particles at higher flow rates.

5.3.3.1 Comparison to literature

The assessment of regional deposition in the human upper airways typically involves the integration of medical imaging techniques and radiolabelled particles. A classic study (Grgic, Finlay, Burnell, et al., 2004) investigated a set of 7 representative realistic mouth throat moulds from 80 airway geometries obtained from MRI scans using radiolabelled drug particles and revealed that the motion of the tongue is crucial for the regional deposition in the upper airway. Compared to their planar image of regional deposition, most of their cases show less deposition in the middle part of the mouth region and higher deposition in the pharynx and larynx region, corresponding to our measurement positions 1,2 and 3, respectively. Our laser deposition data, which indicates a minimal deposition at position 1 (located in the central region of the oral cavity), are consistent with this earlier imaging study. The reduced deposition at position 1 may be attributed to the relatively flat morphology of the tongue in our model, which facilitates direct passage of aerosol jet flow through the oral region and into the deeper pharynx and larynx regions.

The effect of anatomical features on deposition was also investigated by Z. Ma et al.(Z. Ma et al., 2022) using CFD-DPM techniques. Regional deposition was plotted and analysed in that study. As depicted in Figure 5. 7(b), the simulation results (as shown in Figure 5.8) of regional deposition represent the fraction of deposited particles compared to the total deposition in the human airway, thereby demonstrating a consistent trend with our study. This further validates the potential utility of laser techniques for assessing airway deposition in human airway models.

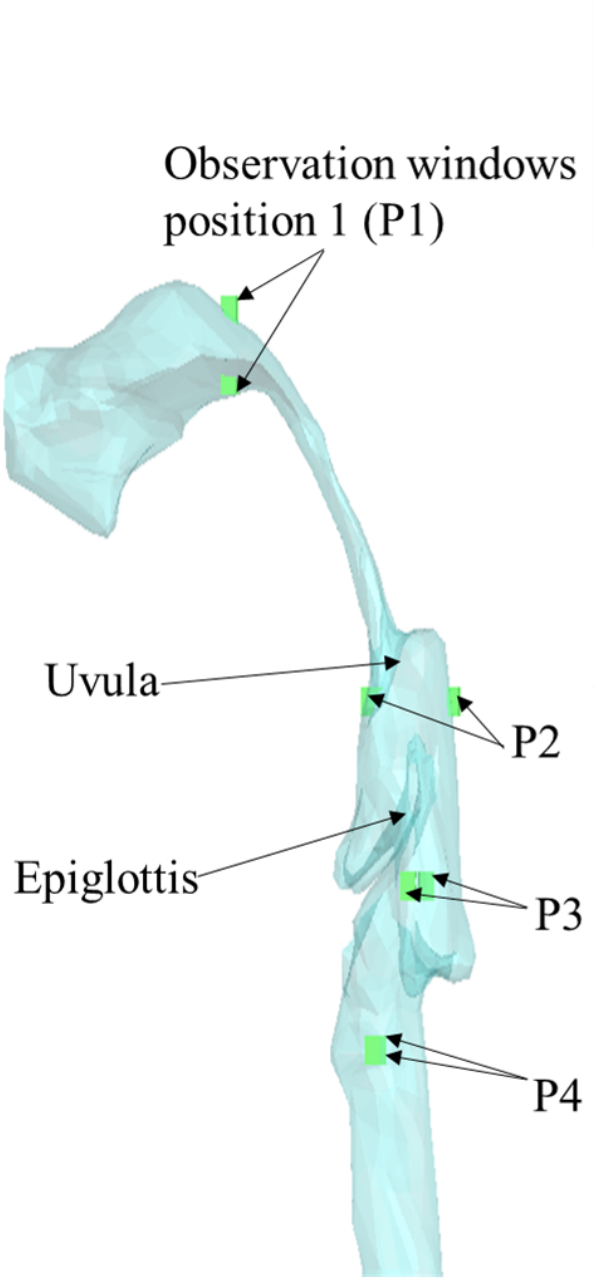

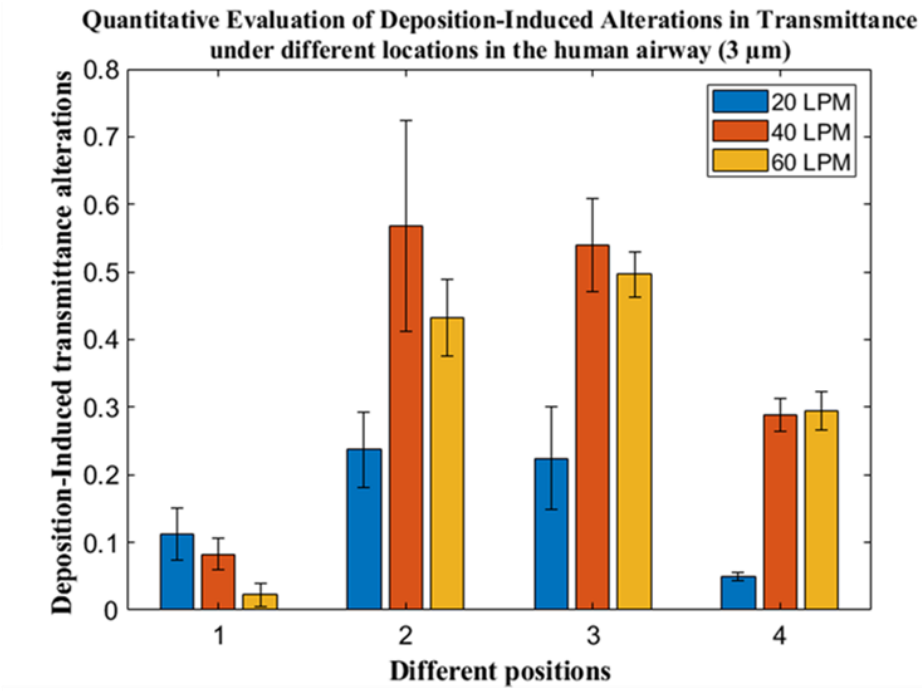

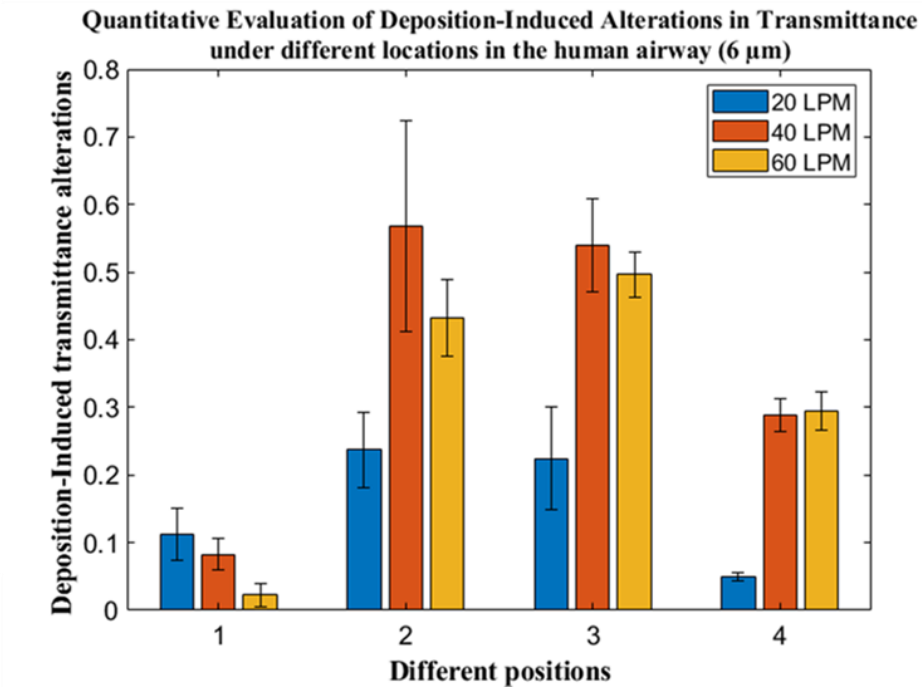

Figure 5. 7: Regional deposition between different positions under different flow rate using two sizes of mannitol. Error bars refer to standard deviations, n=3.

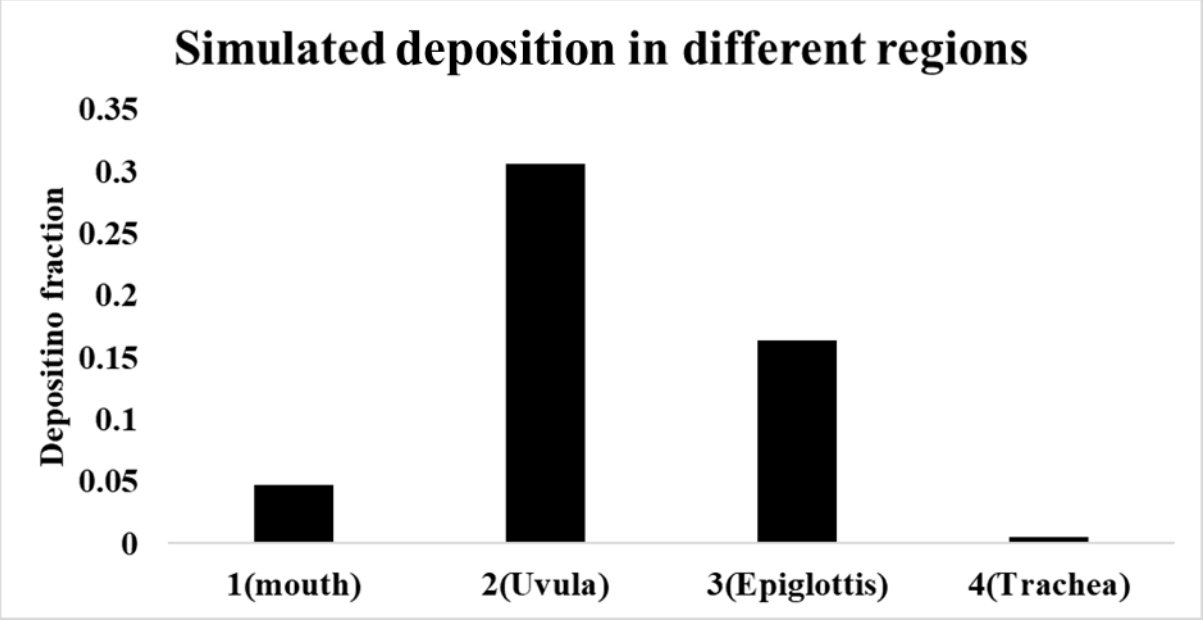

Figure 5. 8: Regional deposition from previous study ((Z. Ma et al., 2022)

5.3.4 Signal fluctuation and turbulence analysis

The aerosol signal is detected by the photodiode as a result of turbulent airflow in the human airway, it will impact the flow of drug aerosols within the human airway and consequently lead to signal fluctuations. By assessing the signal fluctuation at various locations, it facilitates understanding of the correlation between turbulent airflow and regional deposition within different segments of the human upper airway.

Figure 5. 9 illustrates the process of quantifying signal fluctuations. Each collected signal is fitted with a seventh-order polynomial to represent the mean signal during fluctuation analysis. The deviation of the signal is then calculated by comparing the difference between the regional signal and the polynomial fit. Subsequently, the standard deviation for each signal using 3 µm particles is computed and presented in Figure 5.10.

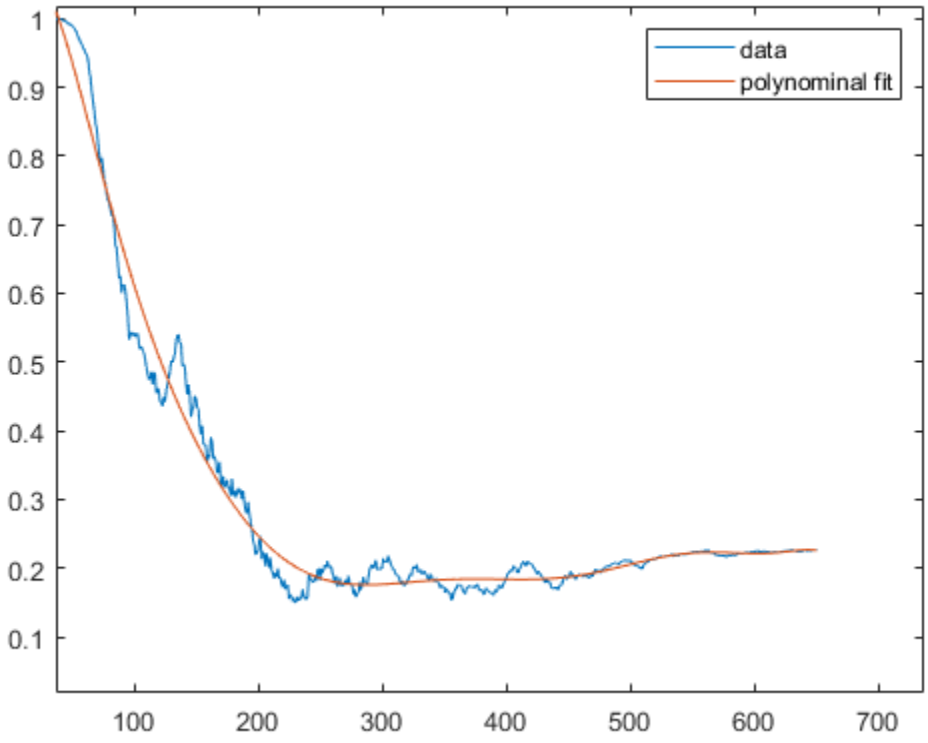

Figure 5. 9: Signal fluctuation with polynomial fit.

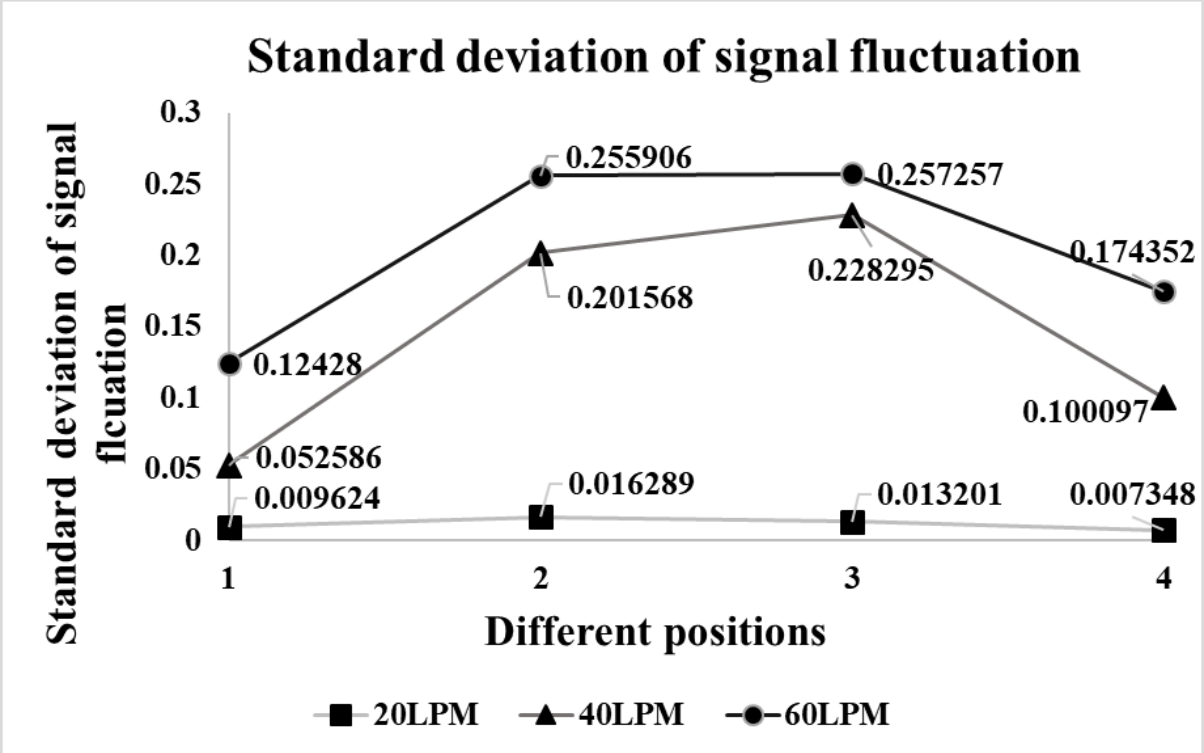

Figure 5. 10: Standard deviation of signal fluctuation

The standard deviation is consistently low at P1 but increases at P2 and P3 before decreasing again at P4. This phenomenon is closely associated with the airway geometry. At the mouth region (P1), the presence of a large cavity results in a lower regional particle velocity, thereby causing minimal fluctuations in signal. Conversely, at positions 2 and 3, where the anatomical geometry becomes more complex and the soft palate region narrows, there is a significant increase in particle velocity leading to a more turbulent flow within that specific area. Subsequently, as the flow enters the trachea region (P4), it gradually becomes less turbulent and homogeneous. Additionally, an observable increase in signal fluctuation occurs when increasing the flow rate.

Interestingly, this similar trend is observed in the regional deposition as depicted in Figure 9. This further implies that the regional deposition in the upper airway is closely associated with flow turbulence. From 20 LPM to 40 LPM, there is a notable increase in signal fluctuation, indicating an enhanced turbulence of regional particle flow. Comparing with Figure 9, there is a remarkable surge in regional deposition from 20 LPM to 40 LPM.

5.3.5 Spectral Analysis of Signals

The signal of drug particles collected from the photodiode in the experiment is a transient signal and therefore lends itself to additional analysis. The wavelet transform has been widely employed in various biomedical applications, such as Computer-Assisted Tomography (CAT), Magnetic Resonance Imaging (MRI), and Functional Image Analysis (PET and fMRI) (Unser & Aldroubi, 1996). In this section, the signal will be analyzed using the wavelet transform, and the relationship between the signal and inhalation aerosol behavior will be discussed.

The Wavelet Transform, particularly the Morlet Wavelet Transform (MWT), surpasses the Fourier and Short Time Fourier Transforms (STFT) by enabling multiresolution analysis, which captures and localizes fine details of non-stationary, transient signals across different time-frequency scales. The Morlet wavelet, a Gaussian-windowed complex sinusoid, provides good time localization due to the second-order exponential decay of the Gaussian function and it is defined as follows (Bialasiewicz, 2015; Mashrur et al., 2021):

$$W_x(s,\tau) = \frac{1}{\sqrt{s}} \int x(t)\psi^*(\frac{t-\tau}{s})dt$$

In which $\psi(t) = \pi^{-1/4} e^{jw_0 t} e^{-1/2t^2}$, where x is the analyzed signal, s is the scale and τ is the position of the signal. The Wavelet coefficient, $W_x(s,\tau)$, represents $x(t)$, and its Fourier transform in the time-frequency region where the energy of the wavelet atom $\psi(t)$.

Scalograms are visual representations of wavelet transforms that are useful for analyzing complex signals and identifying features such as bursts, trends, and patterns in the data (Bialasiewicz, 2015). A wavelet scalogram is defined as the local time-frequency energy density, which quantifies the energy of a signal $x(t)$ within the Heisenberg box of each wavelet $\psi(t)$. The scalogram is defined as follow:

$$P_w x(s,\tau) = |W_x(s,\tau)|^2$$

Where $W_x(s,\tau)$ is Wavelet coefficient, s is the scale and τ is the position.

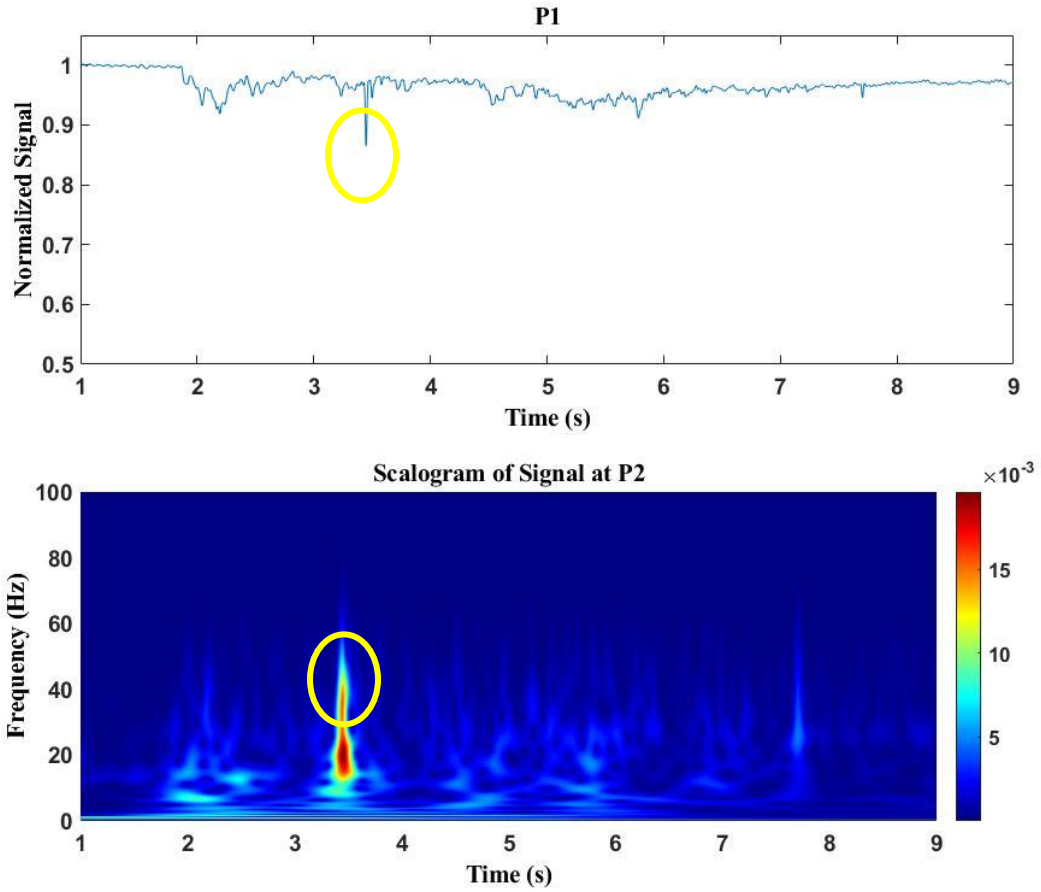

Figure 5. 11: Signal and scalogram under 20 LPM condition using osmohaler measured at Position 1 within the mouth region.

Figure 5. 11 presents the time-domain laser signal and its corresponding scalogram, obtained via wavelet transform, representing aerosol particles emitted from an osmohaler under a 20 LPM inhalation flow rate, measured at Position 1(P1) within the mouth region (as shown in Figure 5.3). The top panel shows the laser signal over time, demonstrating a generally stable pattern with minor fluctuations and a notable dip around the 3-second mark, indicating a transient event or interference that briefly reduces the signal intensity. This relatively stable signal could be due to the suboptimal performance of the osmohaler at the lower flow rate of 20 LPM, leading to a gradual release of drug particles. Since the osmohaler is designed to function optimally at flow rates above 40 LPM, a lower flow rate can cause the capsule to spin more slowly during inhalation, which in turn leads to a slower and more extended release of the powder (Michael Y Yang et al., 2016). The observed fluctuations and isolated dip in the time-domain signal may indicate transient changes in particle concentration or size distribution as the aerosol exits the osmohaler, possibly due to initial aerosolization dynamics or interactions with the inhalation airflow.

The scalogram in the bottom panel offers a detailed frequency analysis over time (X-axis: time (s), Y-axis:frequency (Hz)), revealing a predominance of low-frequency components, which decrease slightly in intensity during the observed dip, suggesting variations in particle dynamics or concentration. The color gradient in the scalogram, with blue representing lower intensity and yellow representing higher intensity, highlights the distribution and intensity of various frequency components. The predominance of blue shades indicates that the aerosol flow is primarily dominated by low-frequency components, most likely characteristic of larger particles or aggregates which have higher inertia and are less likely to respond as rapidly to the surrounding flow. The notable drop around 3.5 seconds (as shown in the yellow circle), as seen in the time-domain signal, corresponds to a reduction in the energy of these frequency components, suggesting a possible interruption or scattering event, likely due to the detection of large particles or particle clusters.

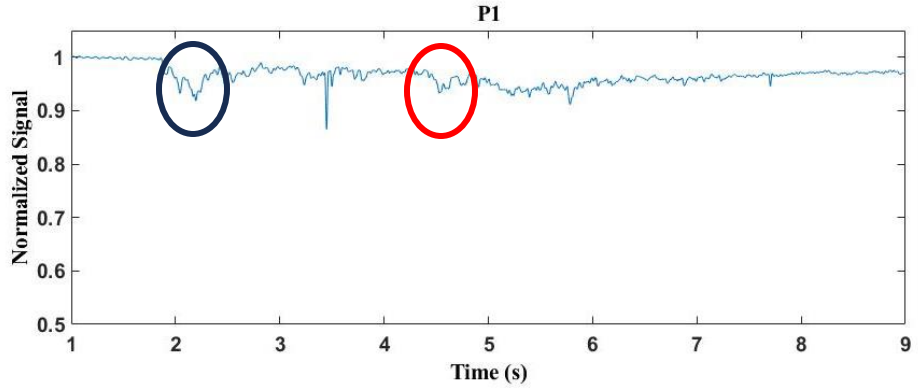
P1
Normalized Signal
Time (s)

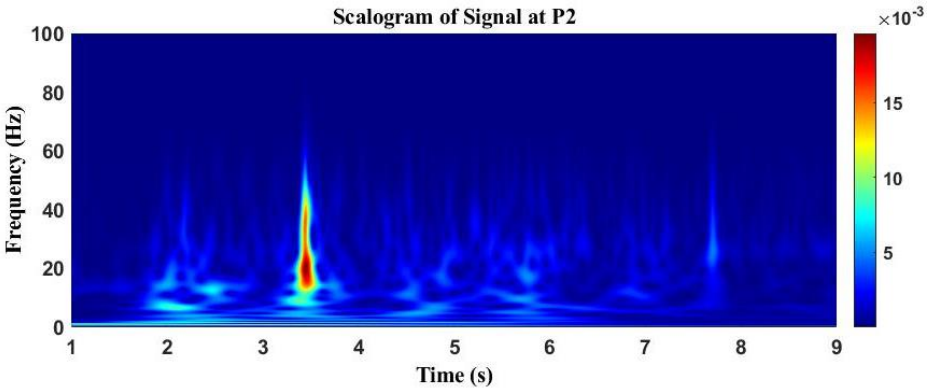
Scalogram of Signal at P2
Frequency (Hz)
Time (s)
×10-3

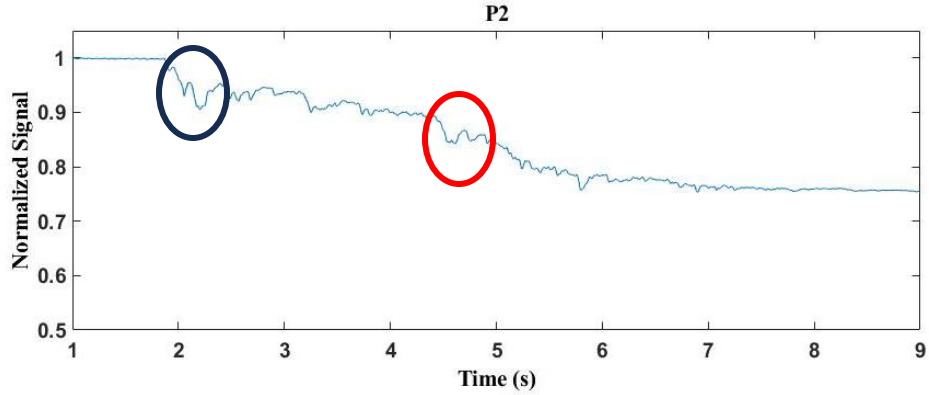
P2
Normalized Signal
Time (s)

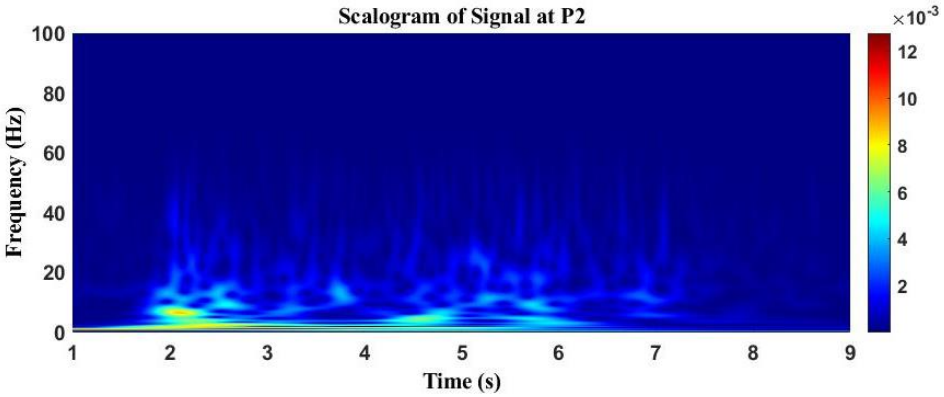
Scalogram of Signal at P2
Frequency (Hz)
Time (s)
×10-3

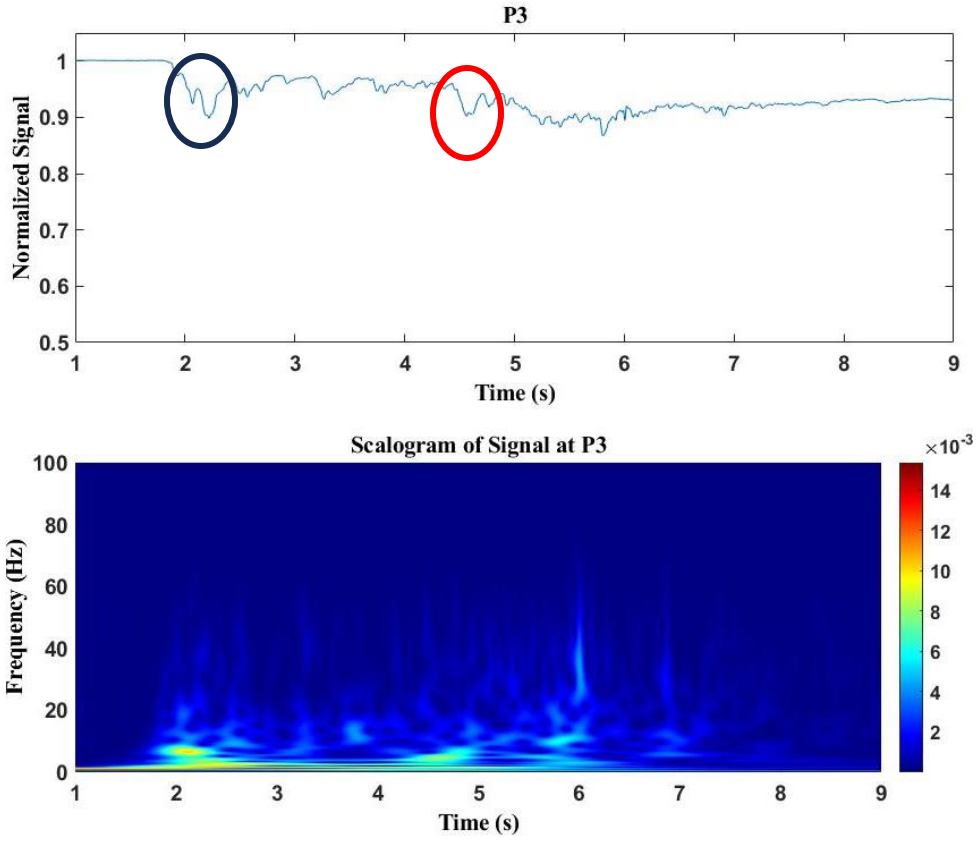
P3
Normalized Signal
Time (s)
Scalogram of Signal at P3
Frequency (Hz)
Time (s)
×10^-3

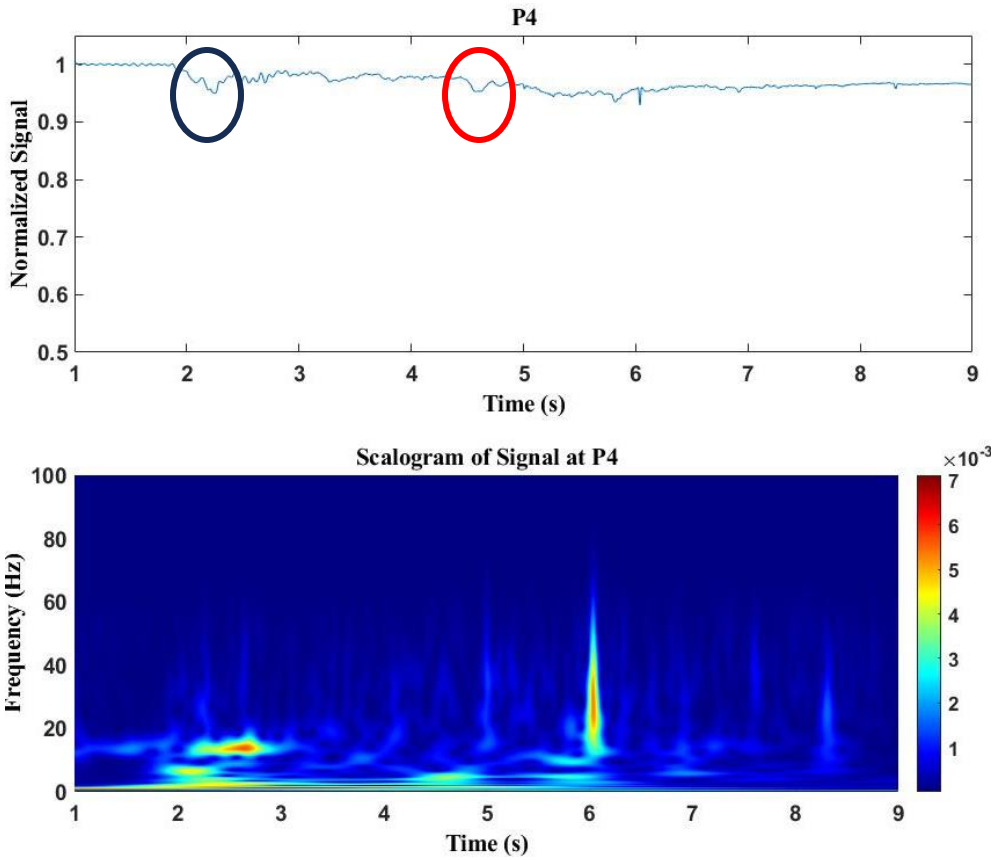
P4
Normalized Signal
Time (s)
Scalogram of Signal at P4
Frequency (Hz)
Time (s)
×10^-3

Figure 5. 12: Signal and scalogram under 20 LPM condition using osmohaler measured at four different Positions (P1-P4) in the upper airway model.

Figure 5. 12 indicates the time-domain signals and corresponding spectrograms of aerosol laser signals recorded at four different positions along the same airway during a single experimental run, labeled as P1, P2, P3, and P4. Each window depicts a distinct temporal and frequency response of the aerosol as it progresses through the airway, with a slight time delay observed between consecutive windows, indicating the sequential arrival of the aerosol at each detection point.

In P1, the time-domain signal is relatively stable with minor fluctuations, suggesting a steady flow of aerosols, while the scalogram shows low-frequency components with moderate intensity, suggesting the presence of larger aerosol particles or clusters. Moving to P2, a noticeable drop in signal intensity is observed, accompanied by a shift towards higher frequencies in the scalogram, possibly indicating the fragmentation or dispersion of aerosol particles. In P3, the signals stabilize again, but the scalograms show variations in frequency content, reflecting the ongoing attenuation of the aerosol as it moves downstream. P4 displays the final stage of the aerosol's progression, with the signal stabilizing again but at a lower intensity than the initial windows, suggesting some aerosol loss or dispersion.

The analysis of these scalograms across different positions provides valuable insights into the dynamic behavior of aerosol particles within the airway. The initial presence of low-frequency components suggests larger particles that may be more prone to deposition in the upper airway. The shift to higher frequencies and the subsequent stabilization indicates a dispersion process, where particle size reduces, potentially improving penetration into deeper lung regions.

As shown in the post-processed signal in Figure 5.12, the patterns marked by the black and red circles can be tracked from P1 to P4. While the main trend of the signal may change, these small patterns maintain a consistent time delay between each position, indicating the successful tracking of the same group of drug particle clusters as they flow through the airway. However, the intensity of signal pattern diminishes from P1 to P4, suggesting the loss or dispersion of these particle clusters due to turbulence and impaction in the airway. Several distinct small patterns can be tracked in the signal from P1 to P4. Based on the signal analysis conducted at these positions, the combination of the scalogram and the signal provides a means to roughly estimate aerosol loss by examining signal dips.

5.4 Limitations

The main objective of this study is to demonstrate the capabilities of laser attenuation in making useful comments about airway aerosol dynamics. However, it is important to acknowledge that the current study design has certain inherent limitations, which should be carefully considered when interpreting the results. Firstly, the limited size of the photodiode surface area and the small surface area of the laser diode restrict the measured regional deposition region, resulting in a small window. The results obtained from the measurements therefore do not fully represent the entire airway though this does not diminish the utility of the data obtained in regions where we could measure. To overcome this limitation, a significant number of laser diodes and photodiodes can be incorporated into the further study this would be rather cost effective and enable these diodes to be integrated within the airway wall itself. Furthermore, the signal drop is a result of the combined effects of particle flow and deposition, and the laser passes through two windows before reaching the photo diode measurement area, making it unknown which side has a higher drug deposition. To solely measure particle flow behavior in the human airway, it is recommended to adjust the window distance from the wall in future experiments. By doing so, this approach can also facilitate clear identification of particle flow and regional deposition patterns. For instance, by controlling one side to have no deposition or ensuring both sides are free from deposition, it becomes possible to discern specific information regarding either side's deposition or particle flow characteristics.

5.5 Conclusions

This study introduced an innovative method using laser and optical sensors to analyze drug particle behavior in the human upper airway, examining two particle sizes across different flow rates. The technique effectively captured spatial and temporal particle dynamics, such as transport velocity, regional deposition, and aerosol escape time. Findings indicate that regional deposition varies with particle size and flow rate, with higher flow rates leading to increased deposition in specific airway regions. By processing signal data, this method measures aerosol transport time and regional deposition, aligning with previous simulations. This approach provides valuable insights into aerosol dynamics and holds potential for assessing different inhaler designs and optimizing drug delivery. Future research can extend this technique to

further explore aerosol behavior in diverse inhalation scenarios, enhancing our understanding of pulmonary drug delivery.

5.6 Appendix

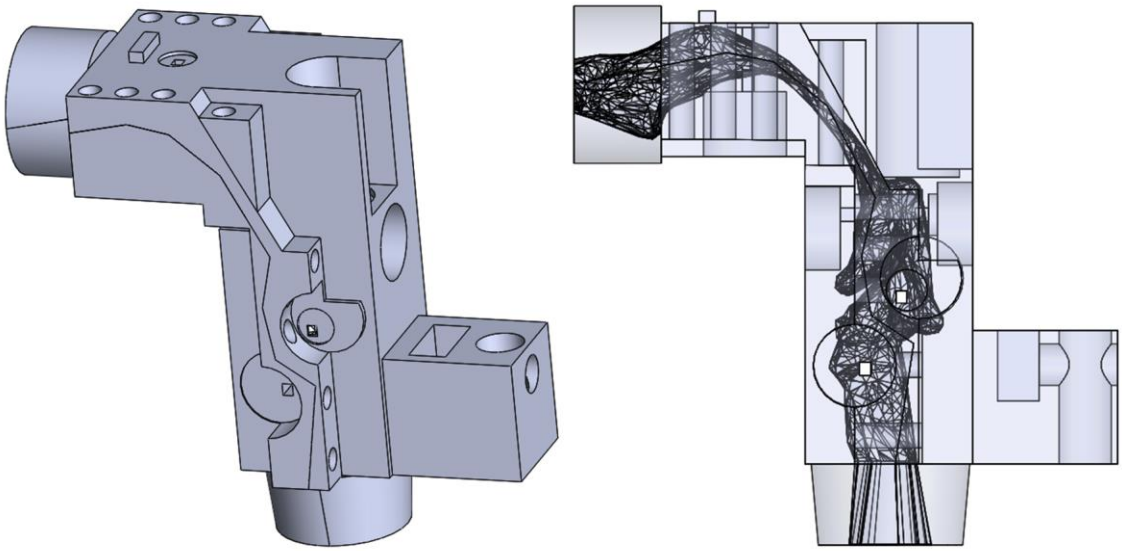

Figure 5. A.1: 3D model of the human airway used in the experiment

5.7 References for Chapter 5

1. Ahookhosh, K., Pourmehran, O., Aminfar, H., Mohammadpourfard, M., Sarafraz, M. M., & Hamishehkar, H. (2020). Development of human respiratory airway models: A review. *European Journal of Pharmaceutical Sciences, 145*, 105233.
2. Anderson, S. D., Daviskas, E., Brannan, J. D., & Chan, H. K. (2018). Repurposing excipients as active inhalation agents: the mannitol story. *Advanced drug delivery reviews, 133*, 45-56.
3. Bialasiewicz, J. T. (2015). *Application of wavelet scalogram and coscalogram for analysis of biomedical signals.* Paper presented at the Proceedings of the World Congress on Electrical Engineering and Computer Systems and Science.
4. Byron, P. R., Hindle, M., Lange, C. F., Longest, P. W., McRobbie, D., Oldham, M. J., . . . Finlay, W. H. (2010). In vivo–in vitro correlations: predicting pulmonary drug deposition from pharmaceutical aerosols. *Journal of aerosol medicine and pulmonary drug delivery, 23*(S2), S-59-S-69.
5. Cai, X., Ma, B., Kourmatzis, A., Salehi, F., Lee, A., Farina, D., . . . Cheng, S. (2022). Potential effects of inhaler mouthpiece size on particle deposition in the human upper airway. *Aerosol Science and Technology, 56*(9), 802-818.
6. Caramori, G., & Adcock, I. (2003). Pharmacology of airway inflammation in asthma and COPD. *Pulmonary Pharmacology & Therapeutics, 16*(5), 247-277.
7. Chan, J. G. Y., Kwok, P. C. L., Young, P. M., Chan, H.-K., & Traini, D. (2011). Mannitol delivery by vibrating mesh nebulisation for enhancing mucociliary clearance. *Journal of pharmaceutical sciences, 100*(7), 2693-2702.
8. Cheng, S., Kourmatzis, A., Mekonnen, T., Gholizadeh, H., Raco, J., Chen, L., . . . Chan, H.-K. (2019). Does upper airway deformation affect drug deposition? *International Journal of Pharmaceutics, 572*, 118773.
9. Chew, N. Y., Bagster, D. F., & Chan, H.-K. (2000). Effect of particle size, air flow and inhaler device on the aerosolisation of disodium cromoglycate powders. *International Journal of Pharmaceutics, 206*(1-2), 75-83.
10. Chew, N. Y., & Chan, H.-K. (1999). Influence of particle size, air flow, and inhaler device on the dispersion of mannitol powders as aerosols. *Pharmaceutical Research, 16*, 1098-1103.
11. Chrystyn, H., Safioti, G., Keegstra, J. R., & Gopalan, G. (2015). Effect of inhalation profile and throat geometry on predicted lung deposition of budesonide and formoterol (BF) in COPD: an in-vitro comparison of Spiromax with Turbuhaler. *International Journal of Pharmaceutics, 491*(1-2), 268-276.
12. Conway, J. (2012). Lung imaging—two dimensional gamma scintigraphy, SPECT, CT and PET. *Advanced drug delivery reviews, 64*(4), 357-368.
13. Delvadia, R. R., Longest, P. W., & Byron, P. R. (2012). In vitro tests for aerosol deposition. I: Scaling a physical model of the upper airways to predict drug deposition variation in normal humans. *Journal of aerosol medicine and pulmonary drug delivery, 25*(1), 32-40.
14. Dyakowski, T., & Williams, R. A. (1993). Measurement of particle velocity distribution in a vertical channel. *Powder technology, 77*(2), 135-142.
15. Fabbri, L. M., Romagnoli, M., Corbetta, L., Casoni, G., Busljetic, K., Turato, G., . . . Papi, A. (2003). Differences in airway inflammation in patients with fixed airflow obstruction due to asthma or chronic obstructive pulmonary disease. *American journal of respiratory and critical care medicine, 167*(3), 418-424.

16. Faizal, W., Ghazali, N. N. N., Khor, C., Badruddin, I. A., Zainon, M., Yazid, A. A., . . . Razi, R. M. (2020). Computational fluid dynamics modelling of human upper airway: A review. *Computer methods and programs in biomedicine, 196*, 105627.
17. Finlay, W. H. (2001). *The mechanics of inhaled pharmaceutical aerosols: an introduction*: Elsevier.
18. Grgic, B., Finlay, W. H., Burnell, P. K., & Heenan, A. F. (2004). In vitro intersubject and intrasubject deposition measurements in realistic mouth–throat geometries. *Journal of Aerosol Science, 35*(8), 1025-1040.
19. Haidl, P., Heindl, S., Siemon, K., Bernacka, M., & Cloes, R. M. (2016). Inhalation device requirements for patients' inhalation maneuvers. *Respiratory medicine, 118*, 65-75.
20. Hoppentocht, M., Hagedoorn, P., Frijlink, H., & De Boer, A. (2014). Technological and practical challenges of dry powder inhalers and formulations. *Advanced drug delivery reviews, 75*, 18-31.
21. Ju, D., Shrimpton, J., & Hearn, A. (2010). The effect of reduction of propellant mass fraction on the injection profile of metered dose inhalers. *International Journal of Pharmaceutics, 391*(1-2), 221-229.
22. Kakade, P. P., Versteeg, H. K., Hargrave, G. K., Genova, P., Williams Iii, R. C., & Deaton, D. (2007). Design optimization of a novel pMDI actuator for systemic drug delivery. *Journal of aerosol medicine, 20*(4), 460-474.
23. Khanal, D., Zhang, J., Ke, W.-R., Banaszak Holl, M. M., & Chan, H.-K. (2020). Bulk to nanometer-scale infrared spectroscopy of pharmaceutical dry powder aerosols. *Analytical Chemistry, 92*(12), 8323-8332.
24. Kourmatzis, A., Cheng, S., & Chan, H.-K. (2018). Airway geometry, airway flow, and particle measurement methods: implications on pulmonary drug delivery. *Expert opinion on drug delivery, 15*(3), 271-282.
25. Labiris, N. R., & Dolovich, M. B. (2003). Pulmonary drug delivery. Part I: physiological factors affecting therapeutic effectiveness of aerosolized medications. *British journal of clinical pharmacology, 56*(6), 588-599.
26. Leung, S. S. Y., Tang, P., Zhou, Q., Tong, Z., Leung, C., Decharaksa, J., . . . Chan, H.-K. (2015). De-agglomeration effect of the US pharmacopeia and Alberta throats on carrier-based powders in commercial inhalation products. *The AAPS journal, 17*, 1407-1416.
27. Liang, W., Kwok, P. C., Chow, M. Y., Tang, P., Mason, A. J., Chan, H.-K., & Lam, J. K. (2014). Formulation of pH responsive peptides as inhalable dry powders for pulmonary delivery of nucleic acids. *European Journal of Pharmaceutics and Biopharmaceutics, 86*(1), 64-73.
28. List, R. J. (1951). Smithsonian meteorological tables. *Smithsonian miscellaneous collections*.
29. Ma, B., Kourmatzis, A., Zhao, Y., Yang, R., Chan, H.-K., Salehi, F., & Cheng, S. (2020). Potential effects of lingual fats on airway flow dynamics and particle deposition. *Aerosol Science and Technology, 54*(3), 321-331.
30. Ma, Z., Kourmatzis, A., Milton-McGurk, L., Chan, H.-K., Farina, D., & Cheng, S. (2022). Simulating the effect of individual upper airway anatomical features on drug deposition. *International Journal of Pharmaceutics, 628*, 122219.
31. Ma, Z., Milton-McGurk, L., Tang, P., Chan, H.-K., Farina, D., Cheng, S., & Kourmatzis, A. (2024). An experimental study of the effect of individual upper airway anatomical features on the deposition of dry powder inhaler formulations. *Journal of Aerosol Science, 177*, 106320.

32. Mahmoudi, S., Elserfy, K., Cheng, S., Chan, H.-K., Hebbink, G., & Kourmatzis, A. (2019). Fluidisation characteristics of lactose powders in simple turbulent channel flows. *Experimental Thermal and Fluid Science, 103*, 201-213.
33. Martin, A. R., Moore, C. P., & Finlay, W. H. (2018). Models of deposition, pharmacokinetics, and intersubject variability in respiratory drug delivery. *Expert opinion on drug delivery, 15*(12), 1175-1188.
34. Mashrur, F. R., Islam, M. S., Saha, D. K., Islam, S. R., & Moni, M. A. (2021). SCNN: Scalogram-based convolutional neural network to detect obstructive sleep apnea using single-lead electrocardiogram signals. *Computers in biology and medicine, 134*, 104532.
35. Milne, S., & King, G. G. (2014). Advanced imaging in COPD: insights into pulmonary pathophysiology. *Journal of thoracic disease, 6*(11), 1570.
36. Mitchell, J. P., & Nagel, M. W. (2003). Cascade impactors for the size characterization of aerosols from medical inhalers: their uses and limitations. *Journal of aerosol medicine, 16*(4), 341-377.
37. Newman, S. P., & Chan, H.-K. (2020). In vitro-in vivo correlations (IVIVCs) of deposition for drugs given by oral inhalation. *Advanced drug delivery reviews, 167*, 135-147.
38. Schröder, A., & Willert, C. E. (2008). Particle image velocimetry: new developments and recent applications.
39. Scichilone, N., Benfante, A., Bocchino, M., Braido, F., Paggiaro, P., Papi, A., . . . Sanduzzi, A. (2015). Which factors affect the choice of the inhaler in chronic obstructive respiratory diseases? *Pulmonary Pharmacology & Therapeutics, 31*, 63-67.
40. Soodt, T., Schröder, F., Klaas, M., van Overbrüggen, T., & Schröder, W. (2012). Experimental investigation of the transitional bronchial velocity distribution using stereo scanning PIV. *Experiments in fluids, 52*, 709-718.
41. Tang, P., Kakhi, M., Albariqi, A., Behara, S. R. B., Walenga, R., Yang, R., & Chan, H.-K. (2023). The role of capsule aperture size on the dispersion of carrier-based formulation at different air flowrates. *International Journal of Pharmaceutics*, 123152.
42. Unser, M., & Aldroubi, A. (1996). A review of wavelets in biomedical applications. *Proceedings of the IEEE, 84*(4), 626-638.
43. USP. (2023). General Chapter, ⟨601⟩ Inhalation and Nasal Drug Products: Aerosols, Sprays, and Powders—Performance Quality Tests. In. Rockville, MD: United States Pharmacopeia.
44. Venegas, J., Winkler, T., & Harris, R. S. (2013). Lung physiology and aerosol deposition imaged with positron emission tomography. *Journal of aerosol medicine and pulmonary drug delivery, 26*(1), 1-8.
45. Vos, T., Lim, S. S., Abbafati, C., Abbas, K. M., Abbasi, M., Abbasifard, M., . . . Abdelalim, A. (2020). Global burden of 369 diseases and injuries in 204 countries and territories, 1990–2019: a systematic analysis for the Global Burden of Disease Study 2019. *The Lancet, 396*(10258), 1204-1222.
46. Weers, J., & Clark, A. (2017). The impact of inspiratory flow rate on drug delivery to the lungs with dry powder inhalers. *Pharmaceutical Research, 34*, 507-528.
47. Wei, X., Hindle, M., Kaviratna, A., Huynh, B. K., Delvadia, R. R., Sandell, D., & Byron, P. R. (2018). In vitro tests for aerosol deposition. VI: realistic testing with different mouth–throat models and in vitro—in vivo correlations for a dry powder inhaler, metered dose inhaler, and soft mist inhaler. *Journal of aerosol medicine and pulmonary drug delivery, 31*(6), 358-371.
48. WHO. (2023). Retrieved from https://www.who.int/news-room/fact-sheets/detail/chronic-obstructive-pulmonary-disease-(copd)

49. Yang, M. Y., Verschuer, J., Shi, Y., Song, Y., Katsifis, A., Eberl, S., . . . Finlay, W. H. (2016). The effect of device resistance and inhalation flow rate on the lung deposition of orally inhaled mannitol dry powder. *International Journal of Pharmaceutics, 513*(1-2), 294-301.
50. Yang, X., Zhang, T., Zhang, Y., Chen, H., & Sang, S. (2021). Global burden of COPD attributable to ambient PM2. 5 in 204 countries and territories, 1990 to 2019: A systematic analysis for the Global Burden of Disease Study 2019. *Science of the Total Environment, 796*, 148819.

Chapter 6 Summary and Conclusion

This thesis explored the complexities of pulmonary drug delivery by examining the effects of specific anatomical features in the human upper airway and developing a novel method to measure the transient flow behavior and deposition mechanisms of drug particles in this region. Due to the intricate and variable geometry of these airways, aerosol aerodynamic performance and deposition mechanisms remain unclear. To fill this knowledge gap, this study systematically isolated different anatomical structures of the human pharynx, including the uvula, epiglottis, and soft palate, to assess their independent effects on airflow dynamics and particle deposition characteristics. Computational Fluid Dynamics (CFD) using established turbulence models was employed to simulate the transport of mono-dispersed particles (3 μm) within realistic airway geometries as a function of flow rate. Furthermore, a standard experimental approach using NGI and HPLC was employed to investigate how anatomical features influence particle deposition in the human airway. The CFD study was validated against these experimental results, and the impact of anatomical features on drug particles reaching the deep lung was also examined. In addition, the existing experimental methods fall short in assessing transient drug particle flow and behavior, so this study also introduced a novel technique using multiple laser diodes and photodiode sensors to simultaneously measure regional deposition and particle cluster velocity in a realistic human upper airway model, enabling real-time, non-intrusive analysis of particle dynamics within complex airway geometries.

A more detailed main findings are listed below:

6.1 Main findings

6.1.1 Simulation study of the impact of individual upper airway anatomical features on drug deposition

Computational fluid dynamics (CFD) simulations revealed the critical role of upper airway anatomical structures in shaping airflow behavior and particle deposition patterns. While the uvula and epiglottis contribute to maintaining symmetrical airflow, their removal had minimal impact on the total deposition fraction within the airway. However, eliminating the soft palate resulted in significant changes in airflow dynamics, leading to a 33% reduction in

localized velocity and deposition. These findings highlight the necessity of including the soft palate in airway models to ensure realistic drug deposition assessments.

Moreover, the study demonstrated that flow rate variations had a less pronounced effect on deposition compared to structural modifications. The removal of specific anatomical features primarily influenced local flow behavior and regional deposition, reinforcing the importance of anatomical accuracy in pulmonary drug delivery studies.

6.1.2 Experimental study of the impact of individual upper airway anatomical features on drug deposition

Experimental findings using realistic 3D-printed airway replicas confirmed the simulation results, showing that the expansion or removal of the soft palate led to an increased fine particle fraction (FPF) and reduced deposition in the upper airway. This was attributed to the increase in airway cross-section and reduced turbulence, as indicated by lower Reynolds numbers.

The impact of anatomical structures was more pronounced in the Osmohaler compared to the Handihaler, likely due to the Handihaler's smaller mouthpiece, which generates higher inlet velocities and turbulence. Furthermore, at higher flow rates, anatomical features had less influence on downstream deposition, as increased deposition near the mouth-throat region at higher Reynolds numbers reduced the mass available for further airway penetration.

The study also found that removing anatomical features reduced both the Reynolds number and Stokes number, key parameters governing particle deposition. An empirical relationship, $Stk \cdot Re^{0.37}$, revealed that at higher Stokes and Reynolds numbers, deposition patterns remained similar, while at lower values, the inhaler type significantly influenced deposition patterns. This highlights the importance of inhaler design and patient-specific airway conditions in optimizing drug delivery.

6.1.3 A new method using laser attenuation measures particle deposition and velocity in a human upper airway model

A new laser attenuation technique was developed to measure particle deposition and velocity in a realistic human upper airway model, providing real-time insights into aerosol dynamics. The experimental results demonstrated the following key findings:

- Higher flow rates (40 LPM and 60 LPM) led to increased turbulence and denser particle clouds, resulting in significant signal attenuation in the optical measurement system.
- At lower flow rates (20 LPM), particle signals exhibited gradual declines across different positions, whereas higher flow rates caused distinct deposition variations between the mouth and deeper airway regions.
- Escape time measurements showed that as flow rate increased, drug particles exited the airway more quickly, emphasizing the importance of consistent inhalation techniques for effective drug delivery.
- Regional deposition analysis revealed increased deposition from the mouth region to the uvula and epiglottis, followed by a decrease toward the trachea, particularly at higher flow rates.
- Signal fluctuation analysis indicated that greater turbulence in anatomical regions, such as the uvula and epiglottis, correlated with increased regional deposition.
- Spectral analysis using wavelet transforms identified a shift from low-frequency components near the inhaler to higher-frequency fluctuations downstream, suggesting potential for deeper lung penetration of aerosols.
- Scalogram analysis enabled the estimation of aerosol loss and regional deposition fractions, demonstrating a practical method for evaluating real-time flow dynamics in pulmonary drug delivery studies.

6.2 Future work

6.2.1 Inhalation profile simulation and experiment combined with laser

- Different individuals have unique inhalation profiles. A future study could simulate inhalation profiles across different groups of people's airways and use the laser attenuation method to validate the results. This approach would help to better understand the variations in particle behavior and deposition, leading to more personalized and effective inhalation therapies.

- Further studies should focus on optimizing the laser measurement setup to capture real-time particle dynamics across a range of flow rates and particle sizes. By doing so, we can enhance the accuracy of regional deposition data, ultimately leading to better predictions of drug delivery efficiency and therapeutic outcomes. This approach will bridge the gap between theoretical models and practical applications, paving the way for innovative inhalation technologies and personalized treatment strategies.

6.2.2 A New Color-Labeled Drug Method to Investigate Particle Distribution in the Airway

- Future research could explore the use of a novel color-labeled drug method to investigate drug particle distribution within the airway. By tagging drug particles with, it would be possible to visually track and analyze the deposition patterns throughout various regions of the airway. This approach could provide detailed insights into how different anatomical structures, airflow rates, and particle sizes affect the distribution and deposition of drug particles. Combining this color-labeled method with imaging techniques could offer a more comprehensive understanding of drug delivery mechanisms, allowing researchers to precisely map particle trajectories and identify areas of high or low deposition. Such detailed visualization would be invaluable for optimizing inhaler designs and developing more targeted drug delivery strategies, ultimately improving therapeutic outcomes for patients with respiratory conditions.

6.2.3 New Laser Method Combined with Inhalers to Test Various Devices

- The laser attenuation based method can be integrated with different inhalers to comprehensively evaluate their performance and effectiveness. By utilizing laser technology, this approach can accurately measure particle velocity, distribution, and deposition patterns in real-time, providing valuable insights into how different inhaler designs influence drug delivery. This method allows for the detailed analysis of how particles behave under various inhalation conditions, including different flow rates and particle sizes. By applying the laser method to a range of inhaler devices, researchers can directly compare their efficacy in delivering medication to targeted regions of the respiratory tract. This will help identify which designs optimize drug delivery, minimize particle loss, and ensure consistent therapeutic outcomes.

6.2.4 Dissolution

- Dissolution testing for oral dosage forms can be introduced to differentiate several formulation types and should allow an estimate of dissolution behavior in vivo. It is routinely used in quality control during development, manufacturing, and storage. In the future, dissolution testing of inhaled powders will likely become an important aspect of pharmaceutical development and quality control processes. A future study could involve using filter paper to collect drug particles from the airway model, and employing either the flow-through cell method or the paddle over disc method to mimic how drugs dissolve in the blood and to study their dissolution rate.